THE FACULTY OF ENGINEERING AND THE BUILT ENVIRONMENT

The Department of Mechanical Engineering

Optical and Thermal Analysis of a Heteroconical Tubular Cavity Solar Receiver

By

Neelesh Maharaj

A dissertation submitted to the Department of Mechanical Engineering, University of Cape Town in partial fulfilment of the requirements for the degree of Master of Science in Mechanical Engineering

DECLARATION

I, Neelesh Maharaj know the meaning of plagiarism and declare that all the work in the document, save for that which is properly acknowledged, is my own. This thesis/dissertation has been submitted to the Turnitin module, and I confirm that my supervisor has seen my report and any concerns revealed by such have been resolved with my supervisor.

Signed by candidate

Neelesh Maharaj

Student Number: MHRNEE002

Date: 25-11-2017

ABSTRACT

Title: Thermodynamic Analysis of a Heteroconical Tubular Cavity Solar Receiver

Author: Neelesh Maharaj (MHRNEE002)

Supervisor: Prof. Tunde Bello-Ochende

University: University of Cape Town

Department: Mechanical Engineering

Degree: Master of Science in Mechanical Engineering (M.Sc. Mech. Eng.)

The principal objective of this study is to develop, investigate and optimise the Heteroconical Tubular Cavity receiver for a parabolic trough reflector. This study presents a three-stage development process which allowed for the development, investigation and optimisation of the Heteroconical receiver. The first stage of development focused on the investigation into the optical performance of the Heteroconical receiver for different geometric configurations. The effect of cavity geometry on the heat flux distribution on the receiver absorbers as well as on the optical performance of the Heteroconical cavity was investigated. The cavity geometry was varied by varying the cone angle and cavity aperture width of the receiver. This investigation led to identification of optical characteristics of the Heteroconical receiver as well as an optically optimised geometric configuration for the cavity shape of the receiver. The second stage of development focused on the thermal and thermodynamic performance of the Heteroconical receiver for different geometric configurations. This stage of development allowed for the investigation into the effect of cavity shape and concentration ratio on the thermal performance of the Heteroconical receiver. The identification of certain thermal characteristics of the receiver further optimised the shape of the receiver cavity for thermal performance during the second stage of development. The third stage of development and optimisation focused on the absorber tubes of the Heteroconical receiver. This enabled further investigation into the effect of tube diameter on the total performance of the Heteroconical receiver and led to an optimal inner tube diameter for the receiver under given operating conditions.

In this work, the thermodynamic performance, conjugate heat transfer and fluid flow of the Heteroconical receiver were analysed by solving the computational governing Equations set out in this work known as the Reynolds-Averaged Navier-Stokes (RANS) Equations as well as the energy Equation by utilising the commercially available CFD code, ANSYS FLUENT®. The optical model of the receiver which modelled the optical performance and produced the non-uniform actual heat flux distribution on the absorbers of the receiver was numerically modelled by solving the rendering Equation using the Monte-Carlo ray tracing method. SolTrace – a ray-tracing software package developed by the National Renewable Energy Laboratory (NREL), commonly used to analyse CSP systems, was utilised for modelling the optical response and performance of the Heteroconical receiver. These actual non-uniform heat flux distributions were applied in the CFD code by making use of user-defined functions for the thermal model and analysis of the Heteroconical receiver. The numerical model was applied to a simple parabolic trough receiver and reflector and validated against experimental data available in the literature, and good agreement was achieved.

It was found that the Heteroconical receiver was able to significantly reduce the amount of re-radiation losses as well as improve the uniformity of the heat flux distribution on the absorbers. The receiver was found to produce thermal efficiencies of up to 71% and optical efficiencies of up to 80% for practically sized receivers. The optimal receiver was compared to a widely used parabolic trough receiver, a vacuum tube receiver. It was found that the optimal Heteroconical receiver performed, on average, 4% more efficiently than the vacuum tube receiver across the temperature range of 50-210℃.

In summary, it was found that the larger a Heteroconical receiver is the higher its optical efficiency, but the lower its thermal efficiency. Hence, careful consideration needs to be taken when determining cone angle and concentration ratio of the receiver. It was found that absorber tube diameter does not have a significant effect on the performance of the receiver, but its position within the cavity does have a vital role in the performance of the receiver. The

Heteroconical receiver was found to successfully reduce energy losses and was found to be a successfully high performance solar thermal tubular cavity receiver.

Key words: Parabolic Trough Receiver, Thermal Receiver, Tubular Cavity Receiver, Ray-Tracing, Monte-Carlo, Concentration Ratio, Reflector, Collector, Optical Efficiency, Thermal Efficiency, Heteroconical, Absorber Tube, Conjugate Heat Transfer, Re-Radiation, High Performance Solar Receiver, Parabolic Trough Reflector, Optical Analysis, Thermal Analysis

ACKNOWLEDGEMENTS

Acknowledgement and thanks are given to my supervisor Prof. Tunde Bello-Ochende for his guidance and continuous encouragement throughout this project.

Thank you to my dear friend Ashwin Vallat for his support.

Special thanks to my mother and brother, Veena and Divesh Maharaj for all the support and encouragement you provided throughout my studies.

Finally, the funding received from the NRF is gratefully acknowledged and appreciated.

TABLE OF CONTENTS

TABLE OF FIGURES

LIST OF TABLES

NOMENCLATURE

Symbols

$\mathcal{N}$	Optimum Position	m
r	Cavity Aperture Width	cm
R	Reflector Width	m
f	Focal Length	m
a	Receiver Aperture Width	cm
C	Specific Heat Capacity	J/kg·K
$\dot{Q}$	Heat Rate (Power)	W
T	Temperature	K
k	Thermal Conductivity	W/m·K
v	Velocity Vector	m/s
g	Gravity Vector	m/s^2
p	Pressure	Atm
$\dot{m}$	Mass Flow Rate	kg/s

Greek Symbols

ψ	Rim angle, degrees	^{0}
ρ	Density	kg/m^3
Φ	Viscous Dissipation Function	-
μ	Dynamic Viscosity	kg/m· s
θ	Cone Angle	^{0}
η	Efficiency	-

Subscripts

opt	Optical
abs	Absorbed
r	Receiver
htf	Heat Transfer Fluid
th	Thermal
o	Total
p	Pressure

Abbreviations

HTC	Heteroconical Tubular Cavity
STC	Simple Tubular Cone
CFD	Computational Fluid Dynamics
RANS	Reynolds-Averaged Navier-Stokes
RNG	Renormalisation Group
CR	Concentration Ratio
RCR	Receiver Concentration Ratio
CSP	Concentrated Solar Power
atm	Atmosphere

Blank Page

CHAPTER ONE

1 INTRODUCTION

1.1 BACKGROUND

The demand for energy is ever-increasing due to urbanization, industrialization and population growth. Energy is also vital in the wellbeing of people as well as in the development of economies and civilization in general. It is an enabler to many societal developments like education, healthcare, transport, innovation and agriculture. Due to this increase in demand and the realization of the finite supply of fossil fuels and the harmful effects caused by the emission of greenhouse gases in obtaining energy, alternate, clean and sustainable renewable energy sources are needed.

Energy is considered renewable and sustainable when the resources are easily replenished once they have been consumed and have little negative impact on the environment, for example, water and sunlight. Non-renewable energy has finite resources like oil, coal, gas, etc. When converted to usable energy, these have many negative effects on the environment, for example, harmful emissions and by-products.

According to the South African Department of Energy, approximately 77% of South Africa's energy needs are provided by coal power stations (DOE, 2018). Transmission lines must be laid across large distances to supply electricity to isolated areas and some areas unfortunately do not receive electricity and are forced to use wood as a means of generated heat for warmth and cooking. A solution is needed to make electricity more accessible without the concern of depleting resources and causing harm to the environment.

In South Africa, there is an abundance of resources, most of them being limited or finite for example, coal, oil, diamonds and gold. However, there is an abundance of irradiated sunlight

which can be converted to solar energy and used as a renewable energy resource. This makes it a very promising alternative to energy converted from fossil fuels. As a result, this development research needs to be directed into harvesting solar energy and using the resource effectively and productively allowing the technology to be useful around the world in solar rich countries.

For all South Africans to have access to affordable and competitive solar power as a source of energy, more efficient and cost-effective small-scale solar-to-electricity technologies are needed. This can be created by optimizing the current forms of solar energy conversion.

One of the means of converting sunlight into a usable from of solar energy is by CSP (Concentrated Solar Power). This method is used if the energy need is electricity and not specifically heat and it is also the more favourable method to store energy for later use rather than immediate use when converted. CSP generates solar power by using reflective materials to concentrate sunlight onto a receiver; this transfers heat to the receiver which then drives a heat engine to provide useful products such as electricity and heated water. There are four main components in CSP:

- Collector / concentrator
- Receiver
- Transporter / storage
- Power conversion

By optimizing all or any one of these components, the overall capability and performance of a CSP system can be enhanced and developed into a more affordable, reliable and accessible system that provides energy in the required form.

1.2 PROBLEM STATEMENT

Solar energy is a renewable energy source and is abundantly available in many areas in South Africa, thus, a means to harvest this energy and use it productively will be a step in the right direction. This will minimise the use of non-renewable energy sources and reduce pollution to ensure the continual existence of a healthy environment.

There are many Concentrated Solar Power (CSP) plants that use line-concentration systems such as parabolic trough and linear Fresnel systems. The receivers of these plants pose the following design challenges. They should capture most of the solar energy entering through their aperture and then transfer this energy to a heat transfer fluid whilst limiting losses. The losses include reflection losses, thermal re-radiation losses and convection losses; the latter due to natural and forced convection (due to wind). An increase in efficiency of the receiver translates directly to an increase in efficiency of the CSP line concentration trough plant.

This novel receiver design intends to address how to effectively capture solar energy by making use of geometry instead of materials. This work focuses on the research and design of a tubular cavity receiver which effectively captures solar irradiance and converts it to thermal energy for a parabolic trough CSP reflector.

1.3 PURPOSE OF THE STUDY

The purpose of this research is to develop and investigate a novel cavity receiver for a line concentrating solar power system, in this case, a parabolic trough system by investigating its thermal and optical response and performance under different operating and geometric conditions.

In this work, the concept of a cavity receiver will be applied to developing a cavity type receiver for a line concentrating system, in this case, a parabolic trough system. This study serves as an

initial analysis into the viability and performance of the proposed heteroconial tubular cavity receiver.

The flow of energy from input energy to output energy in a thermal CSP system is; solar energy (light) irradiates a reflector, which reflects and concentrates this light onto a receiver, the concentrated light undergoes optical interactions with the receiver such as refraction, reflection and absorption. The absorbed concentrated light undergoes conjugate heat transfer processes via conduction, convection and radiation and is transferred to the flowing heat transfer fluid which outputs useful energy in the form of a hot fluid.

The purpose of this work is to accurately model this flow of energy to effectively develop a high-performance solar thermal tubular cavity receiver for a line-concentrating parabolic trough reflector. The optical and thermal response of the receiver under different operating and design configurations will be analysed. Parameters such as heat flux distribution, optical efficiency and thermal efficiency will be analysed to produce a receiver with mechanisms in place that reduce performance losses.

1.4 DISSERTATION ORGANISATION

This dissertation is presented over 7 chapters excluding the current chapter which serves as the introductory chapter. Each chapter is subdivided into sections for good flow and better understanding.

The dissertation is organised as follows:

- Chapter 2: This chapter is dedicated to the review of relevant literature in the field of solar power and concentrated solar thermal energy systems. The use of solar technology is on the rise in South Africa; hence the amount of available solar energy irradiating South Africa and its most promising solar hot spots are reviewed. The workings of a solar thermal CSP system are discussed as well as the various power cycles that CSP systems can be applied to. This

chapter contains information about previous studies on CSP receivers as well as the heat transfer mechanisms associated with solar thermal receivers including a review on how to reduce performance losses from solar thermal receivers.

- Chapter 3: This chapter presents the theoretical background for numerically modelling a solar thermal receiver including the numerical model applied in this work. The optical and thermal governing Equations are described as well as the boundary conditions applied to the receiver. In addition, a mathematical model is presented which describes Equations used to analyse the optical and thermal performance of the receiver. Lastly, the solar tubular receiver analysed and optimised in this work is presented.

- Chapter 4: This chapter is dedicated to the validation of the numerical model described in Chapter 3. Experimental work which included the experimental analyses of a solar thermal tubular receiver for a parabolic trough reflector for different operating conditions was selected. The numerical model was utilised to model the experimental system for each operating condition and simulated. The results of the numerical model are validated against the results of the experimental work.

- Chapter 5: This chapter leads into the core works carried out in this dissertation. Here, the first investigation which focuses on the optical response of the proposed receiver is conducted. The heat flux distribution on the absorbers is analysed under varying design configurations. In addition, the optical response of the receiver is evaluated at varying design configurations. The receiver's geometry is comprehensively analysed in terms of the benefits it provides to optical performance.

- Chapter 6: Decisions based on the results of Chapter 5 were carried into this chapter in which the second core investigation into the proposed receiver was conducted. This chapter primarily focuses on the thermal performance of the receiver. The effect of varying design

configurations on thermal and total performance of the receiver are investigated as well as the thermal benefits of the geometry of the receiver.

- Chapter 7: This chapter focuses on the optimisation of the receiver. Decisions made in previous chapters were implemented in this chapter. This chapter is dedicated to optimising the total performance of the receiver by focusing on varying the diameter of the absorber tubes of the receiver. Once the optimal receiver is established, its performance under varying operating conditions is compared to that of a commonly used commercial tubular parabolic trough receiver as a means of benchmarking the proposed receiver.

- Chapter 8: This chapter brings the dissertation to an end with the presentation of a comprehensive summary on the work conducted throughout this dissertation in retrospect. Conclusions are drawn from the various sets of results and discussions, after which recommendations for future studies are proposed.

CHAPTER TWO

2 LITERATURE STUDY

2.1 INTRODUCTION

This chapter presents an overview of previous research conducted in the solar thermal energy systems field as well as the importance of the use of solar energy in South Africa. A brief overview of solar radiation and heat transfer theory is provided. The literature study contains information on current CSP (Concentrating Solar Power) technologies used in Africa and South Africa as well as previous works done on CSP receiver technologies.

2.2 SOLAR ENERGY IN SOUTH AFRICA

Solar energy is a renewable energy resource that is abundantly available in many areas within South Africa. South Africa receives approximately 24 GWhr/m^2 per year of solar radiation over its 1.2 million square kilometres of land (Bugaje, 2004).

According to the South African Department of Energy, the 24-hour global solar radiation average per annum is approximately 220 W/m^2 for South Africa compared to the USA, which receives 150 W/m^2 and the UK and Europe which receives about 100 W/m^2. Figure 2.1 shows the annual DNI (Direct Normal Irradiance) map of South Africa (Maleka, et al., 2010).

The country was found to have a potential CSP capacity of 262 GW with 51% of the feasible sites located in the Northern Cape (Meyer & van Niekerk, 2011). The Northern Cape is one of the most irradiated areas in South Africa having an average annual DNI of just below 3000 kWh/m^2 (Meyer, 2011).

Greenpeace conducted a study on the “investment attractiveness” for investment in photovoltaic technology and CSP technology. According to Greenpeace, South Africa ranked seventh for

photovoltaic systems and ranked third for CSP technologies. This suggests that future development of solar energy systems in South Africa is viable (Wild, 2015).

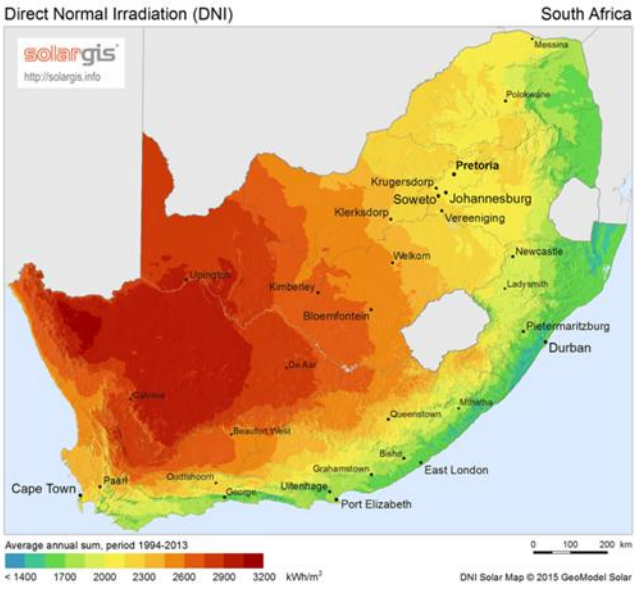

Figure 2.1: Annual DNI map of South Africa (GeoModel SolarGis, 2014)

2.3 SOLAR RADIATION AND IRRADIANCE

The earth receives energy from the sun in the form of solar radiation which is the electromagnetic radiation that is emitted from the surface of the sun. Solar irradiance on the other hand is a measure of the power per unit area produced by the sun.

At the edge of the outer atmosphere of the earth, the total solar irradiance, also called the extra-terrestrial solar irradiance, is occurring at a rate of 1367 W/m^2 and is known as the solar constant (Watt, 1978). A large percentage of irradiance is lost before reaching the surface of the earth as the solar irradiance available at the earth's surface is dependent on the inclination angle of its axis relative to its orbital plane around the sun. However, the largest contributors to the loss of irradiance is its dependency on location as well as climate conditions as the atmosphere and particles in the atmosphere absorbs, scatters and reflects a percentage of the incoming irradiance (William, et al., 2001). Due to these effects, on a very clear day about 70% of the solar constant

reaches the surface of the earth (Watt, 1978). Figure 2.2 shows the losses that occur due to the atmosphere.

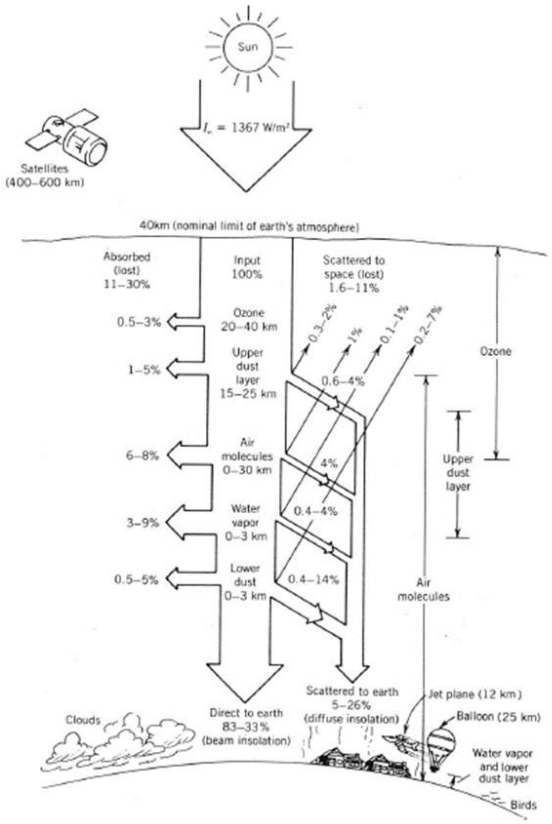

Figure 2.2: Nominal Range of Clear Sky Absorption and Scattering of Incident Solar Energy (Watt, 1978).

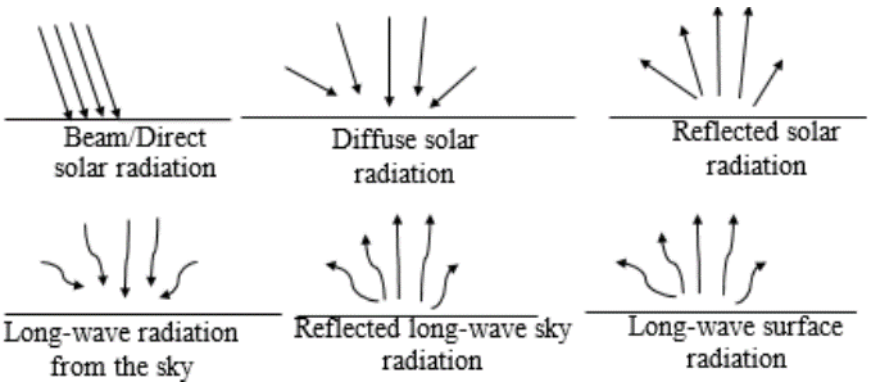

Figure 2.3: Surface Radiation Diagram

On the surface of the earth, there are three types of irradiance that occur. These are known as DNI, diffuse irradiance and reflected irradiance. However, the two main types of irradiance are DNI and diffuse irradiance and combination of these irradiances is known as the Global

Horizontal Irradiance (GHI). Other types of radiation to consider when designing and optimising a solar collector are re-radiation from the solar collector as well as thermal radiation from surrounding bodies and the sky. The total solar irradiance at the surface of the earth is the sum of the direct and diffuse radiation and is given by Equation 2.1 where θ is the normal angle between the sun and the surface.

$$G_{solar} = G_{direct} \cos\theta + G_{diffuse} \quad 2.1$$

Photovoltaic technology makes use of both direct and diffuse irradiance as it works on the photoelectric effect whereas CSP utilises only direct irradiance as the reflected rays are a function of the direct rays falling on the reflector and thus only the effects of DNI are considered in this study.

2.4 POWER CYCLES IN SOLAR POWER PLANTS

A solar power cycle is a device used to convert solar generated thermal energy into mechanical or electrical energy. This section discusses the three most common power cycles used in solar power plants: Rankine, Stirling and Brayton Cycles (William, et al., 2001).

2.4.1 RANKINE CYCLE

80% of the globally produced electricity is by means of a Rankine cycle (Wiser, 2010). There are four stages in a simple Rankine Cycle: compression of working fluid (liquid water) to high pressure via the pump, vaporization of the water via the heat exchanger/steam generator, expansion via the turbine and condensation of the steam back to the initial liquid state via the condenser (Dunham & Iverson, 2014). Water is used as the working fluid. In a DSG (Direct Steam Generation) solar system, the solar receiver acts as the steam generator. In an indirect steam generating solar Rankine Cycle a heat transfer fluid flows through the solar receiver/s in the solar block, gaining thermal energy and then flows through the steam generator, generating high-pressure steam which is used to power the turbine, generating electricity. The spent steam is

then condensed and re-circulated through the power block using a pump and closing the loop. Steam Rankine cycles have been found to offer large thermal efficiencies for temperatures up to 600℃. However, more sophisticated materials are required for the components for temperatures above 600℃. Figure 2.4 shows a schematic of this process.

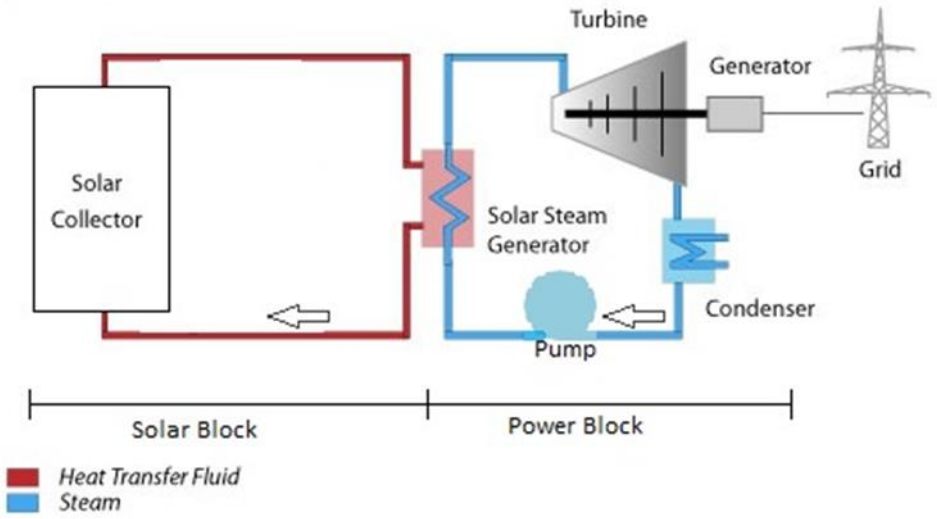

Figure 2.4: Schematic of a Solar Rankine Cycle (Green Rhino Energy, 2016).

2.4.2 BRAYTON CYCLE

Brayton cycles are usually used in point concentration solar systems such as parabolic dish and central tower solar systems. These cycles can be effectively used as a means of generating electricity in a modular solar power set-up by making use of a Brayton micro-turbine. In the case of central tower receivers, the receivers can be either pressurised receivers using the air flowing within the receiver or open receivers which heat the air within the cavity for the cycle.

Brayton cycles applied on a large solar system utilising air as the working fluid are usually open loop in which air is taken from the atmosphere and expelled back into the atmosphere. This is done to prevent reinjection of the warm exhaust air into the cycle. Closed loop Brayton cycles are used when air is not the working fluid, or the system is on a small scale. Closed loop Brayton cycles comprise of four stages: compression, heat addition by the solar collector-receiver system,

expansion through the turbine generating electricity and cooling of the low pressure working fluid to initial temperature required at the compressor inlet (William, et al., 2001).

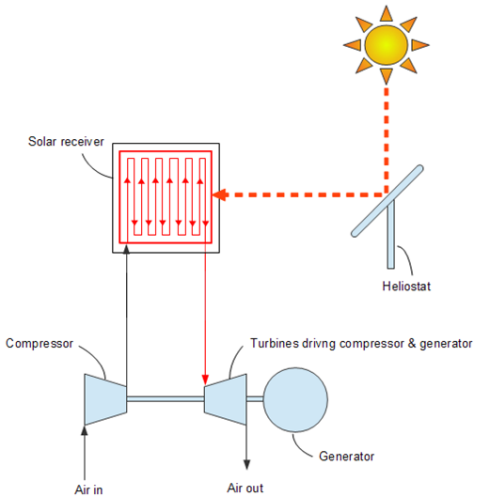

Figure 2.5: Central Tower Receiver Open Solar Air Brayton Cycle (Prometheus Turbine, 2013).

Air Brayton cycles operate at much lower pressure ratios and larger temperatures than Rankine cycles. This is done to keep the Brayton cycle self-sustaining as a Brayton cycle is only self-sustaining for temperatures in excess of 480℃ and requires high temperatures to achieve reasonable efficiencies (Gehring, 2013). Closed Brayton cycles utilising CO_2 as the working fluid were found to have thermal efficiencies over 60% at 30MPa and temperatures exceeding 1000℃ (Dunham & Iverson, 2014). Figure 2.5 shows a schematic of an open Brayton cycle used in a central tower application.

2.4.3 STIRLING ENGINE CYCLE

Stirling engine cycles, like the Brayton cycle, are utilised in point concentration systems, specifically, parabolic dish systems where the engine is mounted together with the receiver at the focal point of the parabolic concentrator which enables power generation by utilising only one dish – however, on a much larger scale.

In a solar Stirling engine, the concentrated solar irradiance is used to heat and expand the working fluid, usually air or hydrogen, which pushes a piston, operating a linear or crank shaft to power an alternator. The working fluid is then cooled by means of a radiator and then fed back into the expansion chamber.

The small size, simple operation and low maintenance need of the Stirling engine makes it an attractive option for stand-alone and distributed solar power generators (Patel, 2006). As a result, most Stirling engines are used in modular parabolic dish systems to generate power. The advantage of a modular approach to solar power generation is mobility and that it can be installed in rural and remote areas to provide a source of electricity to small communities (Kayofa, 2015).

However, due to large costs involved in constructing and installing Stirling engines, Brayton micro-turbines are becoming a more attractive option for the small-scale and modular approach ton solar power generation (Mills, 2004). Figure 2.6 shows a solar Stirling engine parabolic dish system.

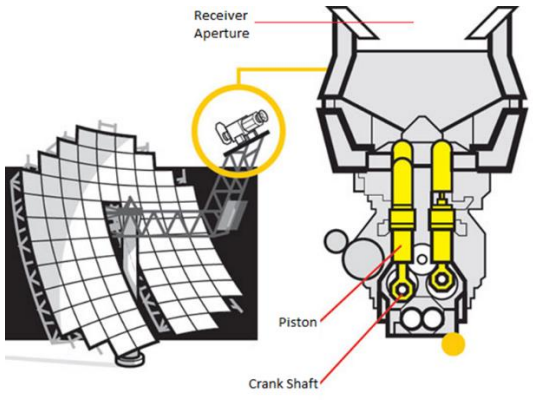

Figure 2.6: Solar Stirling Engine Parabolic Dish System (Piyawat Chalermkanjana, 2008)

2.4.4 COMBINED CYCLES

To increase the efficiency of a power plant, thermodynamic cycles are combined as a means of reducing the amount of wasted energy by using it to operate a second power cycle.

Brayton-Rankine cycles are usually used to increase the efficiency of a power plant. This is accomplished by using the high temperature exhaust gas of the Brayton cycle in a heat exchanger or steam generator in the Rankine cycle to produce high pressure steam to power a secondary turbine, producing electricity (Gehring, 2013).

Another combined cycle makes use of gas turbine. The solar receiver is used to increase the temperature of the flowing air which is then used as the incoming air in a gas turbine. The higher air inlet temperature of the gas turbine increases the efficiency of the power plant (Homann, 2015).

2.5 CONCENTRATED SOLAR POWER SYSTEMS

CSP systems utilise reflective mirrors to concentrate solar radiation onto a receiver in order to generate power. CSP systems are mostly used to transform solar radiation into thermal energy. The receiver contains a heat transfer fluid flowing through it which heats up as it flows through the receiver which is irradiated by the sun. The heated heat transfer fluid is then either used directly to drive a heat engine – in a direct steam system or used in a heat exchanger to vaporise water which in turn drives a heat engine to produce useful products such as electricity and heated water.

CSP systems are usually solar thermal collectors and have mainly four types; parabolic trough, dish, and central tower receiver and linear Fresnel systems. This section provides introductory information on each type or system mentioned.

2.5.1 PARABOLIC TROUGH

Parabolic troughs are made up of large parabolic reflective surfaces or mirrors which are linearly connected and track the movement of the sun throughout the day, using a single-axis tracking system, in order to capture the highest amount of irradiance. This solar irradiance is reflected on the parabolic surface and concentrated on to a receiver which is simply a linear tube located

ideally at the focus point of the parabolic reflector – this type of concentrating technique is known as a line focus system.

The tube is highly absorptive to decrease the amount of reflected radiation and increase the amount absorbed. The tube is encased in an evacuated glass tube to prevent heat loss via convection. The tube contains a flowing heat transfer fluid which is heated by the concentrated solar irradiance and is transferred to the power generation system. Figure 2.7 shows a simple DSG parabolic trough system.

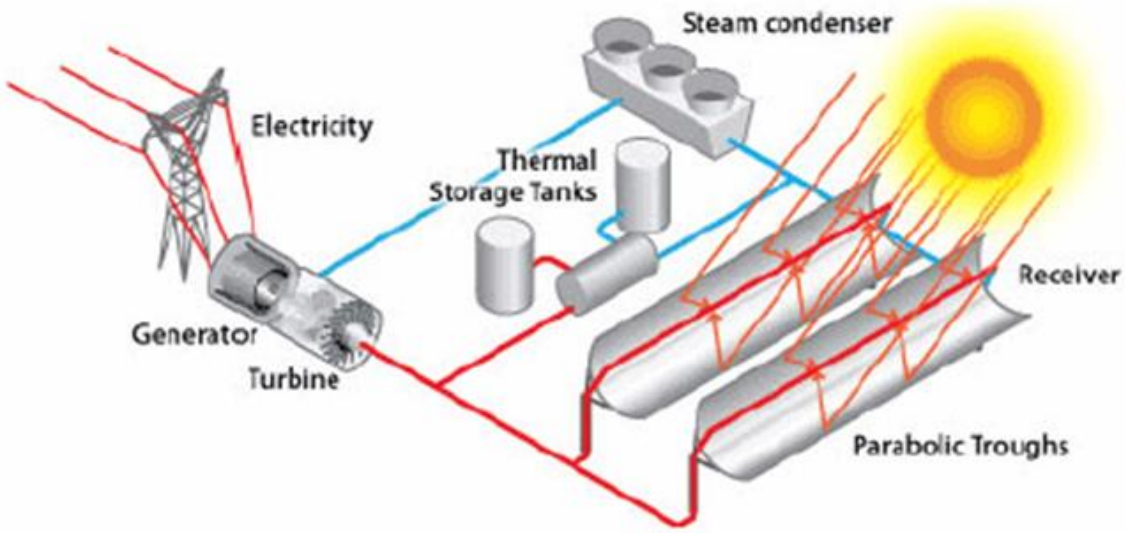

Figure 2.7: Simple Representation of a DSG Parabolic Trough Power Plant (Solar Energy Technologies Office, 2013)

2.5.2 DISH

A parabolic dish consists of mirrors or reflective surfaces that form a dish. This type of solar collector is a point concentration system as the dish reflects the incoming irradiance onto a single receiver located at the focal point of the parabolic dish. Parabolic dish systems comprise of a single solar thermal receiver which converts the concentrated solar irradiance into thermal energy using a circulating heat transfer fluid. In order for the system to work effectively, the optical axis of the receiver must be parallel to the incoming solar rays, thus a two-axis tracking system is utilised.

The receivers used in parabolic dish systems are usually tubular cavity receivers combined with a Stirling engine that converts the thermal energy into electrical energy. For small scale applications, dish type solar collectors are used as solar cookers in rural and domestic environments. Dish systems are widely used for modular electricity generation systems. Figure 2.8 shows a representation of a parabolic dish system.

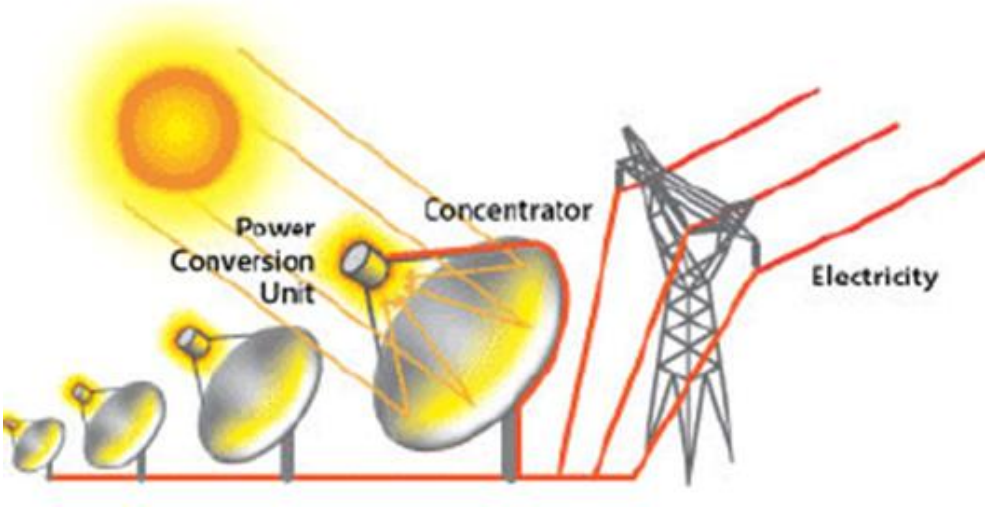

Figure 2.8: Simple Representation of a Parabolic Dish System (Solar Energy Technologies Office, 2013)

2.5.3 LINEAR FRESNEL

Linear Fresnel systems are the most recent addition to CSP technologies. Linear Fresnel collectors utilise many rows of linearly aligned flat reflectors which track the sun to concentrate solar irradiance onto a centralised fixed receiver tube. Most linear Fresnel systems make use of a secondary reflector placed above the receiver as a means of increasing the optical efficiency of the system. An array of linear Fresnel collectors is controlled and positioned in a manner in which a trough shape is mimicked by the many flat reflectors (Feldhoff, 2012b). Linear Fresnel systems are cheaper to construct than parabolic trough systems as flat reflectors are cheaper to manufacture than curved reflectors. Flat mirrors also reduce the wind load acting on the system. These reasons increase the attractiveness of Linear Fresnel systems.

In a study comparing two linear collectors in solar thermal power plants, linear Fresnel collectors were found to have an optical efficiency of 67% while parabolic trough collectors were found to have an optical efficiency of 75%. This resulted in the respective systems of having an overall electric efficiency of 19.25% for the linear Fresnel system and 23.6% for the parabolic trough system (Giostri, et al., 2011). Figure 2.9 shows a DSG linear Fresnel system.

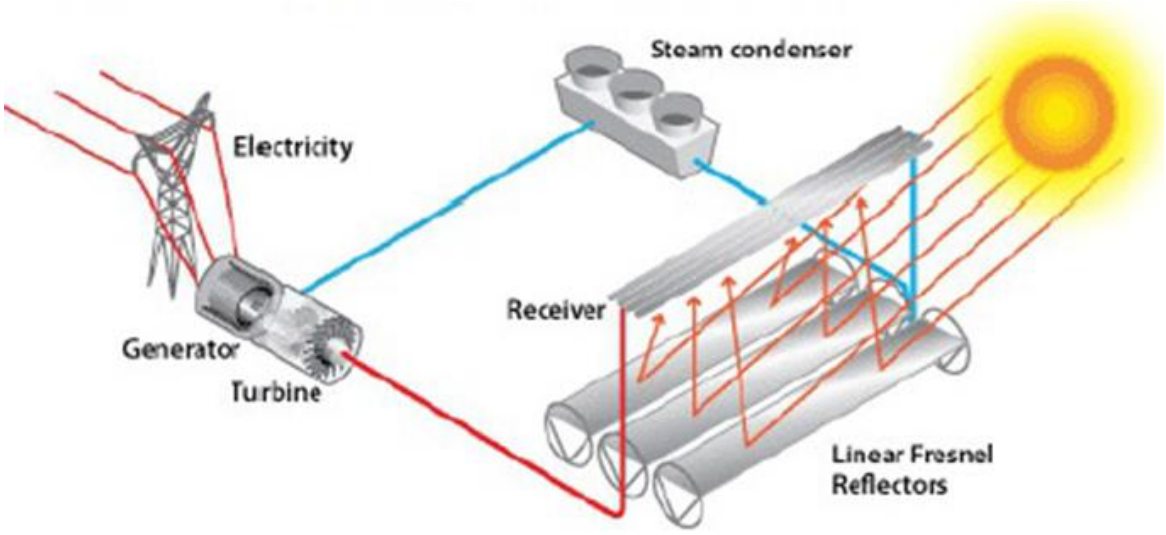

Figure 2.9: Simple Representation of a DSG Linear Fresnel System (Solar Energy Technologies Office, 2013)

2.5.4 CENTRAL TOWER

Central tower solar power systems comprise of three sections: a heliostat field, the solar receiver and the power block. The heliostat field is made up of numerous computer controlled twin-axes sun-tracking flat reflectors which concentrate the incoming solar irradiance onto the central tower receiver. These reflectors are individually controlled in order to ensure that the reflected sunlight is concentrated onto the central receiver. The receiver is located at the top of the central tower. There are three types of receivers, namely tubular cavity, open cavity and volumetric receivers. The receiver absorbs the concentrated solar energy and transforms it into thermal energy by transferring the solar energy to the heat transfer or working fluid. The power block contains the power conversion system similar to that of conventional power plants and other CSP systems,

which is used to transform the thermal energy into electrical energy, usually by means of a steam turbine (Behar, et al., 2013).

Central tower systems (CTS) can be utilised in many power cycles such as Brayton and DSG (Rankine) cycles and in combined systems utilising, but not limited to, molten salt as the heat transfer fluid. The advantages of CTS are that they cope with higher temperatures of up to 1000°C which results in a higher overall efficiency. Open tubular receivers are the most common central tower receivers (Ho, 2013). However, CTS have been found to offer the greatest potential for increasing efficiency and cost reduction by up to 65% (Behar, et al., 2013). According to the U.S. Energy Information Administration, CTS is an attractive option for large scale electricity generation as it only requires a single central receiver which reduces thermal energy losses due to large transport distances such as in linear Fresnel and trough systems. Figure 2.10 shows a simple DSG CTS.

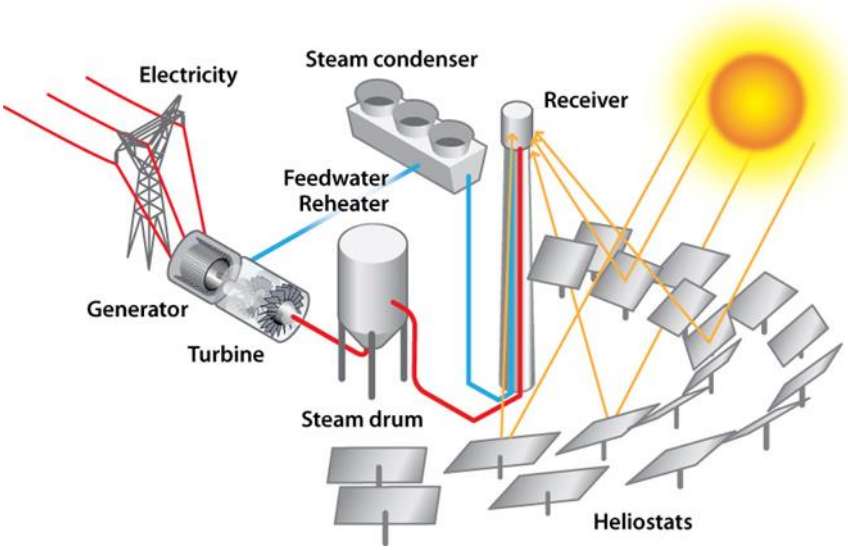

Figure 2.10: Simple DSG Central Tower System (Solar Energy Technologies Office, 2013)

2.6 SOLAR THERMAL RECEIVERS

Solar thermal receivers are devices used to convert solar radiation that is concentrated onto them into thermal energy by making use of a heat transfer fluid. The fluid is used to transport this

thermal energy to the power block of the solar thermal power plant in order to generate electricity. It is important to have a high absorption of radiation and low heat losses.

The receiver must fulfil many geometrical, thermal and optical requirements. The reflected radiation must contact the receiver surface which implies geometric constraints and requirements. The concentrated radiation must be absorbed by the receiver, which implies optical performance considerations. The absorbed radiation must then be converted as completely as possible into thermal energy while limiting losses, which implies thermal performance considerations.

2.6.1 VOLUMETRIC RECEIVERS

2.6.1.1 OPERATING PRINCIPLE

The concentrated solar radiation needs to penetrate the structure and be absorbed by the volume – to allow for this, porous interlocking shapes, knit wire packs or foam made of adequate materials such as metals or ceramics are used as the receiver in the volume. The volumetric receiver material is heated by the solar radiation simultaneously as the heat transfer fluid flows through the receiver and is heated by forced convection, converting the incoming solar radiation into usable thermal energy. The volumetric receivers discussed in this section operate using either gas or transparent heat transfer fluids in order for the volumetric effect to work.

2.6.1.1.1 DIAPR 30-50

The DIAPR 30-50 volumetric receiver utilised a porcupine-like absorber structure within the volume to aid with heat transfer to the working fluid which was separated from the ambient air by a window frustum to minimise re-radiation and reflection losses and allow for high fluid pressures. The type of glass used was a fused silica quartz glass which allowed high transparency and negligible energy losses due to absorbed radiation (Karni, et al., 1997). The receiver was developed by the Weizmann Institute of Science in 1992 and experimental tests showed an

overall efficiency of approximately 70-80% (Avila-Marin, 2011). Figure 2.11 shows a schematic of the DIAPR receiver.

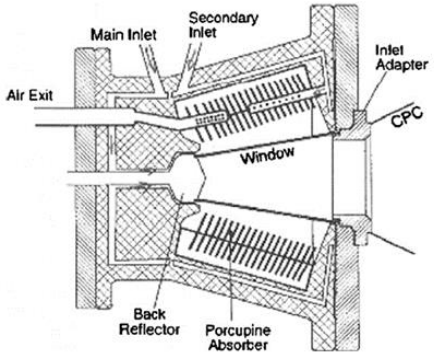

Figure 2.11: Schematic cross-section of the DIAPR (Avila-Marin, 2011).

2.6.1.1.2 REFOS PROJECT

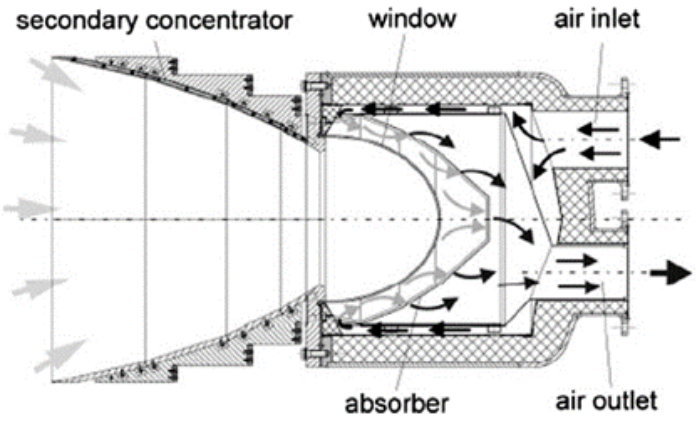

Figure 2.12: REFOS Volumetric Receiver (Avila-Marin, 2011).

The REFOS project began in 1996 and aimed to develop a solar volumetric gas receiver with a minimum efficiency of 80%. The receiver comprised of multiple layers of wire meshes laid upon each other in a semi-dome shape which served as the solar absorber. The receiver was closed off from the ambient air by a dome shaped quartz window. The gas entered the chamber, between the window and mesh absorber, and then passed through the mesh absorber and heated up. This was the main operating principle of the receiver. The receiver consisted of a secondary concentrator which increased the optical efficiency of the receiver by preventing solar leakage. Experimental results showed that the receiver had efficiency in the range of 74.5-86% (Avila-Marin, 2011).

2.6.2 TUBULAR RECEIVERS

Tubular receivers are widely used in solar towers, parabolic troughs, parabolic dish and Fresnel solar power systems as tubular receivers can tolerate higher heat fluxes, low metal temperatures and low pressure drops and allow simple manufacturing while producing high efficiency results.

2.6.2.1 OPERATING PRINCIPLE

The receiver tubes contain a heat transfer fluid, which can be either gas or liquid, flowing through the tubes. The incoming solar radiation is concentrated on the surface of one or more of the receiver's tubes, which have a high absorptivity and thermal conductivity. The heat transfer fluid is heated by forced convection, converting solar irradiation into thermal energy.

2.6.2.1.1 DLR SOLAR TOWER RECEIVER

The DLR designed and manufactured a tubular solar tower receiver with a multi-layered metal tube consisting of copper sandwiched between Inconel material to aid in heat distribution around the circumference of the tube and increase heat transfer to the fluid. Figure 2.13 shows a DLR concept receiver.

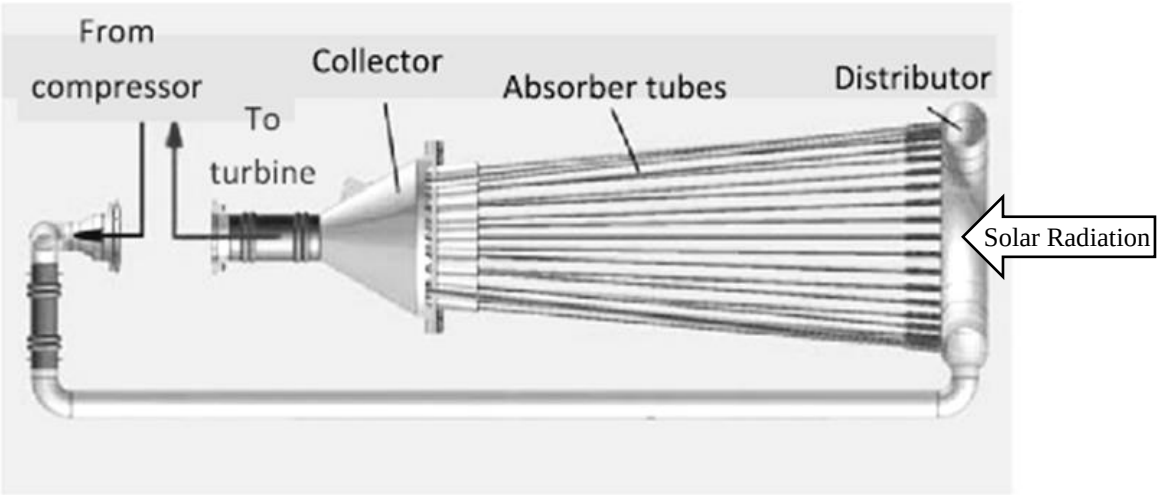

Figure 2.13: Concept of DLR tube air-turbine receiver (Ho & Inverson, 2014).

The receiver was simulated with and without a silica quartz glass window at the aperture, which served to separate the interior air and ambient air as well as reduce heat loss due to natural convection and re-radiation. Simulations of the receiver showed efficiency of 68% without the glass window and 81% with the glass window, showing that natural convection and re-radiation are significant heat loss mechanisms (Ho & Iverson, 2014).

2.6.2.1.2 MODIFIED DISH CAVITY RECEIVER

A study conducted by K.S. Reddy and N. Sendhil Kumar in 2008 investigated the laminar natural convection and surface radiation heat losses for a modified cavity receiver for a dish reflector application with a hemispherical shape as shown in Figure 2.14 (Reddy & Sendhil, 2008). However, since this receiver is a for a dish reflector, it must rotate with the dish to track the sun. Therefore, the receiver has to operate at any orientation.

It was found that the orientation of the receiver influenced the heat loss due to natural convection significantly for orientations less than 45°. Re-radiation losses were greater than convective losses for orientation angles more than 45°. It was also observed that the ratio between the aperture size and the interior surface area significantly impacted the losses due to re-radiation.

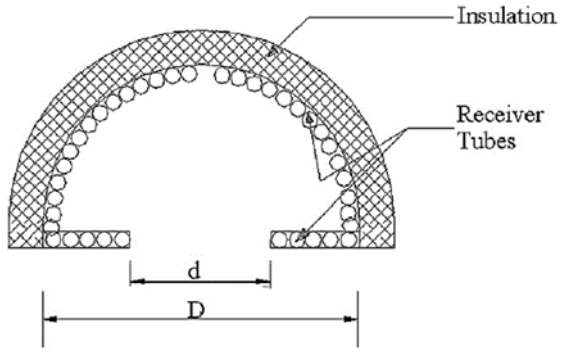

Figure 2.14: Schematic of Modified Hemisphere Cavity Receiver (Reddy & Sendhil, 2008).

A further study was performed which investigated the effect of plate fins placed on the receiver bottom plate as a means of reducing convective heat losses as the angle in inclination increased as

shown in Figure 2.15 (Ngo, et al., 2016). A reduction of a maximum of 20% at a zero-degree inclination was achieved.

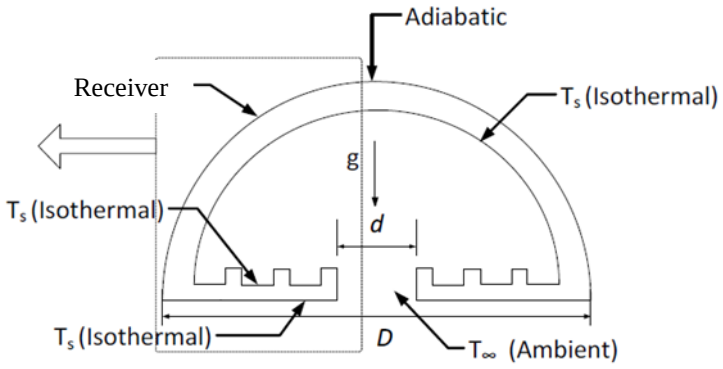

Figure 2.15: Schematic of modified hemisphere cavity with plate fins (Ngo, et al., 2016).

Conical receiver shapes have been shown to be more efficient than any other type of cavity receiver as it undergoes reduced re-radiation, convective and optical losses and has a higher flux generation compared to other cavity types under the same geometric constraints such as position and size (Craig, 2015).

These modified cavity receivers are limited to a parabolic dish system. However, it is the cross-section of the receiver that is focused on here. Aperture size plays a key role in a cavity receiver. The aperture size should be optimised to minimize heat losses and re-radiation losses while allowing solar radiation capture. The higher the ratio between the cavity area and the aperture area, the closer the cavity approaches a blackbody absorber and the smaller the aperture size, the lesser re-radiation losses occur. Ultimately, an optimum aperture size would be a trade-off between maximum radiation capture and minimum radiation losses (Wu, et al., 2010).

2.6.2.1.3 EVACUATED TUBE RECEIVER

Parabolic trough power plants utilising evacuated tube receivers contribute the largest share of installed concentrating solar power technologies (Gunther, et al.).

The vacuum tube consists of two concentric glass tubes. The air in the space between the two glass tubes is evacuated to minimise heat loss via convection from the inner tube, also called the absorber tube. Figure 2.16 shows a typical evacuated tube receiver for a parabolic trough reflector.

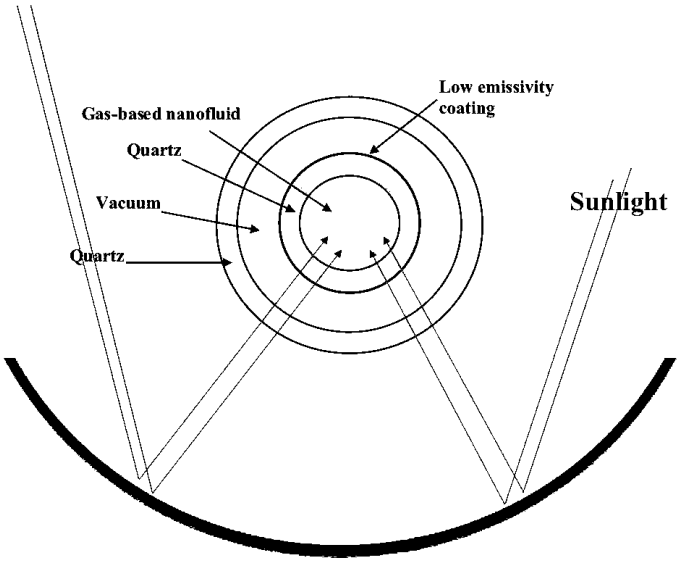

Figure 2.16: Typical Evacuated Tube Parabolic Trough Solar Receiver (Laforgia, 2013)

An experimental study published in 2017 on the thermal properties of a parabolic trough vacuum tube receiver investigated the effect of vacuum pressure and receiver emittance has on heat-loss of the parabolic trough receiver (Yu, et al., 2017). The study showed that radiation heat-loss accounts for approximately 70-90% of the total heat-loss and heat-loss due to convection occupied 10-30% (Yu, et al., 2017).

2.6.2.1.4 MODULAR PYRAMID RECEIVER

A modular pyramid receiver for a solar power tower was proposed in a paper published in 2013. The receiver design was for a molten salt solar central receiver with a heliostat field. The receiver consists of many hexagonal pyramid-shaped elements that are arranged alveolarly with their apexes pointing to the heliostat field (Garbrecht, et al., 2013). Figure 2.17 shows a photograph of the pyramid receiver.

Garbrecht's study investigated the pyramid receiver with regard to its thermal efficiency. The studf found that the receiver produced a thermal efficiency of 91.2% for an incident radiation of 1 MW/m^2. Radiation losses due to reflection were found to be reduced to 1.3% of the incoming radiation and radiation losses due to emission were reduced to 2.8% (Garbrecht, et al., 2013).

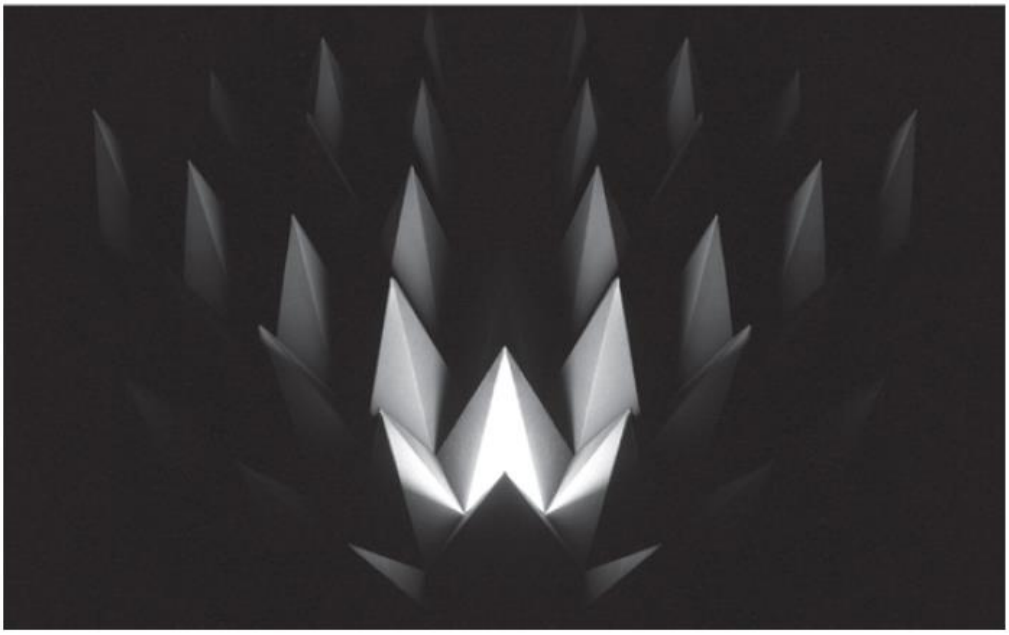

Figure 2.17: Photographic Image of Pyramid Receiver (Garbrecht, et al., 2013)

2.7 HEAT MECHANISMS IN TUBULAR CAVITY RECEIVERS

The tubular cavity will experience heat loss via the three heat transfer mechanisms; however, due to high temperatures experienced by a receiver, re-radiation may become the largest contributor to heat loss.

Heat loss due to convection and re-radiation regarding cavity receivers is minimized due to the design of the cavity. The extent to which heat loss occurs due to convection is greatly reduced due to the occurrence of movement limitations imposed on the fluid within the cavity and thus, the heated fluid within the cavity has a lower chance of escaping the receiver, hence, reducing convective heat loss.

Cavity receivers have a reduced heat loss via radiation due to the design feature regarding the aperture area relative to the absorber/tube surface area as the aperture area is significantly smaller than that of the absorber/tubes. As solar rays enter the cavity through the small aperture, they are reflected multiple times within the cavity resulting in an increase in the absorption of solar radiation and thus reducing the heat loss due to re-radiation as a large portion of the re-radiation is emitted off the surfaces within the cavity, trapping the heat inside the cavity. The efficiency at which this occurs is dependent on the absorptivity and emittance values of the materials of the receiver.

Considering the factors contributing to heat loss in tubular cavity receivers-especially at high temperature, the extent to which each of the heat transfer mechanisms contributes to heat loss is via radiation, convection and conduction in descending order.

In order to reduce heat loss, an understanding of the influential factors on heat loss is required as well as techniques on how to control these factors. Factors such as receiver materials, geometry and orientation are core factors that influence heat loss as well as the heat transfer mechanisms.

Regarding the receiver materials, for maximum radiation absorbance, a material with a low emittance and high absorptivity is required, especially for the tubes. The interior walls of the cavity should consist of a reflective surface to aid in reflecting incoming solar radiation onto the tubes. When introducing a closed cavity, the aperture window should be made of a material with a high transmissibility as well as an inner coating with a low transmissibility; basically, a window which allows rays in, but not out to a certain extent. The outer surface of the cavity should be well insulated or shiny, preferably white or silver as this will decrease the amount of heat emitted by radiation from the cavity walls and reduce the temperature gradient between the inner and outer walls, thus reducing the rate of heat loss through the wall.

The geometry of the receiver plays an important role in absorbing and trapping radiation with the cavity of the receiver. Factors such as aperture size, tube layout, cavity structure and insulation

thickness need to be considered. The tubular layout should be laid out in a manner which allows an even distribution of heat flux/radiation along the length of the pipe. Regarding cavity structure, the purpose of the cavity structure is to vary the heat flux distribution on the inner walls and reduce local hot spots in order to maintain uniformity. The aperture size should be large enough to allow sufficient radiation to enter the cavity as well as small enough as to prevent excess radiation from being reflected out of the cavity.

2.7.1 CONDUCTION

A tubular cavity receiver consists of a cavity, where the tubes are located, and the aperture, where concentrated radiation enters the cavity. In a closed cavity receiver, a glass cover is used to seal cavity and is typically placed at the aperture. Conduction occurs through the cavity walls and the glass aperture. However, the cavity walls are usually well insulated from its surroundings using insulation materials such as foam insulation with low thermal conductivities. This leaves the aperture as the weakest link in the chain of areas of heat loss due to conduction through the glass.

The steady state of heat conduction across a plane wall, the glass aperture in this case, of thickness *L* can be expressed as:

$$\dot{Q}_{cond} = kA_a \frac{\Delta T}{L} \qquad 2.2$$

where ΔT is the temperature change across the wall and the direction of heat transfer from the high temperature side to the low temperature side.

Equation 2.2 shows that heat transfer can be minimised by maximising the thickness of the wall or by minimising the area of the wall surface for a specific thermal conductivity. In the case of a CSP tubular cavity receiver, it is impractical to maximise the thickness of the glass aperture as this will lead to significant amounts of refraction and absorption of the incoming concentrated

solar radiation leaving us with only the aperture surface area to minimise. By reducing the surface area of the aperture, heat loss due to conduction can be reduced.

2.7.2 CONVECTION

Convection and conduction are similar as both heat transfer mechanisms require the presence of a medium. However, they are different in that convection requires the presence of a fluid medium and fluid motion. Heat transfer is enhanced by this fluid motion due to the flowing of warmer and colder volumes of fluid coming into contact with a surface. Therefore, the rate of heat transfer through a fluid is larger by convection than it is by conduction (Cengel & Ghajar, 2011).

The rate of heat transfer due to convection is expressed by:

$$\dot{Q}_{conv} = hA_a(T_s - T_\infty) \tag{2.3}$$

The heat transfer coefficient *h* depends on several factors such as the type of convection; natural or forced, as well as fluid properties and whether the fluid flow is laminar or turbulent. In the case of a CSP tubular cavity receiver, the outside fluid is air and the type of convection is usually natural convection or when it is windy, forced convection. Equation 2.3 shows that heat transfer due to convection can also be minimised by minimising the surface area in contact with the outside fluid. Since the cavity walls of the receiver are heavily insulated, this leaves the aperture as the primary source of heat loss due to convection – hence, by reducing the surface area of the glass aperture, heat loss due to convection can be reduced.

2.7.3 RADIATION

Heat transfer via radiation differs from conduction and convection in that heat can be transferred in the absence of a medium. Regarding a CSP cavity receiver, radiation plays two roles which are the role of a heat gain mechanism and the role of a heat loss mechanism. Radiation plays the role of a heat gain mechanism in that solar radiation is reflected and concentrated onto the receiver

and this energy is then transferred to the heat transfer fluid via conduction through the absorber tubes of the receiver.

Radiation plays the role of a heat loss mechanism in that re-radiation occurs out from the receiver to its surroundings. Equation 2.4 expresses the total solar radiation coming into the CSP system. Since radiation plays both the roles of a heat gain and heat loss mechanism, a net heat transfer rate should be considered.

The net rate of radiation heat transfer to a surface exposed to solar radiation and its surroundings is expressed by:

$$\dot{Q}_{net,rad} = G_{solar} \cdot \eta_{opt} \cdot A_{trough} - \varepsilon A \sigma (T_s^4 - T_{amb}^4) \quad 2.4$$

The first term expresses the amount of radiation absorbed by the cavity tubes or the heat gain term. The incoming solar radiation in W/m^2 is multiplied by the aperture area of the parabolic trough which gives the heat transfer that is entering the trough. This is then multiplied by the optical efficiency, which considers the absorptivity of the tubes as well as geometric conditions of the system, of the receiver which gives the amount of heat transfer being absorbed by the tubes. The second term is the heat loss term which is the amount of energy being lost to the surroundings. The heat loss term shows that heat loss due to radiation can be reduced by reducing the emissivity, radiating surface area and surface temperature of the radiating surface. In the case of a cavity receiver, the cavity walls are well insulated which means the outer walls of the insulation will be close to ambient temperature thus minimal losses would occur.

The greenhouse effect plays a role in radiation losses. The greenhouse effect is when solar radiation irradiates Earth and is absorbed by the ground and heating it up – radiation, in the form of infrared light, is then emitted by the ground towards space. This infrared light is absorbed by molecules in the atmosphere reducing the amount of energy lost due to radiation – resulting in the atmosphere heating up (Litt, 2016). In a parabolic trough receiver, the glass seal or enclosure acts as the atmosphere, reducing the amount of re-radiation which limits radiation losses.

2.8 PARABOLIC TROUGH GEOMETRY

The geometry of the parabolic trough collector has a significant influence on the performance of the entire CSP system. The optical efficiency of the system is significantly influenced by the accuracy with which the parabolic collector is manufactured. Figure 2.18 shows a cross-section of the geometry of parabolic collector. All parabolas have a focal point at which all incoming parallel rays intersect after being reflected from the surface of the parabola. A parabola is defined by Equation 2.5.

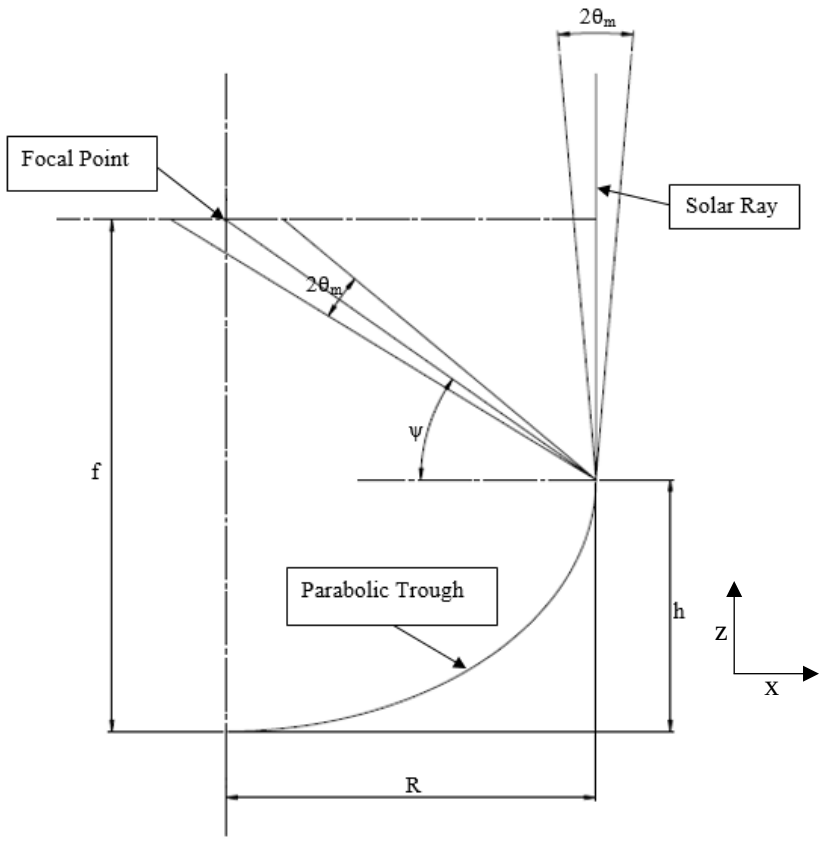

Figure 2.18: Schematic Diagram of a Parabolic Reflector.

$$g(x) = ax^2 \qquad 2.5$$

where

$$a = \frac{1}{4f} \tag{2.6}$$

A combination of Equation 2.5 and Equation 2.6 results in Equation 2.7, which defines the shape of a parabola by its focal length.

$$g(x) = \frac{x^2}{4f} \tag{2.7}$$

A characteristic property of a parabolic reflector is its rim angle (ψ). The rim angle of a solar parabolic concentrator is the angle between the axis of the parabola and the line connecting the parabola edge to its focal point.

The height of a parabolic reflector can be determined by substituting *R* into Equation 2.7. The rim angle of a parabola with a given width *R* and focal length *f* can be calculated using Equation 2.8.

$$\psi = tan^{-1}\left(\frac{f-h}{R}\right) \tag{2.8}$$

Therefore, the width *R*, focal length *f* and rim angle ψ fully define a parabolic reflector.

In reality, not all incoming rays are normal to the plane of the parabolic reflector. Some rays will be coming in at a certain angle from normal due to the sun having a subtended angle of 9.3 mrad.

2.9 SUN SHAPE AND OPTICAL ERRORS

In an ideal world, sun rays entering the atmosphere and travelling towards the Earth's surface would be collimated. However, in reality, these travelling sun rays are not parallel to one another. Therefore, when modelling these sun rays, referred to as Sun Shape in SolTrace, the effect of this non-parallel nature of the incoming rays must be considered.

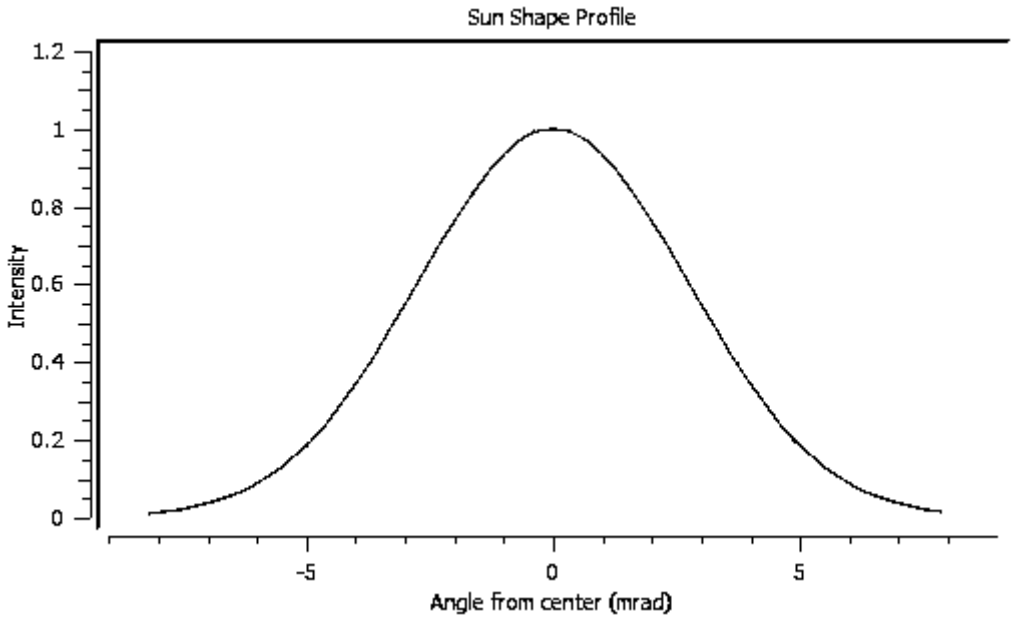

Figure 2.19: Gaussian Sun Shape in SolTrace (Wendelin & Wagner, 2018)

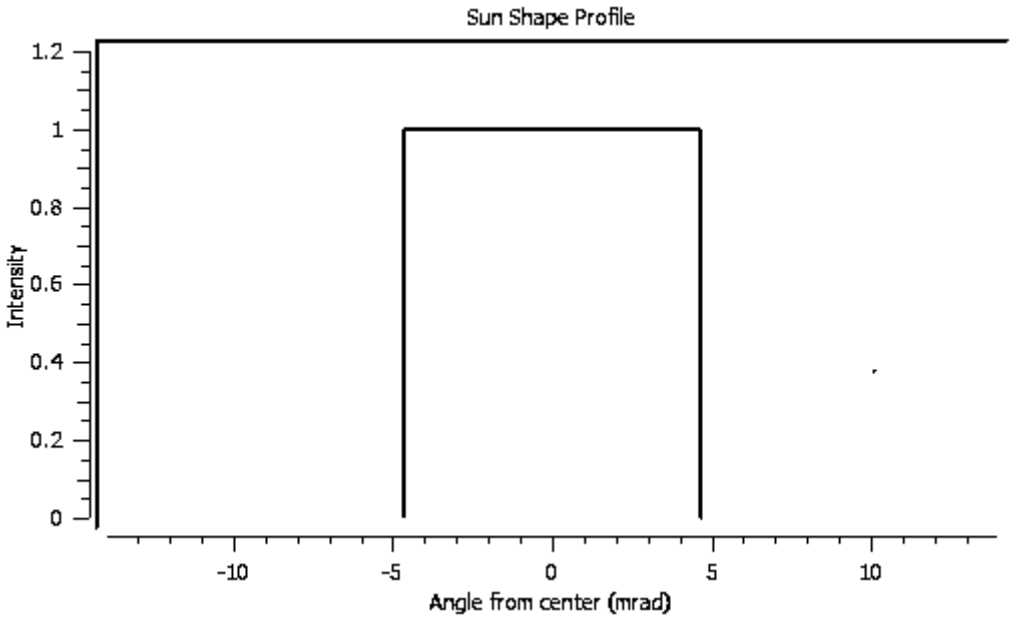

Figure 2.20: Pillbox Sun Shape in SolTrace (Wendelin & Wagner, 2018)

Two common options are available for modelling sun shape in SolTrace developed by NREL (Wendelin & Wagner, 2018). The first is commonly used probabilistic distributions known as the Gaussian sun shape in which the intensity of the incoming rays follows a Gaussian distribution. The second option assumes that all incoming rays are collimated and is referred to as the Pillbox

sun shape (Wendelin & Wagner, 2018). Figure 2.19 and 2.20 show the Gaussian sun shape and pillbox sun shape respectively.

Even though the sun shape is neither truly Gaussian nor pillbox in nature – Gaussian sun shape is not recommended for highly accurate systems unless the system includes large optical errors. Therefore, for most applications and models, the pillbox sun shape is applied (Wendelin & Wagner, 2018).

Surfaces are not exactly smooth. In reality, there are surface slope and surface specularity errors. Surface slope error relates to the unevenness of a reflective surface and surface specularity eeeor relates to the random direction in which a reflected ray would be reflected of a surface (Wendelin & Wagner, 2018). Figure 2.21 and Figure 2.22 show a representation of these errors.

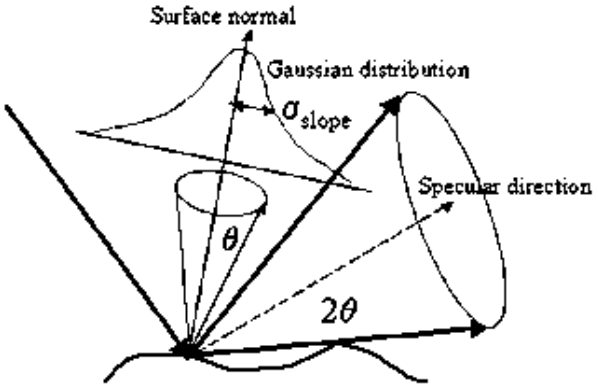

Figure 2.21: Slope Error (Wendelin & Wagner, 2018)

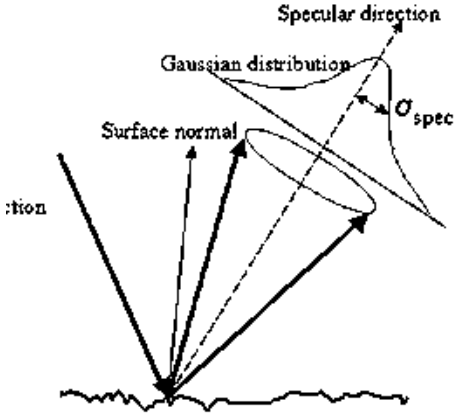

Figure 2.22: Specularity Error (Wendelin & Wagner, 2018)

In this first study, slope and specularity errors are not considered in modelling. However, these should be considered when further or specific research is done on this work.

2.10 SUMMARY

The literature study reviewed the solar resources available in South Africa, the workings of CSP systems, heat transfer modes involved in solar thermal receivers and previous solar thermal

receivers. It was found that South Africa is quite a sunny country and receives an abundant amount of sun light with a high DNI value, which is necessary for CSP systems to output high amounts of energy.

The survey into various tubular receivers showed that the dominant mechanism for heat-loss is due to re-radiation while convections losses come in second. Therefore, the receiver's re-radiative and convective surface area from which most of its losses occur must be minimised in order to minimise heat losses.

Receiver geometry was found to be a strong factor is reducing heat losses. Utilising geometry such that re-radiation is radiated within the receiver showed to be an effective method of reducing radiation losses.

The sun shape was found to be non-parallel in nature. However, literature has suggested that assuming the sun shape is collimated is an acceptable assumption to use when modelling systems without large optical errors such as the system in this work.

This work aims to provide a novel receiver design which utilises geometry to effectively capture solar radiation. As this is a first study into this novel receiver, an idealistic and simplified approach will be maintained in various aspects of the investigation to allow for a well-rounded view of the capabilities and viability of the HTC tubular receiver.

CHAPTER THREE

3 RESEARCH THEORY

3.1 INTRODUCTION

The theory for modelling and analysing the solar thermal receiver as per works carried out in this dissertation is described in this chapter. This chapter starts out with an overview of the numerical method utilised in this work, followed by a description of the modelling procedure applied. Thereafter, the optical model and procedure is presented and described. The governing thermal Equations are presented and discussed, followed by a description of the computational fluid dynamics model as well as the procedure followed. A mathematical model is presented which presents Equations used to analyse the results of the numerical model as well as aid in the design of the novel receiver, including the proposal of a new Equation of predicting the ideal position of a receiver. The chapter is ended by the presentation and description of a novel receiver concept.

3.2 NUMERICAL METHOD

Solar thermal systems convert light (solar irradiation) provided by the sun into heat energy via the use of a heat transfer fluid. Therefore, there is an optical component and a thermal component of the system. As a result, the numerical method utilised in this work is a traditional and commonly used method of modelling CSP systems. The method is to model the solar irradiation by using a ray tracer in which the Monte-Carlo ray tracing method is applied. The resulting absorbed solar irradiation is then applied as a boundary condition in a Computational Fluid Dynamics model to determine the conjugate heat transfer that involves conduction, natural and forced convection and thermal radiation.

The non-uniform solar heat flux acting on an absorber is obtained using the ray tracer which is then applied as a heat source in the CFD model. The solar heat flux is applied as a heat source

using the following procedure, presented in a 2015 paper, using Ansys Fluent (ANSYS, 2012) as the CFD code (Moghimi, et al., 2015):

1. Convert the absorbed irradiation on the absorbers into an interpolation (.ip) file.
2. Define a User-defined scalar (UDS).
3. Interpolate the data to UDS.
4. Copy the UDS to a User-Defined Memory (UDM) using User-Defined Function (UDF).
5. Assign a source term using UDF to patch the load as a volumetric heat source on the absorber.

The benefit of using the aforementioned method is that the optical response and thermal response of the receiver can be analysed separately so as to fully understand the effects of design parameters on the optical and thermal characteristics of a receiver.

3.3 OPTICAL MODEL

The purpose of the optical model is to determine the optical efficiency of a receiver used in a CSP system. A second purpose of utilising a ray-tracing method for the optical model was to generate the heat flux boundary condition acting on the absorber tubes of the receiver as the concentrated heat flux acting on the absorber tubes of the receiver is non-uniform. As a means of tackling this problem, a ray-tracing model of the receiver is used to generate a realistic heat flux acting on the absorber tubes to provide more accurate results.

Monte-Carlo ray-tracing refers to rendering techniques that solve the rendering Equation (Equation 3.1), introduced by James Kajiya in 1986, using Monte-Carlo integration (Kajiya, 1986).

$$I(x,x') = g(x,x')\left[\epsilon(x,x') + \int_S \rho(x,x',x'')I(x',x'')dx''\right] \quad 3.1$$

where:

$I(x,x')$ Is related to the intensity of light passing from point x' to point x

$g(x,x')$ Is a *geometry* term

$\epsilon(x,x')$ Is related to the intensity of the emitted light from point x' to point x

$\rho(x,x',x'')$ Is related to the intensity of the light scattered from x'' to x by a portion of surface at x

The idea of Monte Carlo integration is that we can compute the integral of any function by randomly choosing points in the integration domain and averaging the value of the function at these points. At a high level, in Monte Carlo ray tracing we can use this technique to integrate the amount of light arriving at the camera within a pixel in order to compute the pixel value (Govaerts, 1998).

Using the Monte-Carlo ray tracing method (also simply known as path tracing) offers many advantages. This method is computationally less expensive and provides accurate results.

In this work, SolTrace – a ray-tracing software package developed by the National Renewable Energy Laboratory (NREL) to be used for modelling the optical response and performance of systems of which CSP systems are the most commonly modelled. SolTrace makes use of the Monte-Carlo ray-tracing method. The Monte-Carlo ray-tracing method utilised in SolTrace works by tracing a specified number of rays as they undergo various optical interactions such as refraction and reflection.

The optical model considers the following:

1. Reflectivity, absorptivity and transmissivity of the materials used.

2. Refractive index of any transparent materials used.

3. Specularity and slope errors.
4. Sun Shape
5. DNI

The ray-tracing procedure is as follows:

1. Specify the shape of the sun's distribution of light.
2. Specify the optical properties such as the reflectivity and transmissivity of the surfaces used in the model.
3. Generate the 3-D model of the collector-receiver system using basic geometric shapes. Note that SolTrace does not model the thickness of geometries.
4. Specify the number of rays to be generated and traced.
5. Run the simulation.

One of the objectives of the ray-tracing model is to simulate a realistic pattern in which concentrated light falls upon the absorbers of a receiver as well as allowing the optical response of a receiver to be observed and analysed. This pattern emerges as some areas of a receiver will have high concentrations of final ray intersections and some areas of the receiver will have lower concentrations of final ray intersections. Final ray intersections are the rays that are absorbed by the receiver with given absorptivity. Each ray carries a value known as *power per ray* or *ppr* which is determined by specifying a DNI value and the number of rays to be generated and traced. Hence, by each ray having a value in Watts, the total power, in Watts, acting on the receiver can be determined by simply counting all the final ray intersections and multiplying this value by its *ppr*. To determine how this power is distributed on the receiver means identifying the locations of the high and low concentrations of final ray intersections. In order to accomplish this task, the surface of the receiver must be discretised into surface elements with a specified shape

(e.g. rectangular elements), area and centre point. By computing the number of final ray intersections located within the bounds of each element, it is possible to determine the amount of power acting on each element of the mesh generated on the receiver. This will provide the locations of the areas of different power concentrations located on the receiver, hence providing a realistic power distribution along the surface of the receiver in Watts by simply dividing the total power acting within each element by the area of the element will result in the heat flux, in W/m^2, acting on that element. Repeating this procedure by dividing this elemental heat flux by the thickness of the element will result in an elemental volumetric heat generation rate measured in W/m^3. By applying the same process used to determine the power distribution pattern, a heat flux distribution and volumetric heat distribution pattern can be generated in the form of an interpolation file (Moghimi, et al., 2015).

3.4 COMPUTATIONAL FLUID DYNAMICS MODEL

The purpose of the computational fluid dynamics model (CFD) is to investigate the thermal performance of a CSP thermal receiver utilising a heat transfer fluid. The CFD model allows one to identify areas of heat loss such as heat loss due to re-radiation and convection in order to identify the dominant mechanism of heat loss in the CSP thermal receiver as well identify the areas where majority of heat loss occurs.

The CFD model allows one to simulate a receiver under different operating conditions in order to investigate the influence that different operating and design variables have on the thermal performance of the receiver. Ansys Fluent is a commercial CFD package available and is used in this work to generate CFD models investigated.

The CFD model considers the following:

1. Receiver material properties.

2. Heat transfer fluid properties.

3. Realistic non-uniform heat generation boundary condition.
4. Radiation and Re-radiation to the surroundings and to the sky.
5. Heat loss due to external convection.
6. Heat transfer via conduction.
7. All components of the receiver are included in the CFD model.

These factors are included in the CFD model in order to simulate a receiver in a realistic environment as a means of providing accurate and realistic results.

Once the volumetric heat rate of each element with a known centre point is determined from the data obtained from the optical model; these processed data can be written to and saved as an interpolation file which can be read into Ansys Fluent as a user-defined volumetric energy source which can then be applied as a cell zone condition. This means the volumetric heat generation rate obtained from the optical model can be applied as a volumetric heat source in Ansys Fluent. Each element with a known centre point and respective volumetric heat rate is interpolated onto the mesh of the receiver generated in Ansys Mesher used in the Fluent simulation, resulting in the thermal model of the receiver having a realistic distribution of energy or realistic volumetric heat source.

3.4.1 THE GOVERNING EQUATIONS

Most commercial computational fluid dynamics (CFD) codes use the finite volume method for determining solutions. The finite volume method is a discretization technique which divides the problem domain or geometry domain into control volumes referred to as elements. The governing Equations are applied to each element in the discretised geometry ensuring that the continuity laws are maintained on an element-by-element basis.

The governing conservation laws must always be maintained (Versteeg, 2007). The conservation laws are:

- The mass of a fluid must be conserved – Continuity (aka Conservation of Mass).
- The rate of change of momentum must be equal to the forces acting in on a fluid particle – Conservation of Momentum (aka Second Law of Motion)
- The rate of change of energy must be equal to the sum of heat addition and work done on the system – Conservation of Energy (aka First Law of Thermodynamics)

The governing Equations are derived from these laws which each element must obey. The combination of the continuity, momentum and energy Equations are referred to as the Navier-Stokes Equations and are the basis on which most CFD codes work. Turbulent flow is a type of fluid flow in which the fluid undergoes irregular fluctuations and mixing. Due to this irregular nature, it is difficult to exactly predict turbulent flow (Rajesh Bhaskaran, 2017). A common method of modelling turbulent flow used in CFD code is by decomposing the flow into its time-averaged and fluctuating quantities. Taking the time-average yields the Reynolds-Averaged Navier-Stokes Equations, commonly known as the RANS Equations (Rajesh Bhaskaran, 2017).

This method is used by CFD codes to model turbulent flow. In this study, *u*, *v* and *w* are the velocity components of velocity vector **v** in the *x*-, *y*- and *z*- directions respectively. The RANS Equations for steady, turbulent and three-dimensional flow are:

Continuity Equation:

$$\nabla \cdot (\rho \mathbf{v}) = 0 \qquad 3.2$$

Momentum Equation:

$$\rho(\mathbf{v} \cdot \nabla)\mathbf{v} = -\nabla p + \rho \mathbf{g} - \rho \boldsymbol{u}_i' \boldsymbol{u}_j' \qquad 3.3$$

Energy Equation:

$$\rho C_p \frac{DT}{Dt} = \Phi + k\nabla^2 T \tag{3.4}$$

where;

$$\frac{DT}{Dt} = u\frac{\partial T}{\partial x} + v\frac{\partial T}{\partial y} + w\frac{\partial T}{\partial z} + \frac{\partial T}{\partial t} \tag{3.5}$$

where;

$$\frac{\partial T}{\partial t} = 0; Steady\ flow \tag{3.6}$$

and

$$\Phi = 2\mu\left[\left(\frac{\partial v_x}{\partial x}\right)^2 + \left(\frac{\partial v_y}{\partial y}\right)^2 + \left(\frac{\partial v_z}{\partial z}\right)^2 - \frac{1}{3}(\nabla \cdot \mathbf{v})^2\right] + \mu\left[\frac{\partial v_y}{\partial x} + \frac{\partial v_x}{\partial y}\right]^2 + \mu\left[\frac{\partial v_z}{\partial y} + \frac{\partial v_y}{\partial z}\right]^2 + \mu\left[\frac{\partial v_x}{\partial z} + \frac{\partial v_z}{\partial x}\right]^2 \tag{3.7}$$

The viscous dissipation function is denoted by Φ in Equation 3.4 while T denotes temperature. Furthermore, k refers to the thermal conductivity and C_p is the specific heat capacity at constant pressure. The dynamic viscosity and pressure is denoted by μ and p respectively.

$\rho \boldsymbol{u}_i' \boldsymbol{u}_j'$ refers to the apparent stress which is an unknown that arises when using the RANS method for solving turbulence. There are many turbulent models available in CFD code to solve for the Reynolds Stresses, of which the most widely used is the *k-ε* turbulence model as these models employ the Boussinesq hypothesis and offer a relatively low computation cost (Bakker, 2006). There are three popular types of *k-ε*, these are:

i) The renormalisation group (RNG) *k-ε* model proposed by Yakhot *et al.* (Yakhot, 1992).

ii) The realisable *k-ε* model proposed by Shih. (Shih, 1995).

iii) The standard *k-ε* model by Launder and Spalding (Launder, 1974).

In this first study, the Realisable *k-ε* model was used in this work.

Once the governing Equations and turbulent models were established, the computations were carried out using the commercial CFD package Ansys Fluent. To ensure pressure-velocity coupling, the COUPLED algorithm was used. The momentum, turbulent dissipation, turbulent kinetic energy and energy Equations were solved using the second-order upwind scheme. To account for, radiation was activated and the Discrete Ordinates (DO) model was used and solved using the second order upwind solution method. The outer surfaces of the glass aperture, absorber tubes and insulation were set to radiate at blackbody emissivity. In order to speed up the rate of convergence, the pseudo-transient method was employed.

3.5 MATHEMATICAL MODEL

The mathematical model provides definitions for optical and thermal performance and performance related quantities, useful heat as well as a novel formulation for solving for the optimum position of a solar receiver.

3.5.1 OPTIMUM POSITION

In order to effectively and efficiently design the HTC receiver, it was essential that a method for determining the best position for the receiver to be placed was found. This method eliminated the need for an iterative or lengthy process of determining the optimum position for the receiver at each design configuration.

A mathematical model was developed by Neelesh Maharaj (the researcher) referred to as *Neel's Equation* which relates the size of the aperture to its optimum height such that all concentrated irradiation passes through the aperture exactly. The optimum position (height), with respect to base of the reflector, of a receiver with aperture width, *r*, is given by:

$$\mathcal{N} = \frac{r}{\tan(90^0 - (\Psi \pm \varepsilon))} + f \qquad 3.8$$

The researcher believes that this form of this relationship has not appeared before. Equation 3.8 solves for the z-position such that all reflected irradiation falls exactly on the total surface area of the aperture for a given parabolic reflector of width R and focal length f and specified aperture width r. Figure 3.1 shows a geometric representation of this model where $\mathcal{N}' = \mathcal{N} - f$.

ε is the error term which accounts for the non-collimated nature of sunlight, specularity and slope errors. The sum of these error angles, referenced from the geometric rim angle, is ε. A positive ε decreases the size of the aperture. A negative ε increases the size of the aperture.

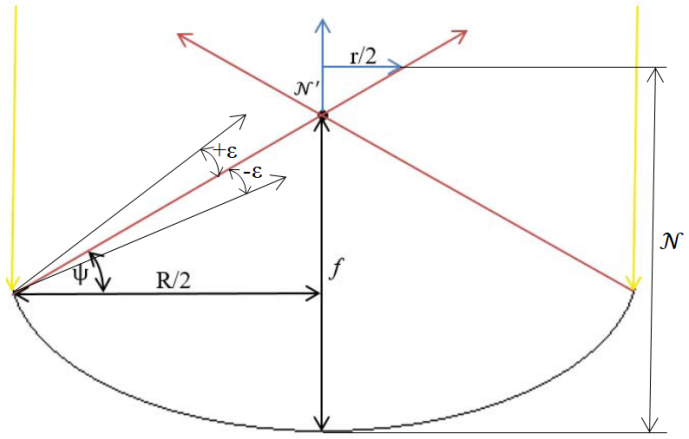

Figure 3.1: Geometric Representation of the Neel's Equation

3.5.2 PERFORMANCE

The performance of the CSP thermal receiver is determined by two non-dimensional properties; these being the receiver's optical efficiency and the receiver's thermal efficiency. The product of these efficiencies is the receiver's overall efficiency which measures its overall performance.

The local optical efficiency or receiver optical efficiency is the ratio of the amount of reflected irradiation absorbed by the receiver's absorbers and the amount of irradiance entering the cavity of the receiver or the amount of irradiance passing through the entrance aperture of the receiver. The overall optical efficiency of the system is the ratio between the total amount of irradiance absorbed by the absorbers of the receiver and the total amount of the irradiance coming into the

system. Equation 3.9 and Equation 3.10 expresses the local optical efficiency and the total optical efficiency respectively.

$$\eta_{opt,r} = \frac{\dot{Q}_{abs}}{\dot{Q}_r} \tag{3.9}$$

$\dot{Q}_{abs}$ and $\dot{Q}_r$ are determined numerically from the optical simulation.

$$\eta_{opt} = \frac{\dot{Q}_{abs}}{I_o \cdot A_{trough}} \tag{3.10}$$

Determining the thermal performance includes determining the external heat transfer coefficient and sky temperature in order to model the receiver accurately and determine accurate results. *O. Garcia-Valladares* and *N. Velazquez* provided Equation 3.11 as a means of determining sky temperature from ambient temperature in their paper investigating the numerical simulation of a parabolic trough solar collector (García-Valladares & Velázquez, 2009). Burkholder and Kutscher propose an accurate expression for determining the heat transfer coefficient due to wind as expressed by Equation 3.12 (Burkholder F, 2009).

$$T_{sky} = 0.0552 T_{amb}^{1.5} \tag{3.11}$$

$$h_w = 4.9 + 4.9 v_w - 0.18 v_w^2 \tag{3.12}$$

The thermal efficiency of the receiver is determined using the inlet temperature, outlet temperature, mass flow rate and the solar irradiance being absorbed by the receiver. The useful heat gain is the heat energy gained by the HTF (heat transfer fluid) during its flow between the inlet and outlet of the receiver. The heat gained by the HTF is expressed by Equation 3.13.

$$\dot{Q}_{htf} = \dot{m} C_p (T_{out} - T_{in}) \tag{3.13}$$

The thermal efficiency of the receiver is defined, in this work, as the ratio of the heat gained by the HTF and the heat absorbed by the absorber tubes, $\dot{Q}_{abs}$, of the receiver which is determined using the optical model.

The thermal efficiency is a measure of the total performance of the system and considers both the optical portion of the performance and the heat transfer capabilities of the system and is given by the the product of the optical and heat-transfer efficiency described by Equation 3.14.

$$\eta_{th} = \frac{\dot{Q}_{htf}}{I_o \cdot A_{trough}} \tag{3.14}$$

The concentration ratio (CR) is defined as the ratio between the width of the cavity aperture *r* and the width of the parabolic reflector *R*. The receiver concentration ratio (RCR) is defined as the ratio between the width of the receiver aperture *a* and the width of the cavity aperture *r*.

3.6 THE HETEROCONICAL TUBULAR CAVITY (HTC) RECEIVER

The HTC receiver consists of an aperture with a width smaller than the width of the inner cavity which allows concentrated irradiation in which is spread inside the cavity and distributed on the absorber tubes. A benefit of having a small aperture is that it reduces the amount of light leaving the receiver cavity which allows the light to bounce around within the cavity and eventually be absorbed. Figure 3.2 show a schematic cross section of the HTC receiver. The width of the entrance aperture of the receiver is denoted by *a* and the width of the cavity aperture is denoted by *r*.

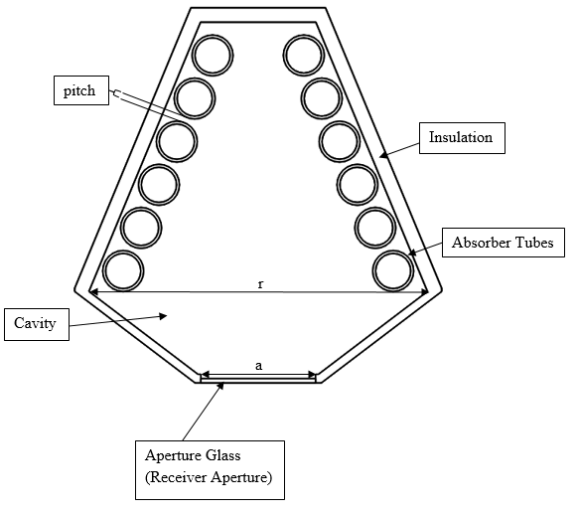

Figure 3.2: Schematic Cross Section of HTC Receiver

3.7 SUMMARY

The numerical model which is composed of the optical model and thermal model was defined in this chapter. The foundation of the optical model is the rendering Equation which was solved by utilising the Monte-Carlo ray tracing method. SolTrace was selected as the software package to generate and simulate the optical model. The thermodynamic model was based on the governing Equations, referred to as the RANS Equations which were laid out including the energy Equation. The thermal model was generated and simulated using the commercial CFD code Ansys Fluent.

A mathematical model was formulated which solved for the ideal position of a receiver with aperture width r for a given parabolic reflector and is defined by Equation 3.8. The Equations used to evaluate the performance of the receiver were defined in this chapter and formed part of the mathematical model.

Lastly, the HTC receiver concept was presented and described. The design of the HTC receiver aims to reduce thermal and optical losses by means of its geometry independently of material considerations.

CHAPTER FOUR

4 VALIDATION STUDY

4.1 INTRODUCTION

This chapter presents the validation of the aforementioned numerical metho as well as the numerical verification of Equation 3.8. To ensure that the numerical model would in fact yield accurate results, the model was validated using previous work. Since the model would have to accurately model the optical as well as the thermal performance of a tubular parabolic trough receiver utilising water as a heat transfer fluid, past work involving all of the aforementioned aspects was chosen to validate the model. The experimental work chosen includes sufficient parameters for this first HTC study (Izweik, et al., 2016). The chapter starts by discussing the previous work, followed by the experimental set-up. Thereafter, the results of the previous work are presented. The numerical model is then discussed and applied to the experimental set-up, followed by the presentation and discussion of the numerical results. To bring the chapter to a close, Equation 3.8 is verified numerically using SolTrace, followed by a discussion of the findings.

Since the SolTrace data is interpolated onto each tube of the HTC receiver, the aim of this study is to determine if the interpolation method employed in this work is a valid method of generating a heat source boundary condition on the tubes of the HTC receiver. Therefore, in this first HTC study, a simple parabolic trough tubular receiver is selected to be validated against as it is assumed that if the computational method accurately models a single tubular receiver, it would be able to model a receiver consisting of multiple independent tubes.

4.2 MESH INDEPENDENCE TEST

A mesh independence test was performed for several mesh refinements to ensure the accuracy of the numerical results. The convergence criterion for the outlet heat transfer fluid temperature as the monitored quantity was:

$$\gamma = \left| \frac{(T_{out})_i - (T_{out})_{i-1}}{(T_{out})_i} \right| \ll 0.01 \qquad 4.1$$

where *i* is the mesh index. As *i* was increased, the mesh was more refined. The *i-1* mesh was determined as a converged mesh when the criterion (4.1) was satisfied.

Table 1 shows the results of the mesh independence test performed under the conditions of validation experiment 3. Very coarse, coarse, medium and fine computational cell densities of 67436, 89487, 165771 and 299676 respectively were used for the mesh independence test. The results show that each cell density does meet the convergence criterion. The results show that an almost identical result was predicted when 165771 cells were used. Therefore, an increase in cell density above 165771 has a negligible effect on the results.

Table 4.1: Mesh Independence Test – Experiment 3 Conditions

Nodes	**Cells**	$\mathbf{T_{out}}$	$\boldsymbol{\gamma = \left\| \frac{(T_{out})_i - (T_{out})_{i-1}}{(T_{out})_i} \right\|}$
101195	67436	325.24	-
132084	89487	324.31	0.002868
212820	165771	324.62	0.000955
364504	299676	325.38	0.002336

4.3 EXPERIMENTAL STUDY

The developed numerical method was thoroughly validated against experimental results from the Sabratha Engineering College at the Sabratha University for overall efficiency which validates

the optical method of analysis as well as the thermal method of analysis. The experimental study tested a parabolic trough collector for process heat applications (Izweik, et al., 2016). The research involved the design, construction and testing of a parabolic trough collector constructed using available local materials and experimentally investigated under the local climate conditions of Sabratha City located in Libya. The heat transfer fluid chosen by the researchers was water. The research paper showed that small scale parabolic trough collectors have the potential to meet the increasing demand for water heating systems.

4.4 EXPERIMENTAL SET-UP

The parabolic trough collector consisted of a parabolic trough reflector and absorber tube set-up. The absorber tube was placed at the focal point of the parabolic trough and was coated in heat resistant black paint. As seen in Figure 4.1, the experimental reflector was a parabolic trough and has a width of 1m, a length of 4.8m and a focal length of 0.5m. The surface of the reflector was aluminium foil with a reflectivity of 0.85. The absorber tube was made of mild steel and coated in heat resistant black paint with an absorptivity of 0.83; had an outer diameter of 0.021m and an inner diameter of 0.017m. The centre of the absorber tube with a length of 4.8m was placed at the focal point of the reflector.

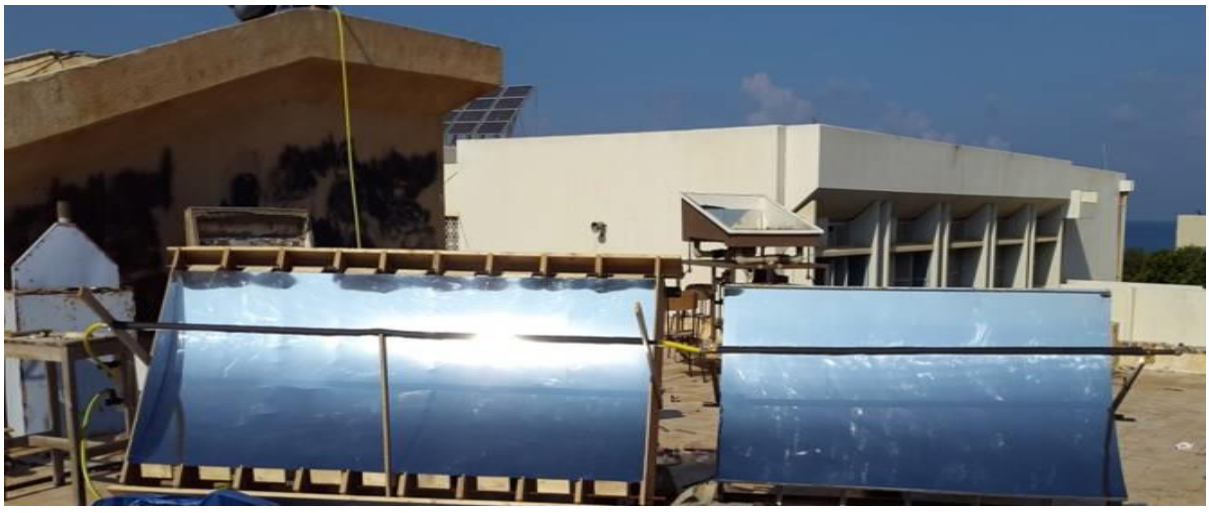

Figure 4.1: Experimental Set-Up (Izweik, et al., 2016)

The trough was manually controlled in order to track the sun and is assumed to be perpendicular to the incoming solar radiation at every data collection point.

Table 4.2 tabulates the specifications of the measuring devices used during the experiment.

Table 4.2: Measuring Instrument Specifications (Izweik, et al., 2016)

Device	Type	Fluid	Operating range	Accuracy
Thermometer	Tastotherm MP2000	Water	Temperature: (-200–1300) ^{0}C	± 2 ^{0}C
Anemometer	GM8901-2-#7183	Air	Temperature: (0– 45)^{0}C Velocity : (0 –45) m/s	± 2^{0}C ± 3 %
Flowmeter	MPB	Water	Flow rate : (0 –50) g/s	± 2 %
Pyrheliometer	METEON CMP6	Solar radiation	Irradiance: (0 – 2000) w/m^2	16.34x10^{-6} v/w/m^2

Water was pumped through the system and the inlet; ambient and outlet temperatures were measured at every data collection point.

Five experiments were conducted. Each experiment had different operating conditions which are listed in Appendix A, along with the results of the experiments. The average wind speed was 1.1m/s. This value will be used to determine the convection heat transfer coefficient.

4.5 EXPERIMENTAL RESULTS

The following section contains results obtained experimentally which would then be compared to the numerical results.

A comprehensive discussion of the results will follow to explain any discrepancies between the experimental and numerical results.

The experimental study presents the efficiency of the system for each experiment. The experimental study only included the thermal efficiency of the system. Therefore, the thermal efficiencies of the numerical and experimental results are compared.

Results

Figure 4.2 graphs the thermal efficiency of each experiment. The thermal efficiency was 53% and the minimum thermal efficiency was 40%. The results and operating conditions of the experiments are listed in Appendix A.

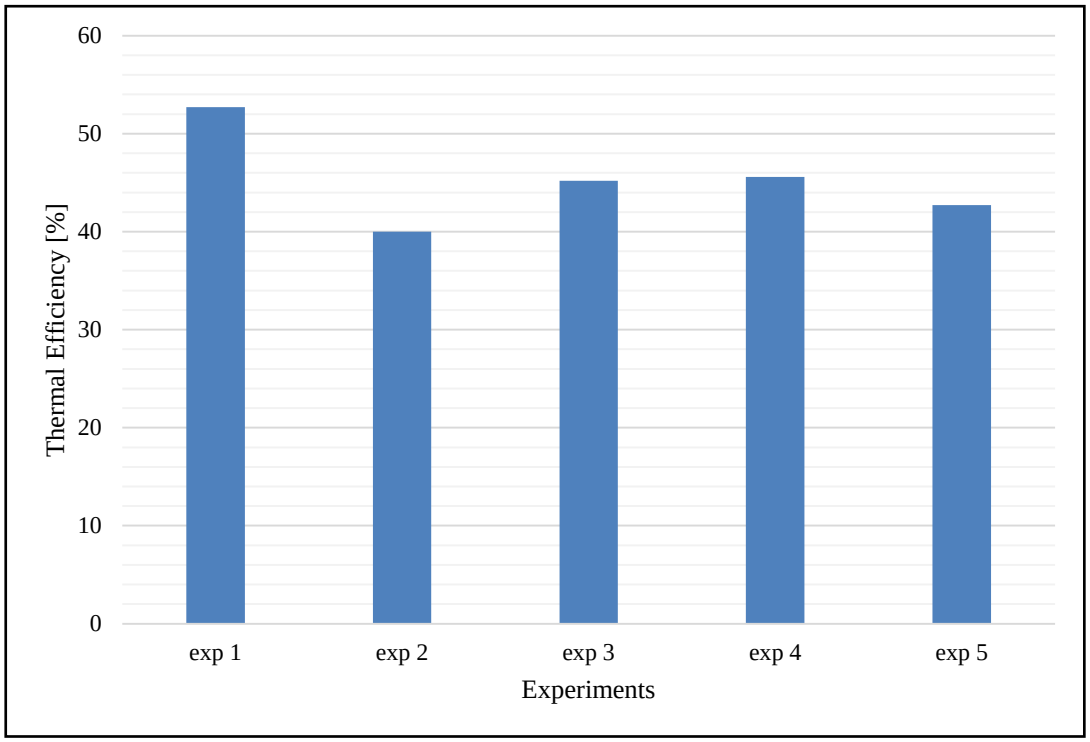

Figure 4.2: Experiment Results

4.6 NUMERICAL MODEL

The numerical model of the experimental set-up follows the method proposed in Chapter 3 utilising the combination of SolTrace and Ansys Fluent to accurately model a CSP thermal system.

4.6.1 OPTICAL MODEL

The optical model made use of SolTrace as the ray-tracing software. The parabolic trough collector was generated in SolTrace with the same geometric and reflective properties used

during the experimental study. The absorber tube was modelled using the same absorptivity and geometric properties used during the experimental investigation as well.

To reduce the computational load and simplify the problem at hand, the following optical assumptions were made:

1. Constant geometric properties.
2. Negligible slope and specularity error.
3. Constant material optical properties.
4. Constant DNI (per simulation).
5. The sun is positioned at noon. Rays are normal to the plane of the reflector.
6. Specularity Error (0.0001 mrad).
7. Slope Error (0.01 mrad)

Figure 4.3 shows the SolTrace model of the experimental set-up. Figure 4-4 shows a ray-tracing model of the absorber tube. Since the sun is positioned at noon, it is assumed that the incoming rays are perpendicular to the parabolic trough aperture and the ray-tracing model is modelled with this property to simplify the model of this first HTC study.

Figure 4.3 shows that the absorber tube creates a shadow on the parabolic reflector. Regarding Figure 4.4, it is also observed that the lower half of the absorber tube is irradiated while the top half of the absorber tube is not irradiated by concentrated irradiation. This implies that majority of heat losses will occur from the lower half of the absorber tube.

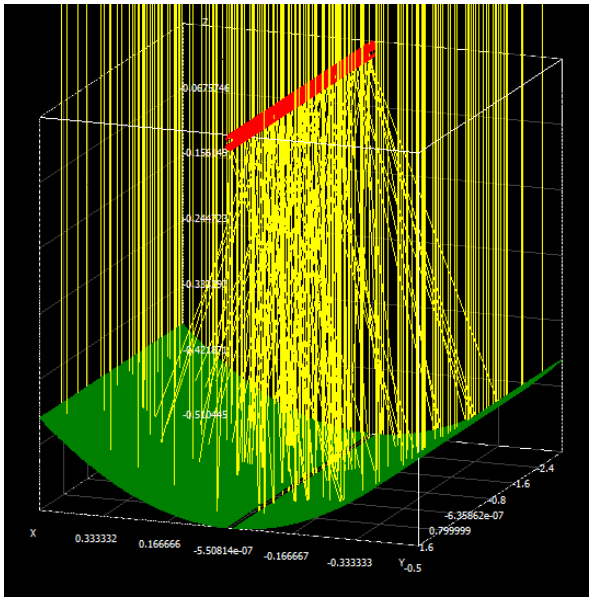

Figure 4.3: SolTrace Simulation of Single Tube Receiver in a Parabolic Trough

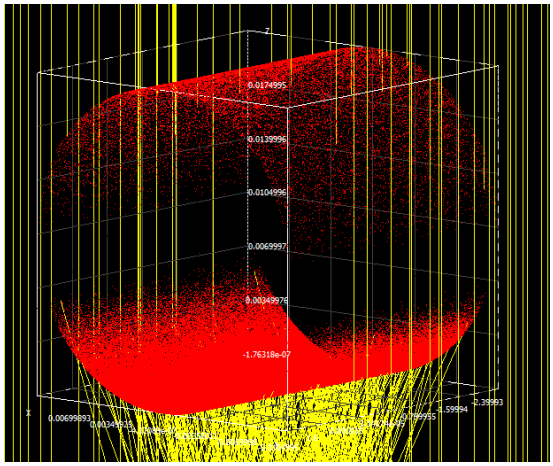

Figure 4.4: Ray-Intersection on Absorber Tube.

The optical model is used to determine the optical efficiency of the system as well as to determine a realistic heat flux distribution acting on the absorber tube to be used to generate a realistic heat flux boundary condition to be used in the CFD model of the system.

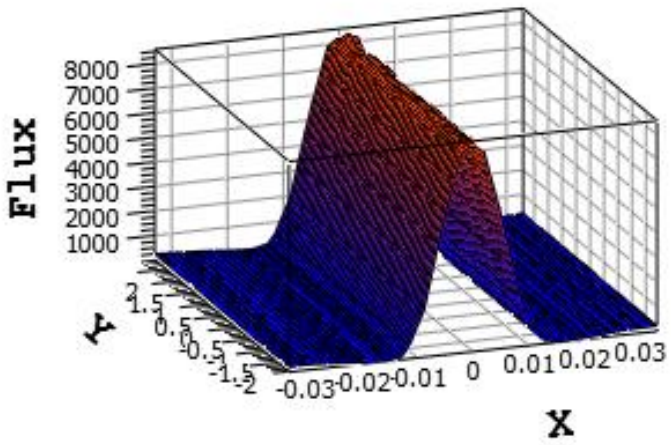

Figure 4.5: 3-D Plot of Flux Intensity of Absorber Tube, DNI = 243 W/m^2

Figure 4.5 shows the heat flux intensity along the surface of the absorber tube for a DNI of 243 W/m^2. Figure 4.5 shows that the bottom half of the tube experiences high concentrated heat flux while the upper half experiences non-concentrated irradiance from the sun.

4.6.2 COMPUTATIONAL FLUID DYNAMICS MODEL

The computation fluid dynamics model was done using Ansys Fluent. The model of the experimental set-up included:

1. A realistic heat generation boundary condition.
2. Materials used in the physical experiment.
3. Heat transfer via conduction.
4. Re-radiation to the sky and surroundings.
5. Heat transfer via convection.

These conditions were included in the CFD model in order to simulate the experiment in a realistic environment similar to that of the physical experimental conditions.

To reduce the computational load and simplify the model, the following assumptions were made:

1. Constant fluid properties.
2. Steady state operating conditions.
3. Constant material properties.
4. Constant boundary conditions.

A convection and radiation mixed boundary condition was set on the outer surface of the absorber tube. The top half of the tube was set to radiate to sky temperature and the bottom half of the absorber tube was set to radiate to the surroundings at ambient temperature. The $k - \varepsilon$ turbulence

model was selected and set to standard properties to solve for the fluid motion of the heat transfer fluid. The COUPLED solution scheme was selected as the solving method. Radiation was enabled, and the Discrete Ordinates method was applied and solved using the second order upwind scheme.

Figure 4.6 and Figure 4.7 show the mesh used for the absorber tube.

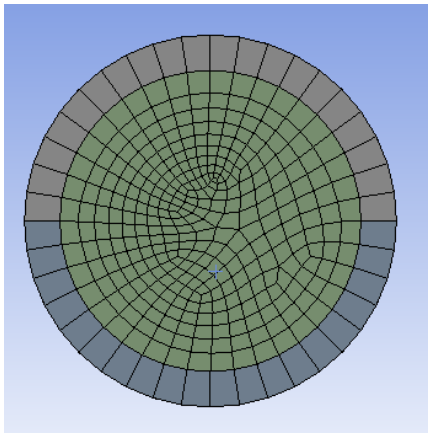

Figure 4.6. Front View of Absorber Tube Mesh.

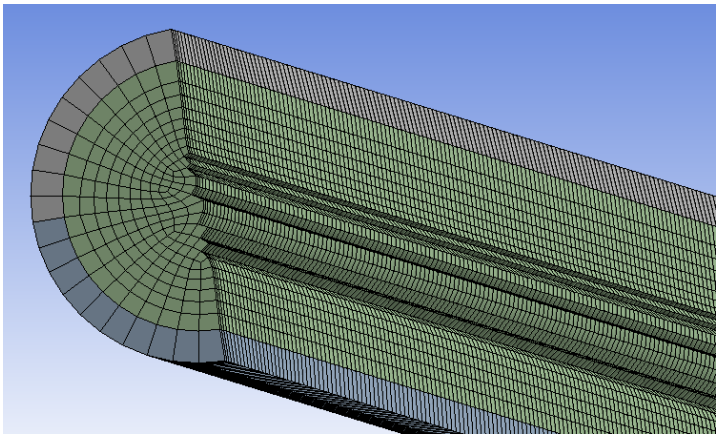

Figure 4.7. Isometric Section View of Absorber Tube Mesh.

A swept mesh was used to mesh the system. An edge sizing method was added to refine the mesh and 40 divisions were selected around the circumference of the absorber tube.

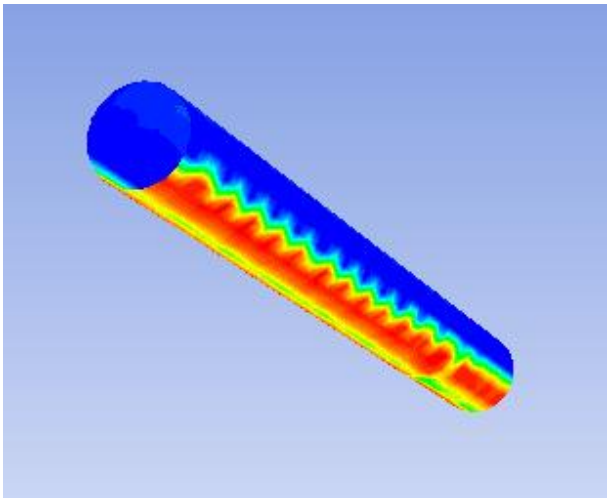

Figure 4.8: Non-uniform Heat Flux on Absorber Tube.

The SolTrace data was converted into a realistic heat generation interpolation file and applied as a user-defined heat generation boundary condition to the absorber tube. Figure 4.8 shows the distribution of solar irradiance on the absorber tube. Appendix A summaries the simulation set-up.

4.7 NUMERICAL RESULTS

This section presents the results obtained from the optical and thermal models of each of the physical experiments conducted. The results of the numerical investigation are listed in Appendix A. Figure 4.9 shows thermal efficiency predicted by the numerical model for each experiment.

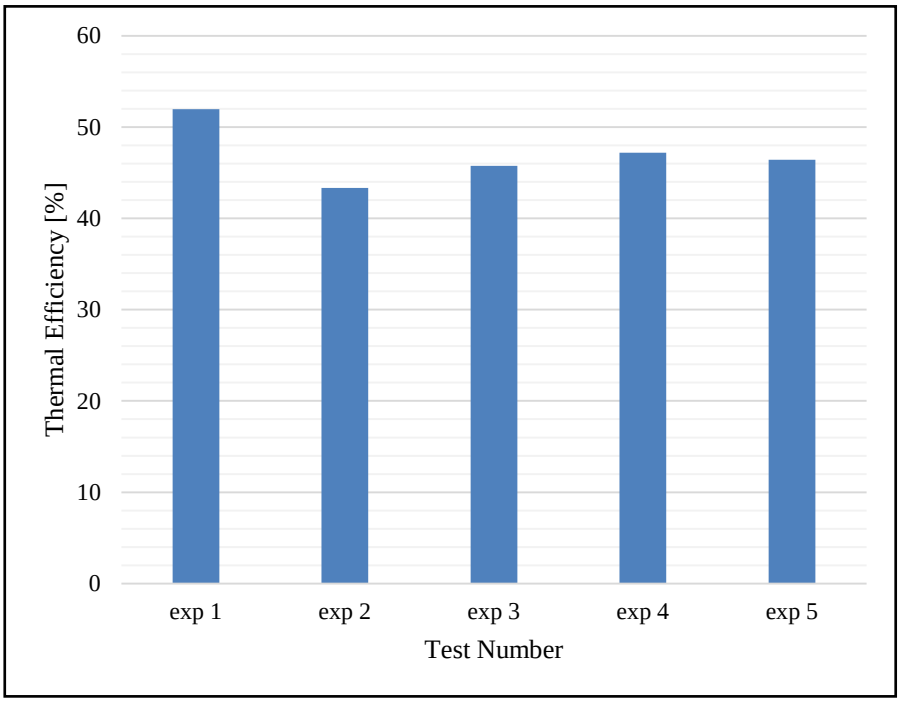

Figure 4.9: Numerical Results

The geometry of the system and the optical properties of the components remain constant, resulting in a constant optical efficiency of which was found to be 60% for this set-up. The maximum numerical thermal efficiency was determined to be 52% and the minimum to be 43%.

4.8 COMPARISON OF RESULTS

This section provides a discussion and comparison between the numerical and experimental results of a simple parabolic trough system with a single absorber tube placed at the focal point of the trough. Appendix A lists the overall efficiency of the experimental system and the numerical system and includes the discrepancies between these results. Optical efficiency is a property characteristic to the receiver geometry and materials; hence it remains constant which is further shown by the numerical results. Figure 4.10 graphs the efficiency of the experimental set-up and the efficiency of the numerical model side by side.

The discrepancy in efficiencies between the experimental and numerical overall efficiencies of the five experiments range between 0.54% and 3.73%, with an average discrepancy of 1.69%. The discrepancies between the numerical and experimental results could be due to inconsistent weather conditions experienced during experimentation, errors inherited from the accuracy of the measuring equipment on the experimentation side and assumptions made for wind speed and sky temperature on the numerical side.

An additional factor that may have led to these discrepancies may be the quality of the experimental set-up such as the quality of the absorber tube, the consistency of the water pump and the consistency of the DNI irradiating the CSP system during measurements.

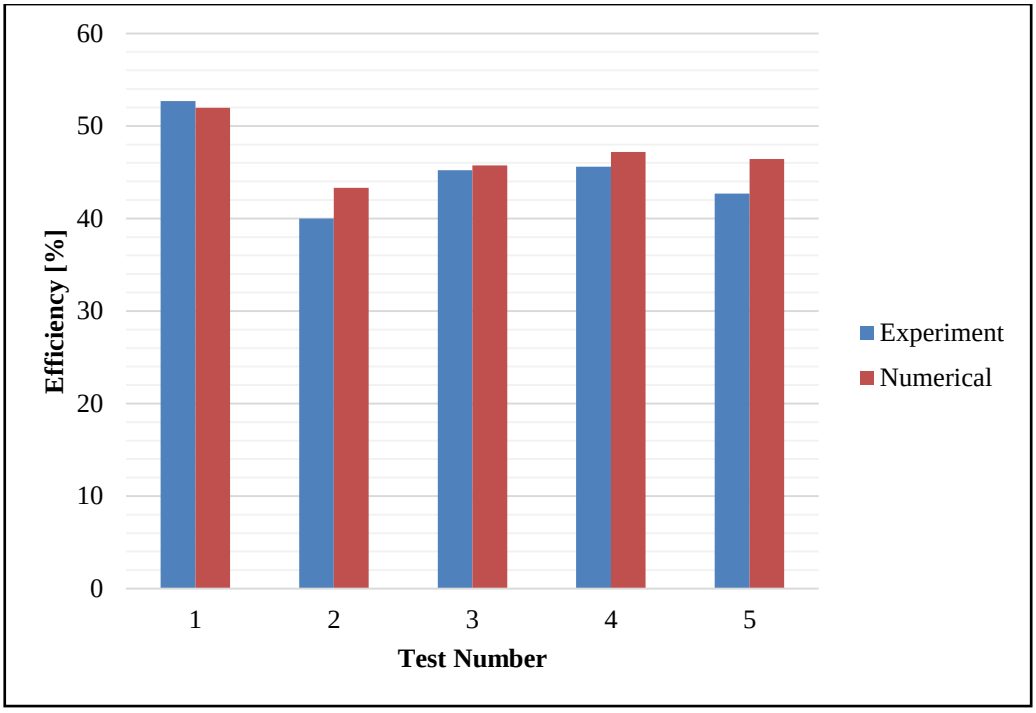

Figure 4.10: Experimental vs Numerical Efficiencies

4.9 VERIFICATION OF IDEAL POSITION EQUATION

SolTrace simulations were conducted to verify that Equation 3.8 effectively and accurately predicts the ideal position for a receiver. For the simulation, a flat plate, treated as an ideal absorber, was positioned above a parabolic trough with a width of 4m and focal length of 1.732m according to its width. Six simulations were conducted with the width of the plate varying from 5cm to 30cm in increments of 5cm. In this first HTC study, 1 000 000 rays were fired. The parabolic reflector was treated as an ideal reflector. Figure 4.11 shows a plot of the error between the number of actual ray intersections and the number of ray intersections predicted by Equation 3.8.

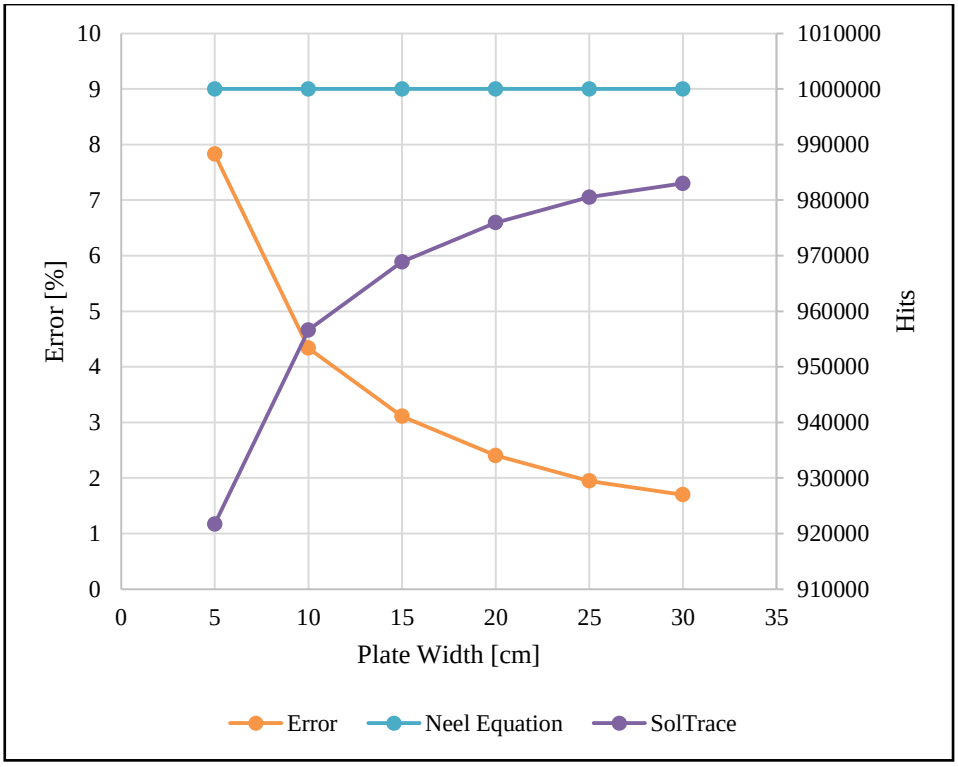

Figure 4.11: Error Plot for the Neel Equation

The theoretical error of applying Neel's Equation (Equation 3.8) is zero in the absence of optical errors. However, there are optical errors, minimum specularity and default slope errors, present in SolTrace resulting in an error between the predicted number of hits and the actual number of hits in SolTrace. The maximum error occurs at the smallest plate width of 5cm with an error of 7.8% while the minimum error occurs at the largest width of 30cm with an error of 1.7%

Figure 4.11 shows that there is an inverse proportionality between the error and the width of the plate, which can be substituted with aperture in this context. The results show that as the width of the plate increases the error decreases. This shows that as the computational accuracy of applying Equation 3.8 increases as the size of the aperture increases.

4.10 DISCUSSION

Although the results of the experiment and numerical model compared well with each other with an average discrepancy of 1.69%, discrepancies were still noticed. These discrepancies could be

attributed to measuring apparatus, numerical errors, specularity errors or limitations of the physical and numerical model. For instance, the thermometer had error of $\pm 2℃$.

There is an agreement between the numerical results of the applying Equation 3.8 and the theoretical predictions made by it. However, there are discrepancies. These discrepancies may be due to the optical errors included in this numerical set-up.

4.11 SUMMARY

Experimental validation of the numerical model was performed. The results showed that the numerical model is conservative, however, there was good agreement found between the experimental and numerical results. Therefore, the numerical model was validated as a model that can be used to accurately model the optical and thermal response of a parabolic trough concentrated solar power system.

Equation 3.8 was applied to a simple scenario and modelled in SolTrace. It was found that the proposed Equation effectively identifies the ideal position of a receiver in a parabolic reflector system under ideal theoretical conditions. However, it was found that there was an error between the theoretical predictions and numerical results due to specularity errors. Therefore, optical errors such as the specularity error must be considered and accounted for in the Equation to accurately position a receiver in a parabolic set-up under real-world conditions,

CHAPTER FIVE

5 OPTICAL INVESTIGATION INTO THE HTC GEOMETRY

5.1 INTRODUCTION

This chapter presents a study into the optical response of the HTC geometry under different geometric conditions as well as the mechanisms at work which affect the optical performance of the receiver design. The chapter starts by laying out the purpose of this study followed by a description of the numerical model which includes the model set-up, assumptions, constraints, analysis tools and a description of the analysis method. Thereafter, the results of the simulations are presented, followed by a comprehensive discussion. To bring the chapter to an end, a summary of the findings is presented.

5.2 PURPOSE OF INVESTIGATION

This study aimed to fulfil the following purposes with regards to the HTC receiver:

1. Identify the effect of cavity geometry on heat flux distribution within the receiver.
2. Identify the effect of cavity geometry on the optical performance of the HTC receiver.
3. Investigate the influence of the addition of the inverted bottom conical structure on heat flux distribution within the receiver and on the optical efficiency of the receiver.

5.3 ANALYSIS TOOLS

Raw data can sometimes be misleading when comparing a set of results for one receiver with given properties to another receiver of different properties as the size and shape of both receivers vary. This issue is overcome by making use of dimensionless properties as a means of levelling the playing field. The heat flux distribution along the cavity walls of the receiver was

investigated; dimensionless heat flux was used to generate the heat flux distribution curve. Since the height of each receiver varies, dimensionless position was used as a comparison parameter.

Figure 5.5 shows a representation of the crude mesh generated for capturing data along the cavity walls of the receiver.

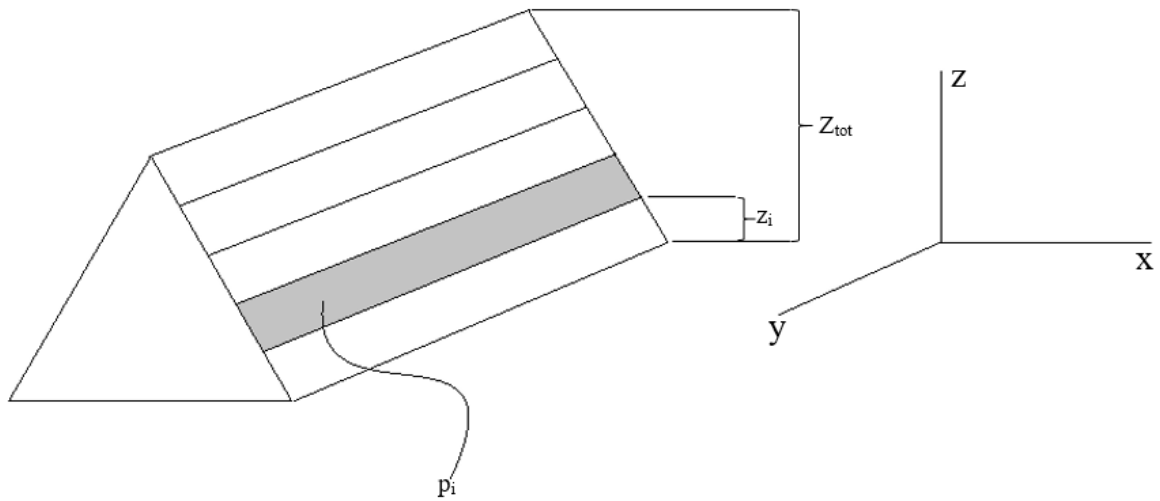

Figure 5.1: Crude Mesh Representation of Upper Cavity Walls.

Equation 5.1 gives the dimensionless heat flux, P_i, acting on an element in position *i* which is the ratio of the heat flux acting on the element, p_i, and the total heat flux acting on the whole surface of the cavity wall, P_{tot}. Equation 5.2 gives the dimensionless position of the element being analysed in a similar manner to that of Equation 5.1.

$$P_i = \frac{p_i}{P_{tot}} \tag{5.1}$$

$$Z_i = \frac{z_i}{Z_{tot}} \tag{5.2}$$

The optical efficiency of the receiver is given by the ratio of the amount of irradiation absorbed by the walls and the total irradiation entering the receiver. Optical efficiency is given by Equation 5.3;

$$\eta_{opt} = \frac{\dot{Q}_{sol,abs}}{\dot{Q}_{sol,tot}} \quad 5.3$$

To better understand and interpret the effect that a change in radii has on power distribution and optical efficiency, each set of geometric conditions was defined by its cone angle, its receiver concentration ratio (RCR) and its concentration ratio (CR). RCR is only applicable to the HTC receiver as the RCR is the ratio between the width of the cavity aperture and the width of the entrance aperture. The concentration ratio applies to both the standard and HTC receiver as it is the ratio between the width of the parabolic trough and the width of the cavity aperture. Note that the ratio between surface area is not used as both the trough and receiver have the same longitudinal length. RCR and CR are given by Equation 5.4 and Equation 5.5 respectively;

$$RCR = \frac{r}{a} \quad 5.4$$

$$CR = \frac{R}{r} \quad 5.5$$

The results are an indication of how well each concept performs as a solar receiver based on optical efficiency. Optical efficiency was chosen as the criterion on which to select a final geometry because the heat transfer rate is directly affected by how much irradiance is acting on the surface area of the tubes.

5.4 METHOD OF INVESTIGATION

The optical efficiency of the HTC cavity geometry was investigated. As mentioned previously, the concentration ratio of the cavity, denoted by CR, was varied along with the shape of the cavity. Once the optical computations were completed for one design configuration, the next design configuration was selected, and a new optical model was generated and simulated. The optical properties used during this investigation are listed in Table 5.1. The geometric properties of the parabolic reflector were kept constant in this work. The parabolic trough was selected to have a width of 4m, a focal length of 1.732m, a rim angle of 60º and a length of 0.5m.

In order to find the optimum design configuration for the given reflector, certain dimensions were assigned the role of design parameters. To vary the concentration ratio, the width of the cavity aperture, denoted by *r*, was selected as a design parameter. The cone angle of the cavity, denoted by θ, was selected as a design parameter which allowed for the shape of the cavity to vary. A minimum and maximum concentration ratio was specified in order to keep the system realistic. The maximum concentration ratio was set to 40 and the minimum set to 10. The maximum and minimum width *r* were set accordingly. This corresponded to a maximum width of 0.4m and a minimum width of 0.1m for a CR of 10 and 40 respectively.

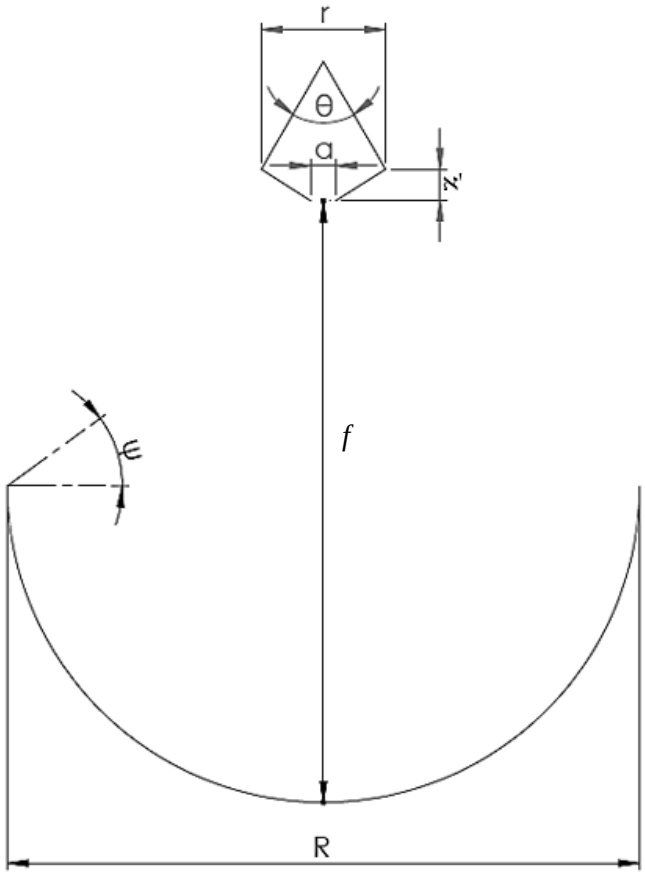

Figure 5.2: Schematic of HTC Receiver with Parabolic Reflector

The minimum cone angle was selected to be 45º and the maximum cone angle was selected to be 90º. Four concentrations ratios were selected and are listed in Appendix B. The cone angle was varied by 1º from 45º-90º. At each concentration ratio, the receiver was simulated for every cone angle. This was done in order to investigate the effect of a varying HTC cavity geometry on the

optical response of the receiver design. Figure 5.1 shows a schematic diagram of the HTC receiver and parabolic reflector.

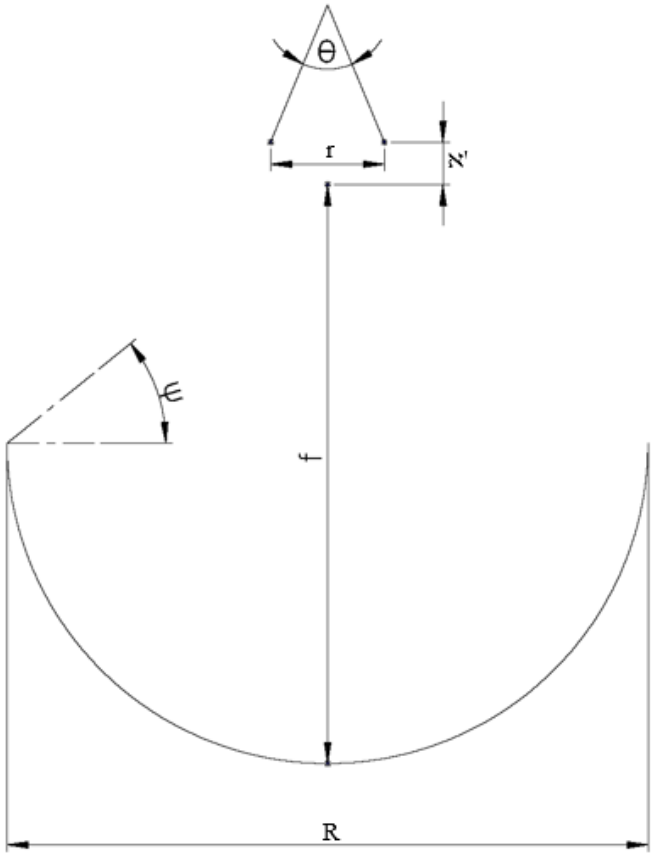

Figure 5.3: Schematic of STC Receiver with Parabolic Reflector

A heat flux distribution plot was generated for the receiver geometry. The geometry of the receiver was discretized into linear elements along their z-axis (vertical height) of equal length. The number of final ray intersections was counted in each element (bin) and plotted against the centre point of each bin in order to generate a heat flux distribution plot for each receiver geometry.

In order to investigate the influence of the bottom inverse cone on heat flux distribution and optical performance, the numerical model and investigation method was applied to a receiver with the same geometric properties as the HTC, excluding the bottom inversed cone. This receiver is referred to as the Single Cone Tubular (STC) receiver. Figure 5.2 shows a schematic of an STC receiver with a parabolic reflector.

5.5 OPTICAL MODEL

In order to determine the optimum cavity geometry for the HTC receiver, various combinations of design parameter specifications were simulated. For a specularity error of 0.0001 mrad (minimum allowed in SolTrace), it was found that an entrance aperture width of 0.04m was sufficiently large to allow all the concentrated irradiation to enter the receiver. The cavity width and cone angle were varied in order to find the optimum combination of both.

In order to model the receiver, certain assumptions were made to simplify the problem at hand.

Assumptions

- Constant DNI (1000 W/m^2).
- Constant optical properties.
- Ideal Reflector (Reflectivity = 1).
- Specularity Error (0.0001 mrad).
- The plane of the reflector was normal to the incoming rays.
- Only the cavity walls were included in this model.
- The Monte-Carlo Ray-Tracing Method was used to model the ray interactions.
- A Pillbox Sun Shape was selected.
- The simulation traced 1 000 000 rays.
- Slope Error (0.01 mrad)
- Refraction through aperture was not considered in this first HTC study.

The ray-tracing model of both the STC geometry and the HTC geometry were simplistic models in that only the cavity walls and glass aperture were generated in the simulation. The parabolic trough was modelled as an ideal reflector as the optical performance of the receiver is the subject of the investigation. Glass was used as the aperture surface and modelled as a transparent flat surface with its respective optical properties. Refraction through the glass aperture was not included in this first study.

The upper cavity walls are modelled as a surface coated in heat resistant black anodized paint similar to that found on modern braai stands with a reflectivity of 0.27 (Alucobond Architecture , 2012). The lower cavity walls' purpose is to reflect back re-reflected radiation and is modelled as a smooth reflective surface similar to that of aluminium foil with a reflectance of 0.93.

The optical properties of the SolTrace model elements are listed in Table 5.1:

Table 5.1: Optical Properties of SolTrace Elements

		Aperture Window	**Upper Cavity Walls**	**Lower Cavity Walls**	**Trough**
Reflectivity	Outer Surface	0.93	0.27	0.93	1
	Inner Surface	0.93	0.27	0.93	1
Transmissivity	Outer Surface	0.91	0	0	0
	Inner Surface	0.91	0	0	0

Figures 5.3 and 5.4 show a SolTrace ray-tracing model for an HTC receiver at a concentration ratio of 40 and cone angle of 45^0.

As a means of reducing computing time, it was assumed that the heat flux acting on the receiver does not vary along its length and only varies along the receiver's height (z-axis). This enabled the discretisation of the receiver into equal sized one-dimensional elements in the z-axis forming

a crude one-dimensional mesh which was used to obtain the heat flux distribution along the height of the receiver.

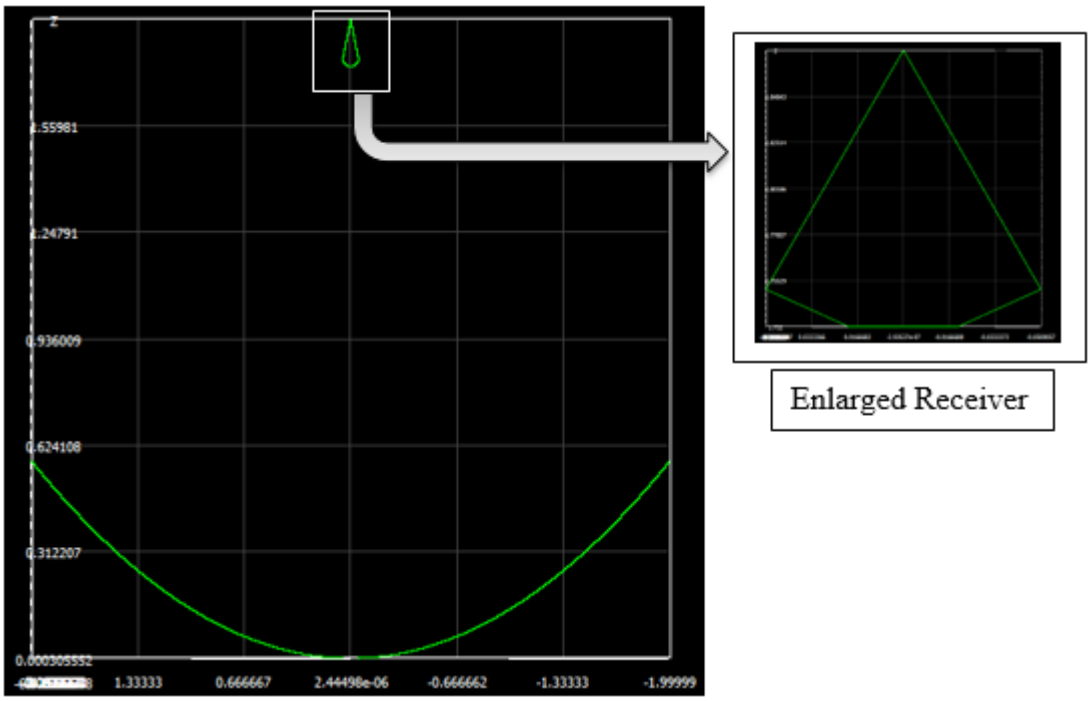

Figure 5.4: SolTrace Model of HTC (CR=40, RCR= 2.5, θ=45^{0})

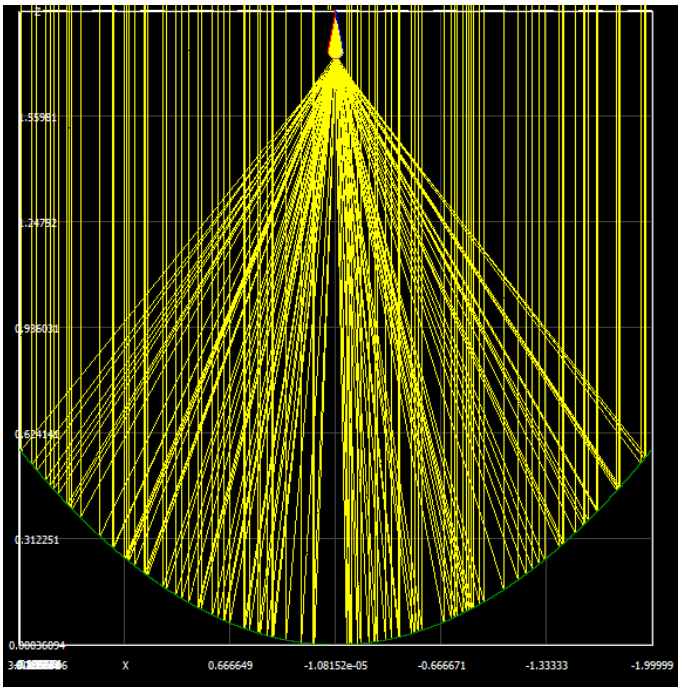

Figure 5.5: Cross-section View of SolTrace Model with Ray Interactions, HTC, CR=40, θ=45^{0}.

5.6 RESULTS

The results of the simulations performed on the STC and HTC receivers are presented in this sub-section.

5.6.1 STC RESULTS

The optical results of an STC geometry were used as a benchmark to compare the HTC receiver results as a means of checking the viability of the HTC concept. Figures 5.6 and 5.7 show a ray-tracing model of an STC. Figure 5.6 shows a model of an STC receiver with glass aperture which includes the ray-interactions and it is observed that the large aperture allows for a larger entrance for radiation to enter the cavity, however at the same time, acts as a large outlet for re-radiation to leave the receiver which can be observed in Figure 5.7.

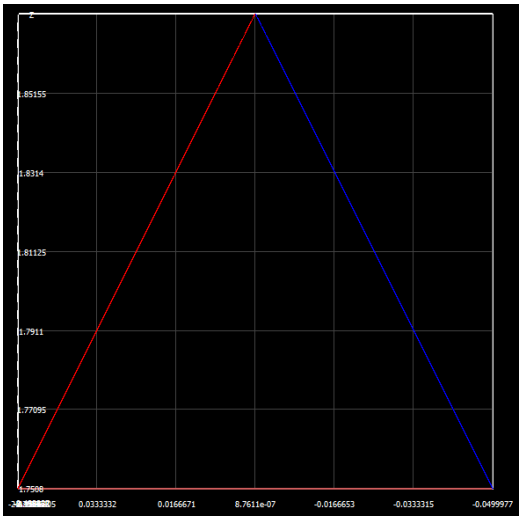

Figure 5.6: SolTrace model of STC Receiver.

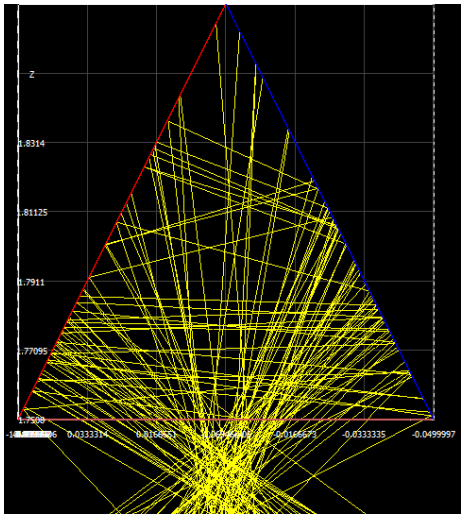

Figure 5.7: SolTrace model of STC showing ray interactions.

Figures 5.8 – 5.11 show the heat flux distribution plots at different cone angles at different concentration ratios for an STC geometry cavity.

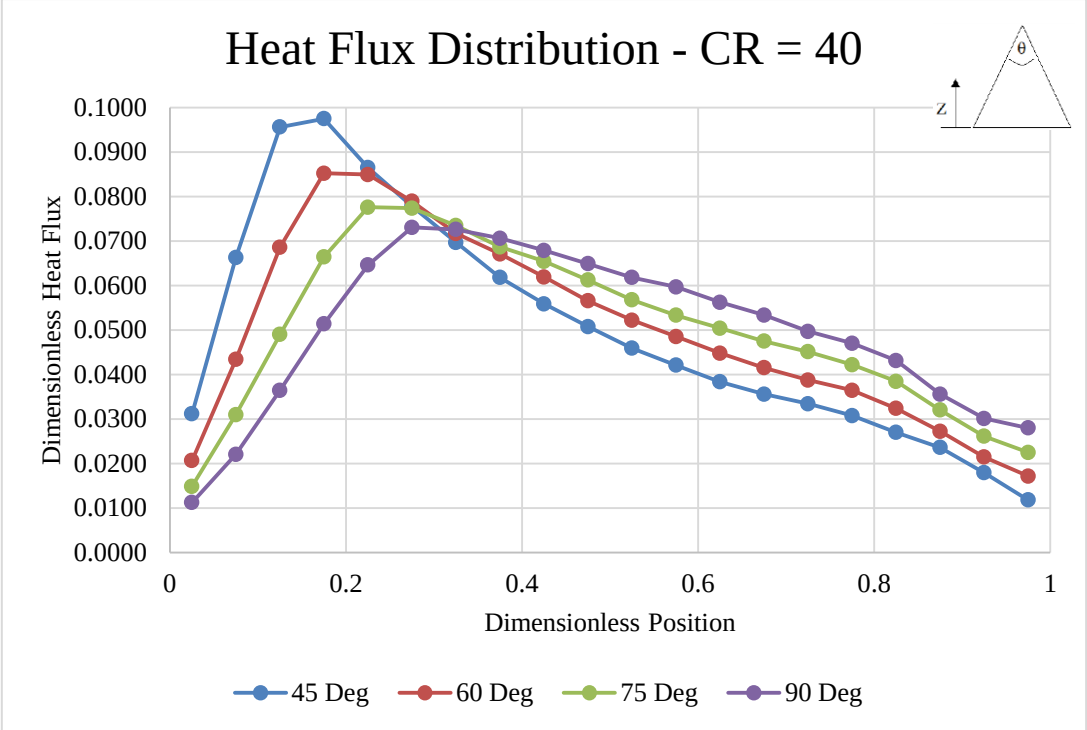

Figure 5.8: Heat Flux Distribution Plot, CR=40, STC.

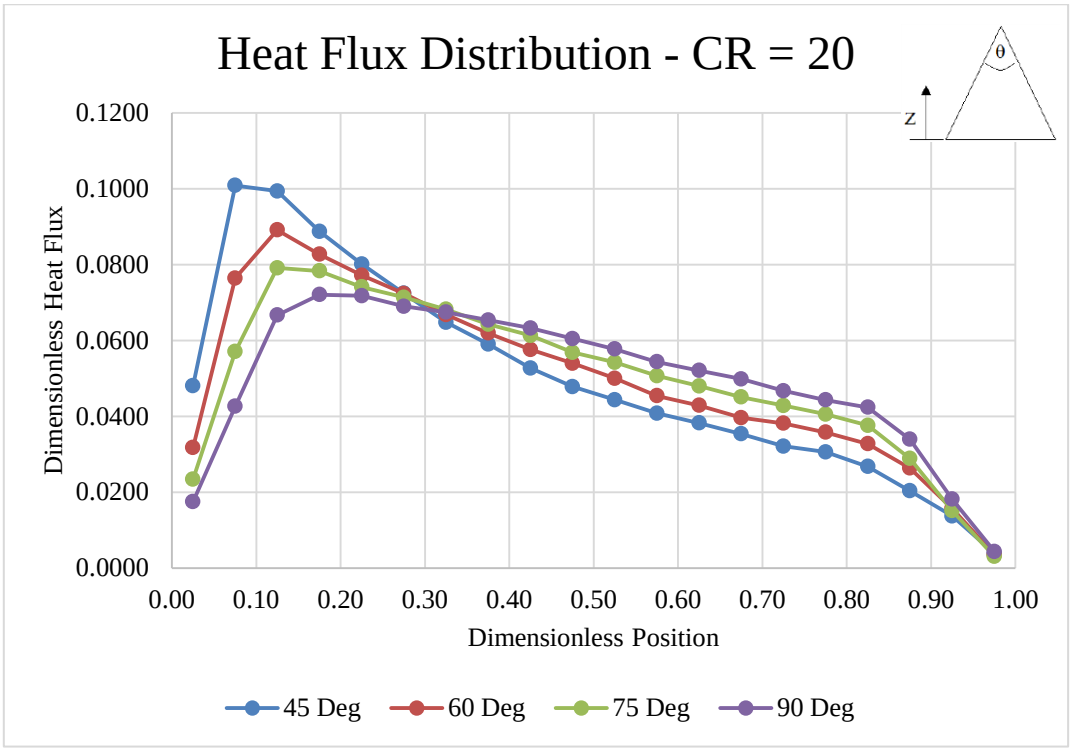

Figure 5.9: Heat Flux Distribution Plot, CR=20, STC.

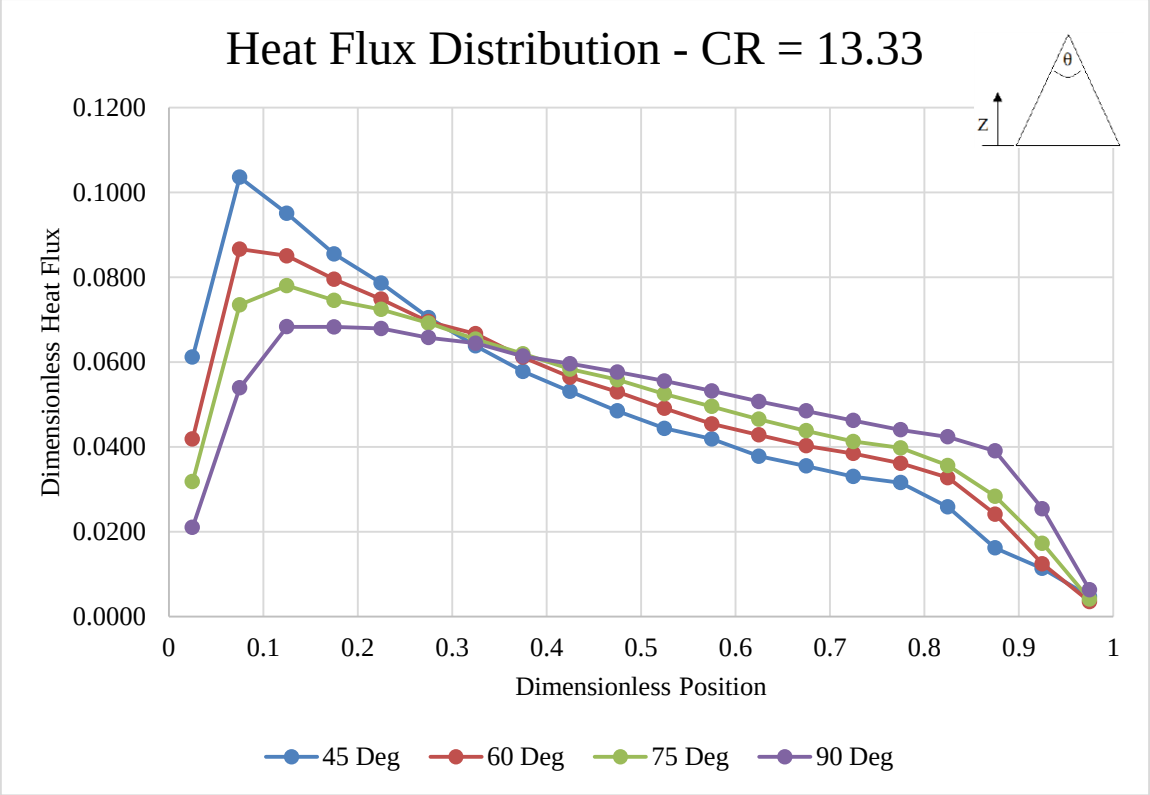

Figure 5.10: Heat Flux Distribution Curve, CR=13.33, STC.

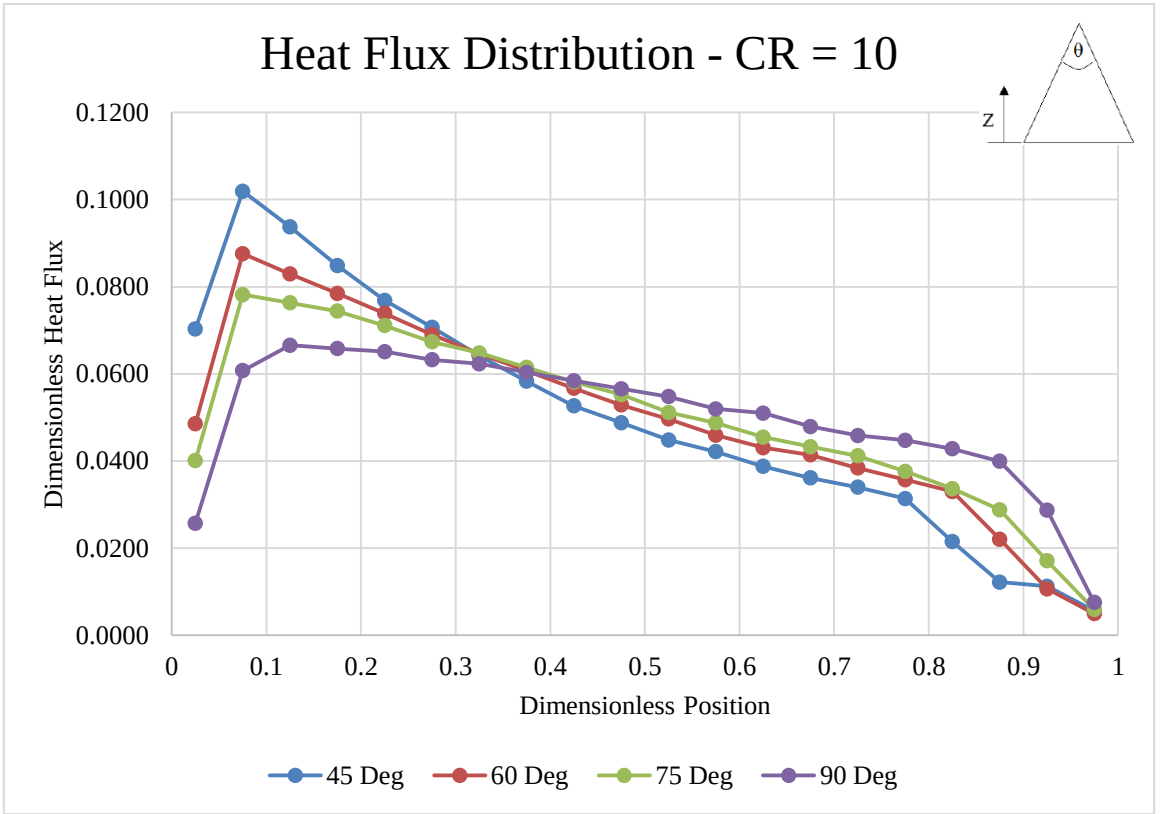

Figure 5.11: Heat Flux Distribution Curve, CR=10, STC.

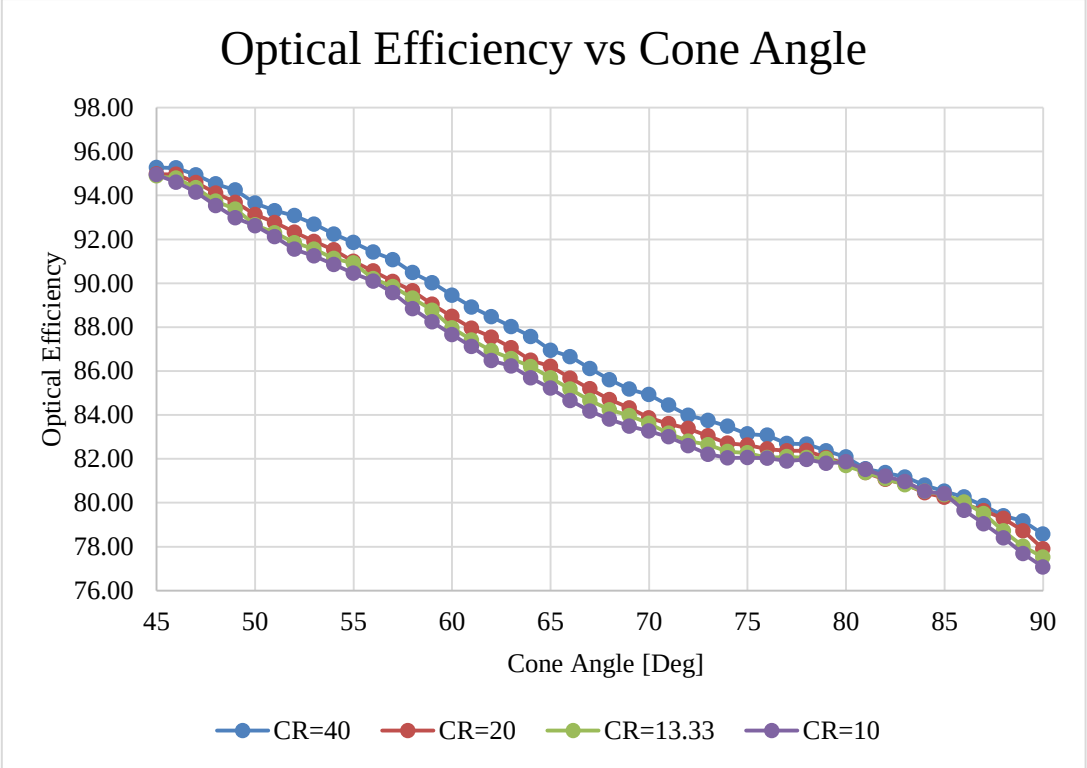

Figure 5.12: Optical Efficiency vs Cone Angle, STC.

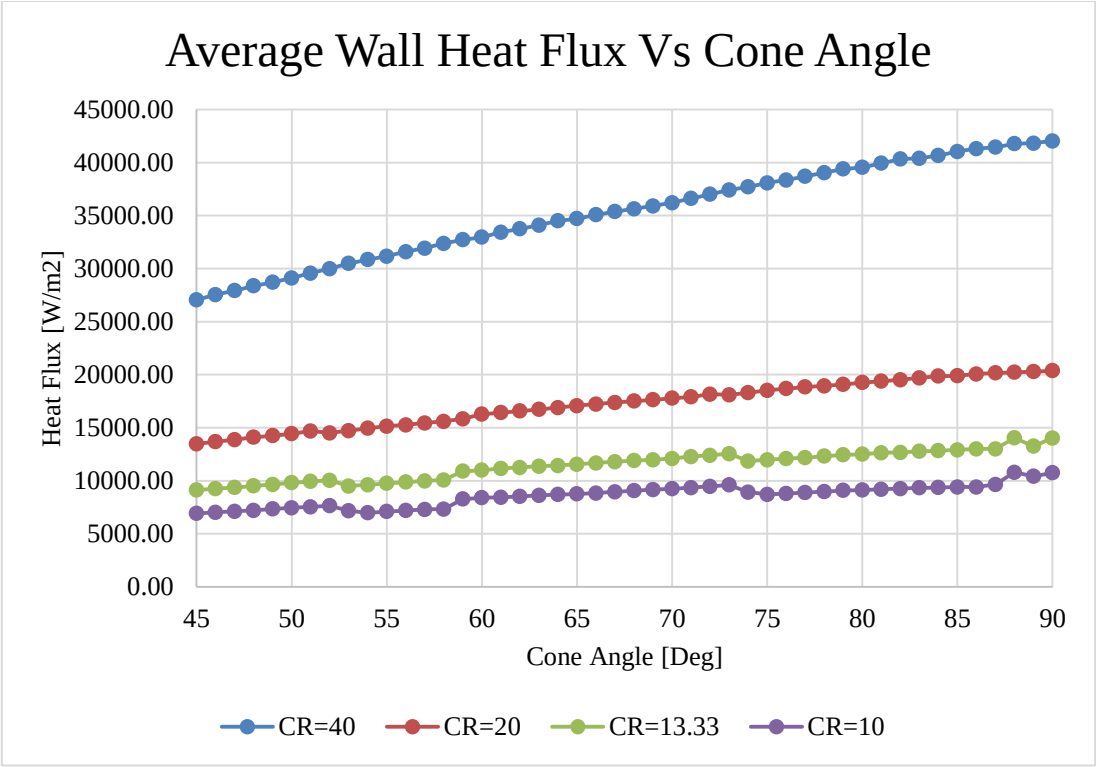

Figure 5.13: Average Wall Heat Flux Plot, STC.

Regarding Figures 5.8 – 5.11; it is observed that the shape of each curve at a given cone angle is similar in its shape. It is noticed that the shape of the curve at each concentration ratio for different cone angles are significantly different. The plots show that as the cone angle increases, the more uniform the heat flux distribution becomes. It is observed that the intensity of heat flux decreases as it propagates along the height of the receiver. It is observed that there is a sudden spike in heat flux at the bottom of the receiver.

Regarding Figure 5.12; it is observed that as the cone angle of an STC receiver increases, the optical efficiency of the receiver decreases. In other words, there is an inverse proportionality between the cone angle and optical efficiency of an STC cavity. Figure 5.12 also shows that there is a decrease in optical efficiency of the receiver as the concentration ratio decreases suggesting that there is a direct proportionality between concentration ratio and optical efficiency of an STC cavity.

Figure 5.13 shows the average heat flux acting on the cavity walls of the receiver plotted against cone angle for each concentration ratio. A DNI of 1000 W/m^2 was used to determine the heat flux. The purpose was to show the influence that cone angle has on heat flux. It is observed that there is a directly proportional relationship between heat flux and cone angle at a given concentration ratio.

5.6.2 HTC RESULTS

The purpose of testing the heteroconical shape under different geometric conditions was to investigate the design's ability to accomplish its purpose which is to trap as much radiation as possible within its cavity. Figures 5.14 and 5.15 show a SolTrace model of the HTC geometry. Figures 5.16 – 5.19 show the heat flux distribution plots for the HTC receiver cavity at different concentration ratios.

It can be seen in Figure 5.15 that the addition of the bottom inverted cone prevents some irradiation from escaping the cavity of the receiver due to the small entrance aperture width. The inside surface of the bottom cone reflects escaping rays back into the cavity.

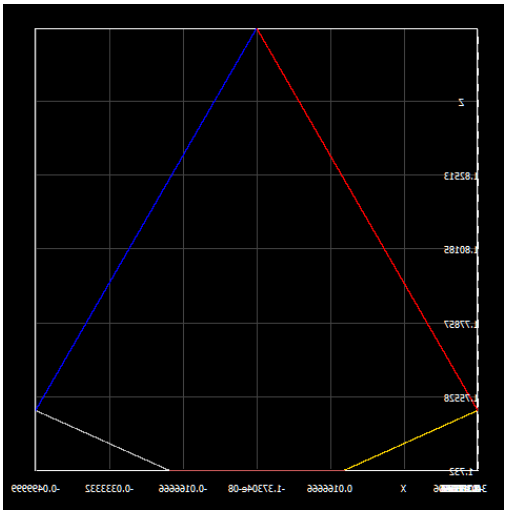

Figure 5.14: SolTrace model of HTC Receiver.

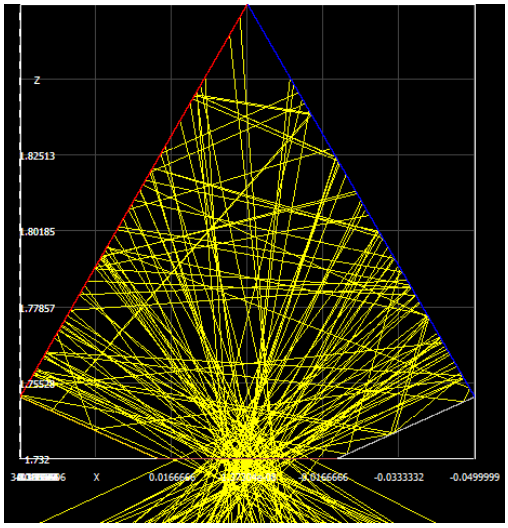

Figure 5.15: SolTrace model of HTC Receiver showing ray interactions.

Regarding Figure 5.16 – 5.19, it is observed that the shape of each curve at a given cone angle is similar in its shape. It is noticed that the shape of the curve at each concentration ratio for different cone angle is significantly different. Figures 5.16 – 5.19 show that, at each concentration ratio, the peak value of the heat flux decreases with an increase in cone angle.

It is also observed that the gradient of the heat flux distribution curve, after its peak value, increases with an increase in cone angle – this observation is present at each of the considered concentration ratios. The dip in heat flux noticed in the plots of the heat flux distribution curves of the STC receiver are still present in the plots of the HTC receiver, however the HTC design seems to reduce this dip in heat flux allowing more heat flux to be present at the top of the receiver unlike the STC receiver cavity.

The configurations of Cases 1-4 are listed in Appendix B. It was decided that each case be simulated for four cone angles; 45^0, 60^0, 75^0, 90^0, as a means of reducing the computational load while providing enough data to be analysed to allow for sufficient insight into the response of the receiver.

Figure 5.20 shows a graph of the optical efficiency HTC cavity for each case. At a CR of 40 which corresponds to an RCR of 2.5 (Case 1), it is seen that the receiver has a maximum optical efficiency of 97.7% at a cone angle of 45º and decreases to a minimum optical efficiency of 87.3% at a cone angle of 90º. The rate of its optical efficiency dropped significantly from a cone angle of 80º.

Cases 2, 3 and 4 all show a minimum optical efficiency of approximately 99%. They show a stable optical efficiency around this region from 45º to approximately 54º, 56º and 58º for cases 2, 3 and 4 respectively, after which the optical efficiency begins to decrease at a significant gradient. However, the gradient at which their optical efficiency decreased drops significantly for cases 2, 3 and 4 from approximately 74º, 69º and 68º respectively. The results show that the optical efficiency of cases 2, 3 and 4 begin to increase from 83º, 78º and 75º respectively.

The results show Case 4 is the optimal cavity configuration with a maximum optical efficiency of 99.5% and a minimum optical efficiency of 95.8% at a cone angle of 56º and 78º respectively.

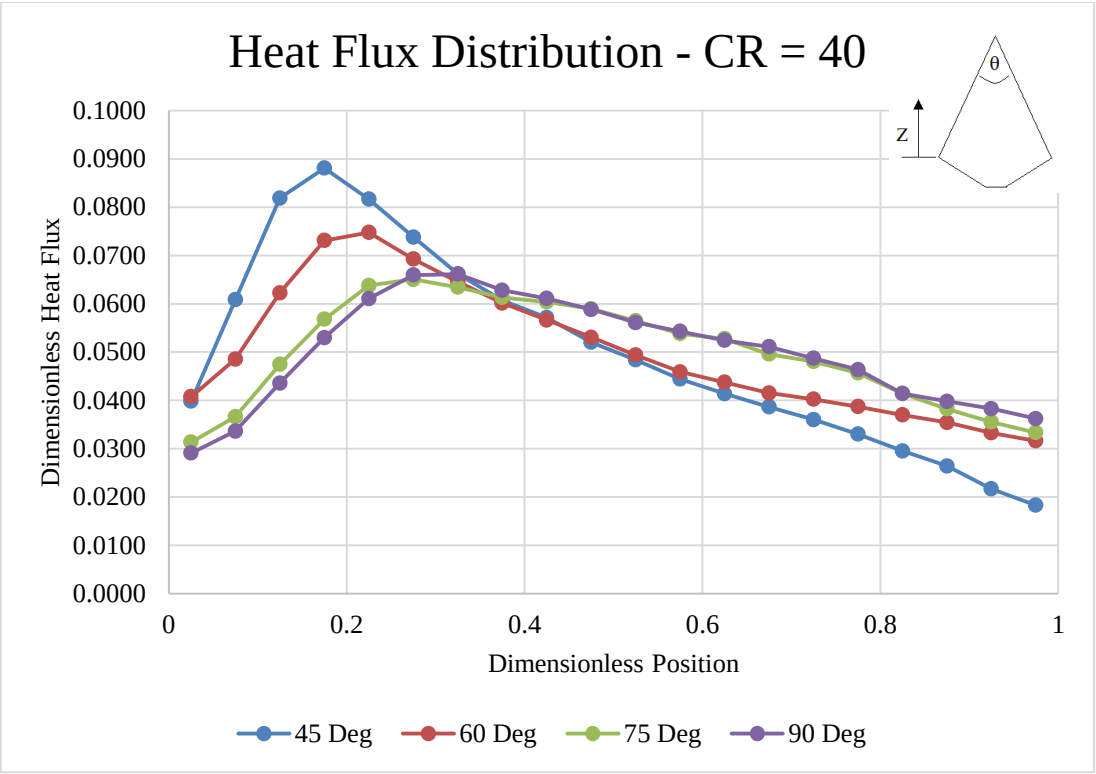

Figure 5.16: Heat Flux Distribution Curve, CR=40, HTC.

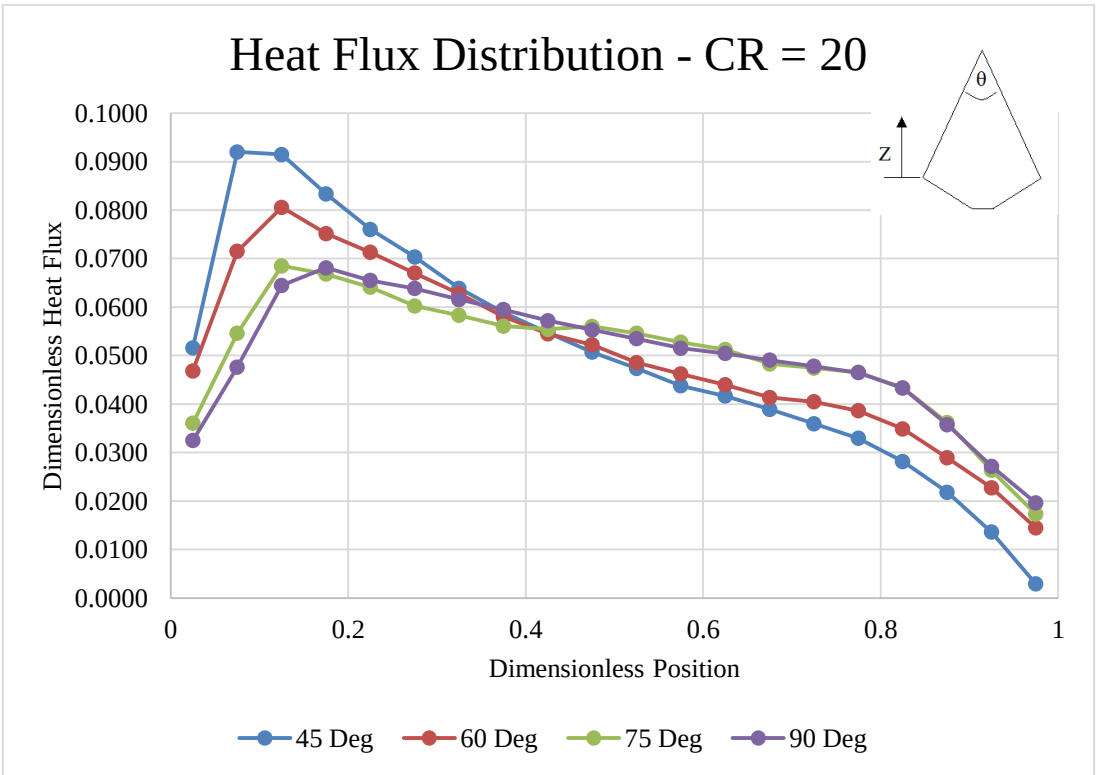

Figure 5.17: Heat Flux Distribution Curve, CR=20, HTC.

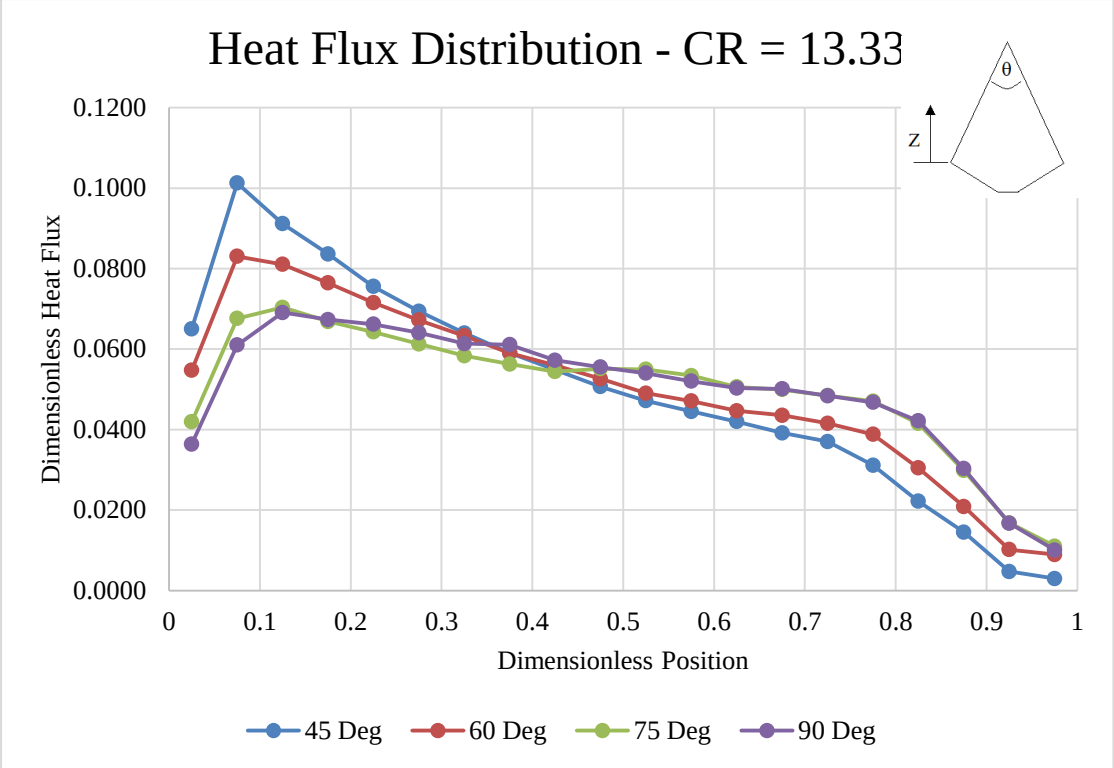

Figure 5.18: Heat Flux Distribution Curve, CR=13.33, HTC.

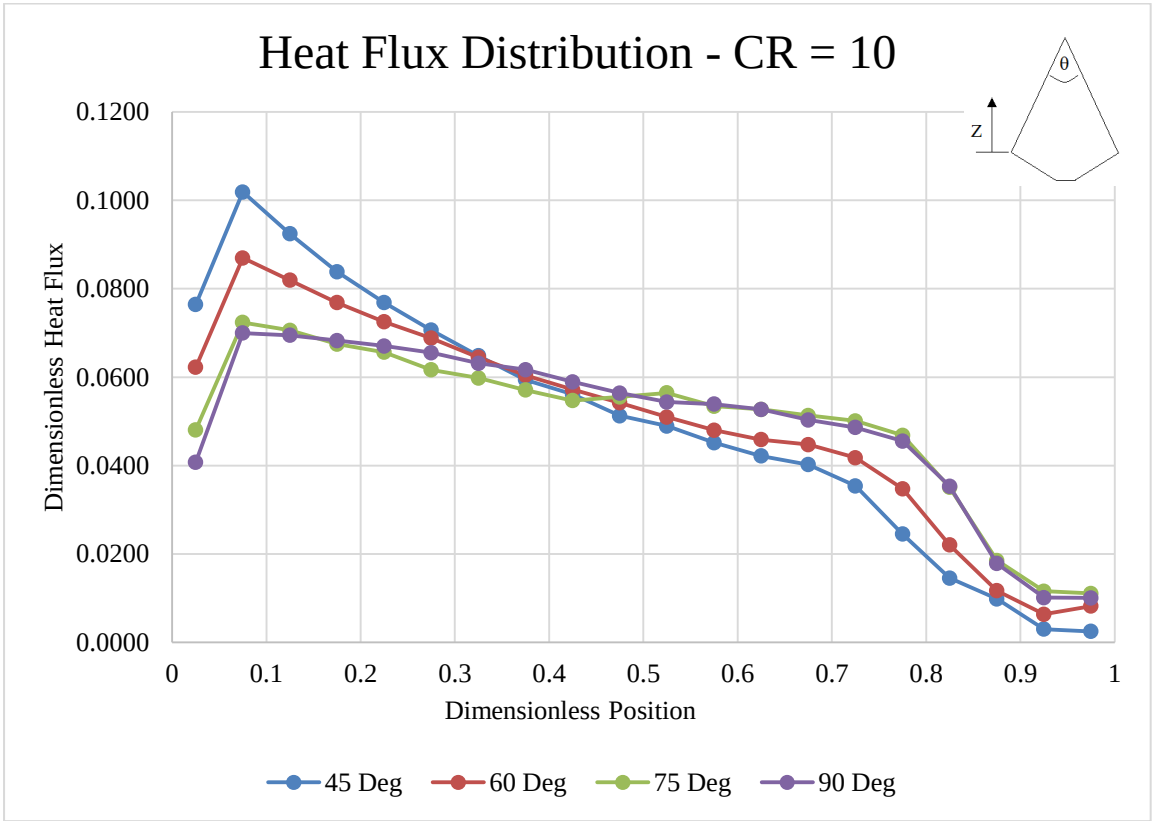

Figure 5.19: Heat Flux Distribution Curve, CR=10, HTC.

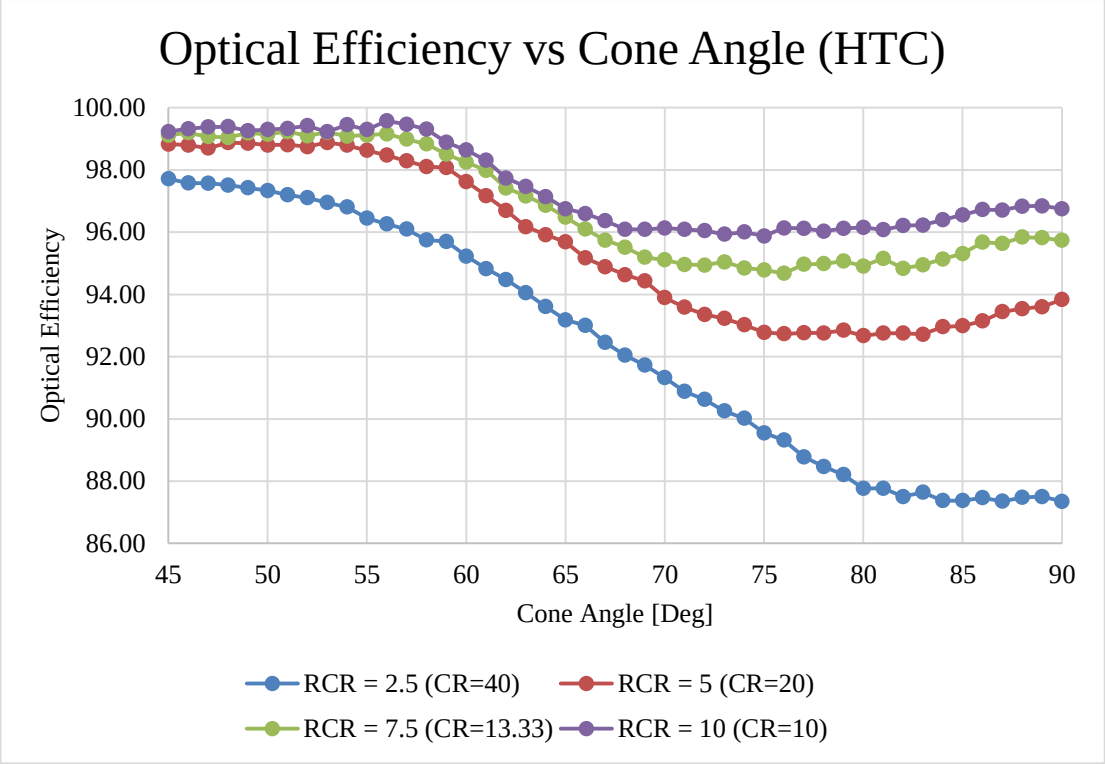

Figure 5.20: Optical Efficiency Plot, HTC.

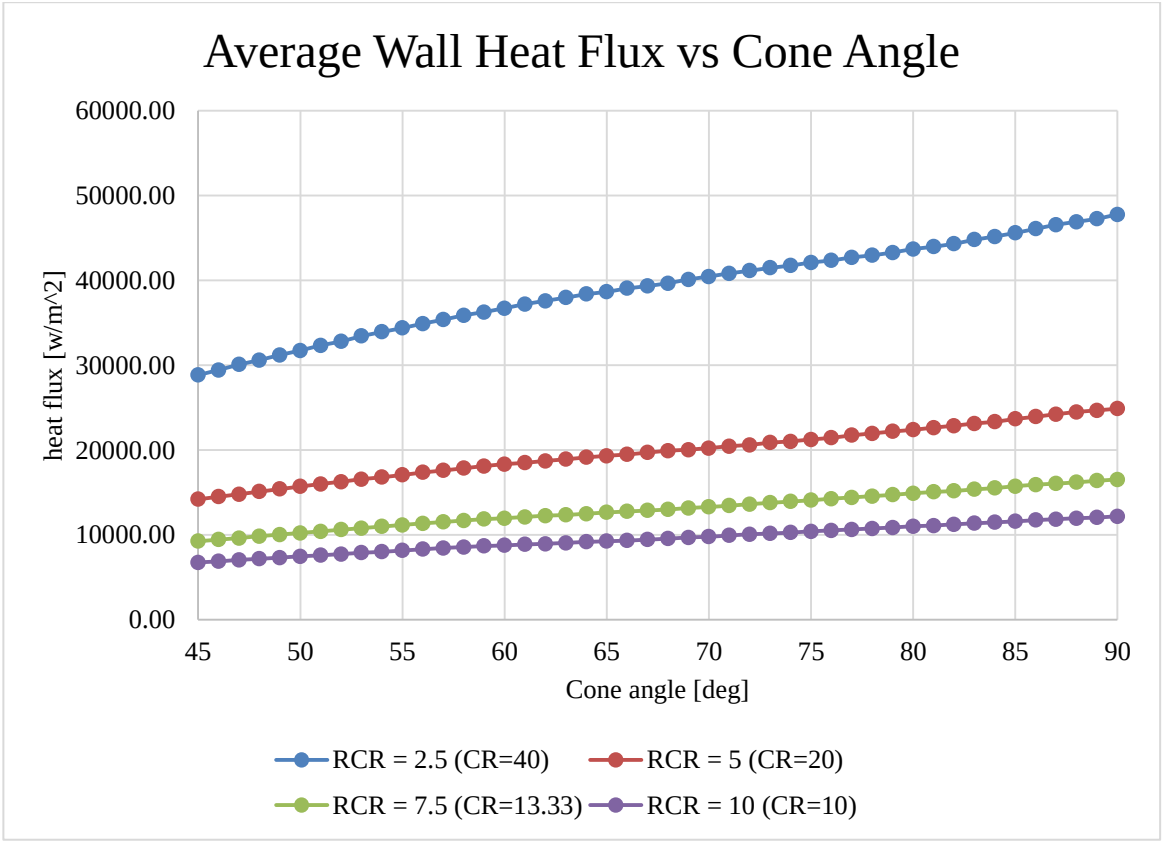

Figure 5.21: Average Heat Flux Acting on Cavity Wall of HTC Cavity

5.7 DISCUSSION

Figure 5.20 shows the optical efficiency plot of the HTC geometry. It is observed that the design has a large theoretical optical efficiency irrespective of receiver concentration ratios and cone angles. These large optical efficiencies are a result of introducing the bottom cone and smaller entrance aperture as the smaller entrance aperture also acts as a smaller exit aperture, hence more radiation is trapped inside the receiver to bounce around more until absorbed.

Figures 5.22 – 5.25 show the SolTrace models of Cases 1 and 4 at their respective cone angles. Regarding these figures, the difference in optical efficiencies between the cases show that light does escape from the cavity and the amount of light that escapes increases as the cone angle increases. The optical efficiency of the HTC is also observed to be affected by the RCR as a smaller RCR would allow light to be internally reflected for a shorter period of time than a larger RCR allowing less light to be absorbed.

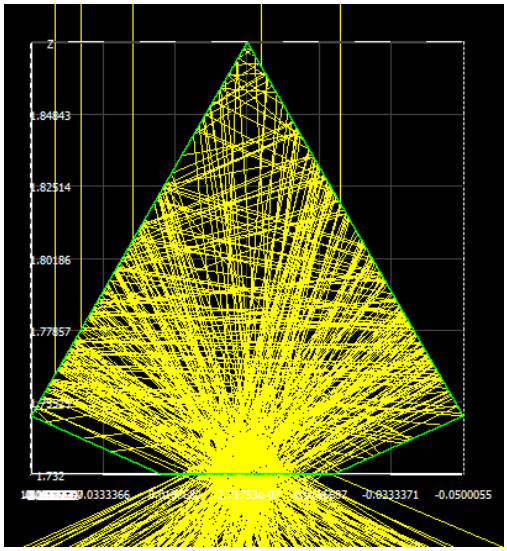

Figure 5.22: HTC Cavity (Case A, θ=45^0)

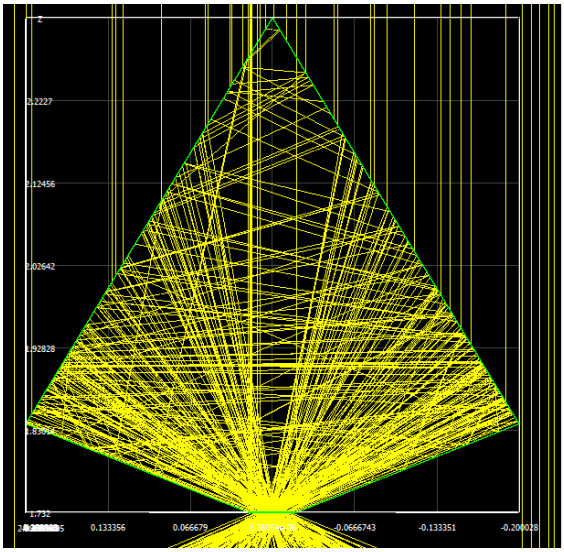

Figure 5.23: HTC Cavity (Case D, θ=45^0)

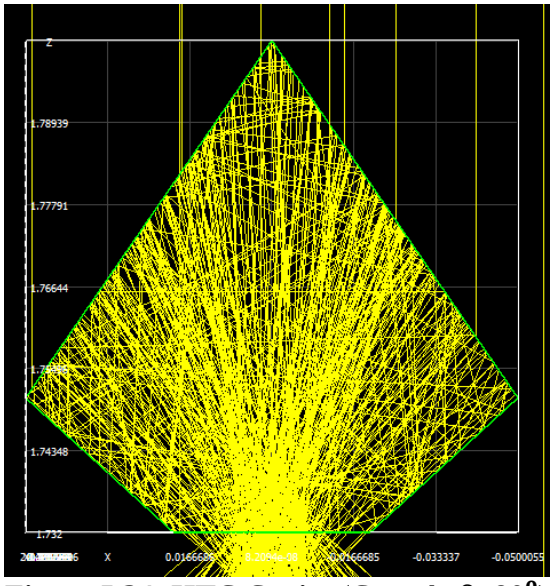

Figure 5.24: HTC Cavity (Case A, θ=90^0)

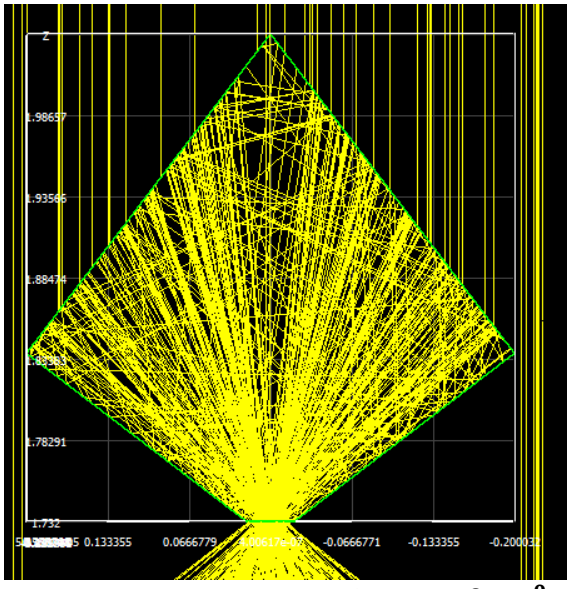

Figure 5.25: HTC Cavity (Case D, θ=90^0)

Comparing the results from the STC geometry and HTC geometry it can be noticed that the HTC receiver does have a more uniform distribution compared to that of a STC geometry. This can be explained by the geometry itself, as the rays reflected by the upper cavity walls are re-reflected by the lower cone and re-distributed along the surface of the upper cavity. There is a noticeable difference in the two distribution patterns simply because there is a significant difference between their receiver concentration ratios. In other words, a larger receiver concentration ratio means there is a smaller gap, compared to the cavity, for rays to escape from.

Compared to that of a STC receiver, it can be observed that the HTC design offers larger and more consistent heat fluxes. This is due to the shape which increases optical efficiency and aids redistribution of re-radiation within the cavity resulting in a larger average wall heat flux at all cone angles investigated.

The dip in heat flux noticed in the plots of the heat flux distribution curves of the standard receiver are still present in the plots of the HTC receiver, however the HTC design seems to reduce this dip in heat flux allowing more heat flux to be present at the top of the receiver unlike the STC receiver.

These sudden dips or ‘shadow regions’ are caused by the lack of radiation being reflected and concentrated to and at this location due to the shadow that the receiver casts on the parabolic trough. One could say that the shadow it casts is being cast back at it. This observation implies that the smaller the concentration ratio, the larger the shadow region.

5.8 SUMMARY

Optical models of the STC and HTC cavity geometries were generated and simulated for varying cone angles at different concentration ratios. The optical efficiencies and heat flux distribution curves for these geometric configurations were determined and presented.

The effect of concentration ratio and cavity shape on heat flux distribution and performance was investigated on both the STC and HTC cavity types. It was found that the heat flux distribution was not significantly affected by a change in concentration ratio. However, it was found that the cavity shape does influence heat flux distribution significantly. It was found that as the cone angle of the HTC receiver increases, the gradient of the heat flux distribution curve after its peak value approaches zero – in other words, the heat flux acting on the absorber walls of the HTC receiver becomes more uniformly distributed as its cone angle increases.

The results showed that the optical performance of the HTC cavity was affected noticeably by both a change in concentration ratio and a change in cavity shape. A lower concentration ratio (higher RCR) was found to produce higher optical efficiencies. The optical efficiency of the HTC cavity was found to decrease with an increase in cone angle; however, the HTC cavity seemed to approach a minimum optical efficiency at each concentration ratio.

The addition of the bottom cone was found to significantly reduce the amount of optical losses due to reflection out of the receiver. The optical efficiency of the STC cavity continued to decrease as its cone angle increased. The HTC receiver seemed to have a minimum optical

efficiency for each concentration ratio. Therefore, it can be stated that this effect is a characteristic of the HTC cavity.

The HTC cavity was found to produce optical efficiencies up to 99% for Case 4 and up to 98% for Case 1. The HTC cavity was shown to be an effective and efficient high-performance cavity receiver type due to its design.

CHAPTER SIX

6 THERMAL INVESTIGATION INTO THE HTC GEOMETRY

6.1 INTRODUCTION

This section presents a study into the performance of an STC and HTC receiver in which its optical performances as well as thermal performance are studied by utilising ray-tracing and CFD models respectively as discussed in Chapter 3 and validated in Chapter 4.

The chapter starts by outlining the purpose of this investigation which lists the main aims of the study followed by a description of the numerical model which includes the definition of the geometry of the models as well as lays out the optical and thermal models. Thereafter, the results of the numerical analysis performed are presented followed by a comprehensive discussion of the analysis. The chapter ends with a presentation of a summary of the findings of the investigation.

6.2 PURPOSE OF INVESTIGATION

This study aimed to fulfil the following purposes with regard to the HTC and STC receiver:

1. Identify the effect of concentration ratio of the thermal performance of the receivers.
2. Identify the effect of cavity shape on the thermal performance of the receivers.
3. Investigate the influence of the addition of the bottom inverted cone on performance.

6.3 METHOD OF INVESTIGATION

The optical and thermal efficiency of the HTC and STC receiver are investigated in this study.

The results of the investigation into the cavity shape showed that the optimum cavity configuration of the HTC receiver occurred at a CR of 10 and cone angle of 56º. This configuration was deemed too large to be practical and would consist of too many tubes which

results in a low heat flux per tube, shown in Figure 5.21. Therefore, considering the results of the aforementioned investigation, four configuration cases were decided upon for this investigation. Case A and B being a receiver configuration with a concentration ratio of 40 (r = 10cm, RCR = 2.5) and a cone angle of 45^0 and 90^0 respectively. Case C and D being a receiver configuration with a concentration ratio of 20 (r = 20cm, RCR = 5) and a cone angle of 45^0 and 90^0 respectively.

In order to investigate the influence of the addition of the bottom inversed cone on performance, these cases were applied to the STC geometry and numerically modelled.

For each configuration case, for both the STC and HTC receiver, an optical model was generated and simulated after which a thermal model was generated and simulated.

6.4 NUMERICAL MODEL

The numerical model was applied to both the STC and HTC receivers and consists of an optical and thermal model. This subsection outlines the geometry of the receivers as well as describes the factors considered in the optical and thermal models. The numerical model was modelled according to the specifications set out in Chapter 3.

6.4.1 GEOMETRY

The geometry of the optical model composed of the following components:

1. Cavity Shell
2. Absorber Tubes
3. Aperture Window
4. Parabolic Reflector

The geometry of the thermal model included the following components:

1. Cavity Shell – Insulation
2. Absorber Tubes
3. Aperture Window
4. Cavity Air
5. Heat Transfer fluid – Water

The width of the entrance aperture *a* was kept constant at 40mm. The thickness of the insulation and absorber tubes was kept constant at 5mm and 1mm respectively. The thickness of the aperture glass was fixed at 2mm along with the distance between the tube outer edge, referred to as the pitch, at 2mm.

A common tube diameter of $\frac{1}{2}$ inch was selected and kept constant for the absorber tube inner diameter. In order to reduce the cost of computation, the length of the receiver and parabolic trough was kept constant at 0.5 m. The number of absorber tubes within the cavity of the receiver is determined by stacking as many tubes of diameter Dt with inner diameter Di according to the cone geometry with a 2 mm pitch, *p*, in such a manner that no tube is placed with majority of its surface area overlapping into the shadow region.

Cross-sections of the STC and HTC designs are shown in Figure 6.1 and Figure 6.2 respectively. The parabolic trough was selected to have a width of 4 m, a focal length of 1.732 m, a rim angle of 60º and a length of 0.5 m. The geometric specifications of the parabolic trough were kept constant throughout this work.

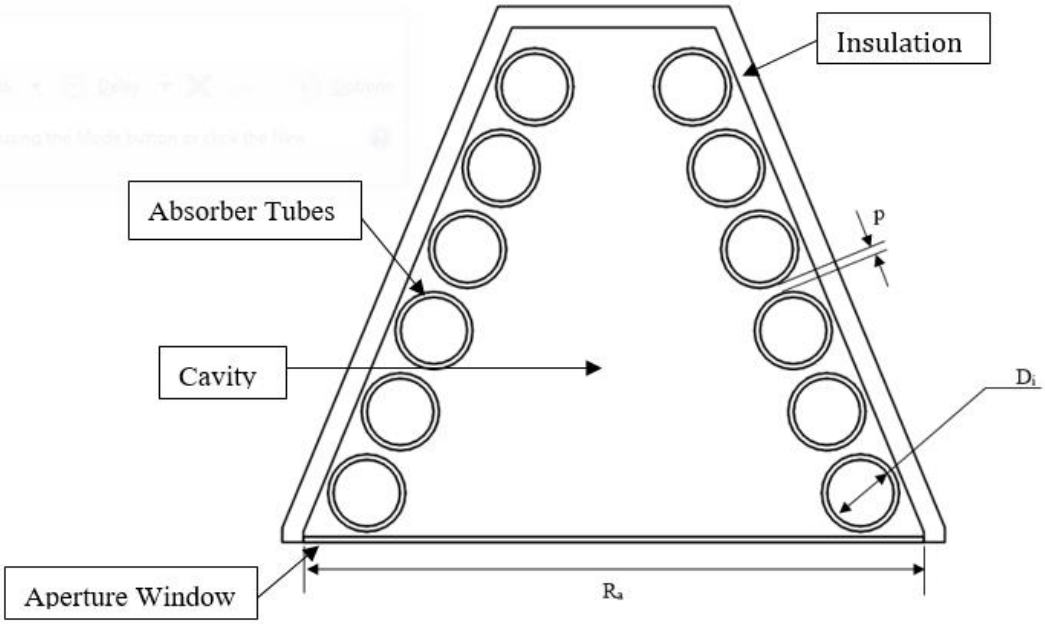

Figure 6.1: Cross-Section View of STC Receiver

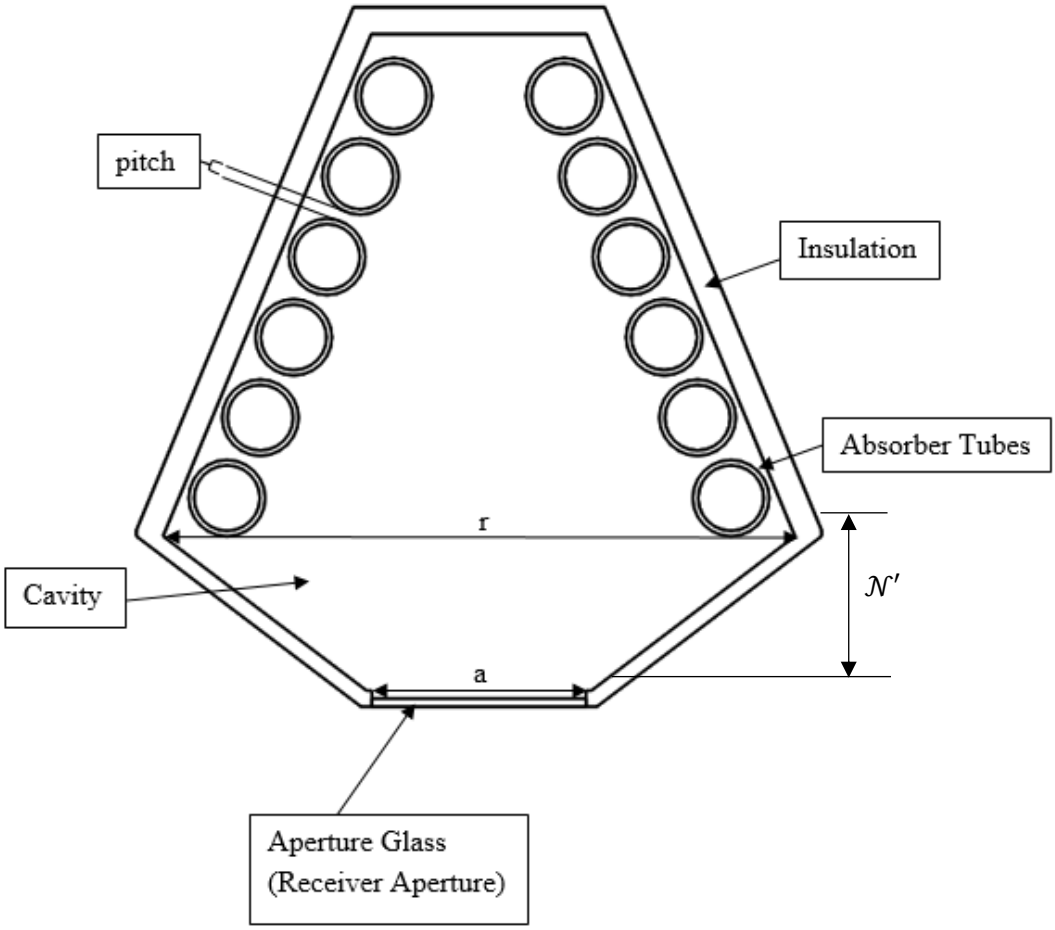

Figure 6.2: Cross-Section View of HTC Receiver

6.4.2 OPTICAL MODEL

The optical model of the system was generated and simulated in SolTrace. Each model consisted of an outer shell with inner and outer optical properties, a glass window aperture, the absorber tubes and the reflector. The absorber tubes were modelled as being painted with black paint. Each element was modelled with its respective optical properties. The parabolic trough was modelled as an ideal reflector (reflectivity = 1) because the focus of this investigation was on the optical performance of the receiver. The inner and outer surface of the receiver shell was modelled with the optical properties of aluminium foil as this reduces the amount of irradiance absorbed by the cavity walls within the receiver and reduces the external surface temperature of the receiver which in turn reduces the amount of heat loss due to re-radiation from the receiver. Table 6.1 lists the optical properties of each element used in the SolTrace model of the SCT and HTC receiver.

Table 6.1: Optical Properties of SolTrace Elements

Element	**Reflectivity**		**Transmissivity**	
	Inner	Outer	Inner	Outer
Glass Window	0.93	0.93	0.91	0.91
Cavity Walls	0.97	0.97	0	0
Tube Surface	-	0.27	0	0
Parabolic Trough	1	1	0	0

In order to model the receiver, certain assumptions were made to simplify the problem at hand.

Assumptions

- Constant DNI (1000 W/m^2).
- Ideal Reflector (Reflectivity = 1).
- Specularity Error (0.0001 mrad).
- The plane of the reflector was normal to the incoming rays.

- A Pillbox Sun Shape was selected.
- Transparent, non-absorbent glass aperture to maximise re-radiation losses out of the receiver.

The simulation traced 1 000 000 rays as this showed the most accurate results (Moghimi, et al., 2015). The heat flux acting on the absorber tubes was exported using the procedure described in Chapter 3 to be used as a volumetric heat source condition in the CFD model. The performance of the receiver was determined by applying the Equations described by the mathematical model presented in Chapter 3.

6.4.3 CFD MODEL

The purpose of the thermal analysis was to investigate the thermal performance of the receiver with different design configurations as well as identify influencing factors in heat loss and how to address them. Heat transfer analysis was performed on the different design configurations to determine the thermal efficiency of the receiver in order to calculate the overall efficiency of the receiver under different geometric configurations.

The mass flow rate and environmental conditions were kept constant throughout the simulations to maintain consistency between the results of each design configuration.

Polished copper was selected as the material of the tubes due to its high melting point and high thermal conductivity. These tubes are modelled as being painted black with black heat resistant paint to increase absorptivity. The selected insulation material of the receiver was foam insulation encased in shinny aluminium. The aperture window selected was glass.

6.4.4 CFD MODEL SET-UP

The following factors were considered in the CFD model:

1. Air within the cavity of the receiver.

2. Radiation absorption.

3. Heat transfer via conduction.

4. Heat transfer due to internal and external convection.

5. Re-radiation to the sky and surroundings.

In order to model the receiver, certain assumptions were made to simplify the problem at hand.

Assumptions

- Uniform heat generation rate on glass window.
- Negligible irradiation absorbed by cavity walls.
- Steady state operating conditions.
- Constant solid material properties – low operating temperatures.
- Atmospheric pressure outlet boundary condition.
- Constant mass flow rate inlet boundary condition.
- Constant fluid properties – low operating temperatures.

A swept mesh meshing method consisting of quadrilateral elements was used to mesh the receiver throughout the numerical analysis as the flow is parallel to the direction of the tube and the insulation was made two elements thick to account for temperature gradients. The absorber tubes are thin walled tubes and modelled with a single element thickness to reduce the cost of computation. Figure 6.3 and 6.4 show a meshed STC and HTC receiver respectively.

6.4.4.1 CELL ZONE CONDITIONS

The absorber tubes are modelled with a heat generation cell zone condition and are set to participate in radiation. The solar irradiation heat source generated from SolTrace is applied as the heat generation source to the absorber tubes. The absorber tubes re-radiate energy through the cavity air. Some of this energy exits through the receiver aperture. To maximise the amount of re-radiation losses from the cavity, the glass aperture window is assumed to be transparent and non-absorbent to this re-radiation.

The air within the receiver, cavity air, through which re-radiation from the absorber tubes is transmitted is modelled as a solid zone. The cavity air zone is set to participate in radiation with zero absorptivity and the refractive index of air in a vacuum. Therefore, the fluid flow and turbulence model equations are not solved for the cavity air, reducing the computational cost of the simulations (Craig, et al., 2014).

The HTF is modelled as a fluid that does not participate in thermal radiation as the absorber tubes are thin walled and the internal tube surface and outer surface as locally at similar temperatures. Therefore, the computational load is reduced as the intensive discrete ordinates Equations are not solved in this zone.

The aperture of the receiver is modelled as a non-absorbent semi-transparent glass boundary wall with a thickness of 3 mm that participates in radiation. Therefore, emitted radiation by the absorber tubes will pass through the window, maximising re-radiation losses.

6.4.4.2 MATERIAL PROPERTIES

The material properties used in the CFD simulations are listed in Table 6.2.

Table 6.2: Material Properties

Property	**Material**					
	Water	Air	Insulation	Glass	Copper	Aluminium

ρ **[kg/m^3]**	998.2	1.225	12	2650	8978	2719
C_p **[J/kg·K]**	4182	1006.43	871	200	381	871
k **[W/mK]**	0.6	0.0242	0.039	1	387.6	202.4

The thermal properties of the fluid are taken at 20℃ as the HTC and STC system are operating at heat transfer fluid temperatures below 40℃.

6.4.4.3 BOUNDARY CONDITIONS

An ambient temperature of 293K was used. A sky temperature of 276.84K was calculated for an ambient temperature of 293K. A wind velocity of 6 m/s was selected as a means of considering moderately breezy conditions (Milwaukee Area Skywarn Association, 2011). This results in a heat transfer coefficient of 26.55 W/m^{2}K. In this first HTC study, the effect of wind direction on heat transfer coefficient was neglected.

The glass aperture absorbs a portion of the incoming radiation, the glass will heat up, which in turn will cause the cavity air to heat up; which will follow through to heat being transferred to the heat transfer fluid.

To account for this in the CFD simulation, the amount of radiation absorbed by the glass was determined by a simple SolTrace simulation by setting the glass transmissivity to 0.91 which implies an absorptivity of 0.09. The power absorbed by the glass was then divided by the volume of the glass to determine the heat generation rate and set as a mixed boundary condition with shell conduction together with convection and radiation boundary conditions. The glass aperture was set to re-radiate to the surroundings, being the parabolic trough, as this is what the aperture was facing.

The radiation acting on the inner aluminium foil surrounding the absorber tubes was not considered in the CFD simulation as it is assumed to have a negligible thermal influence as the

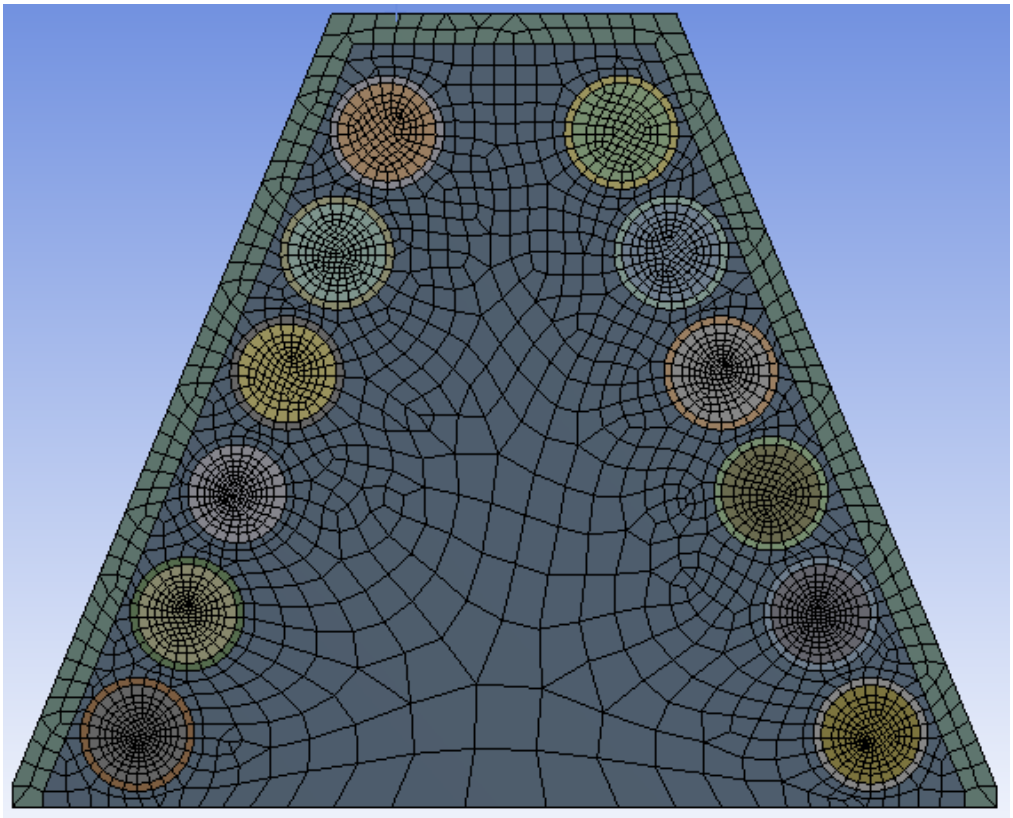

Figure 6.3: STC Receiver Mesh (CR=40, θ=45^{o})

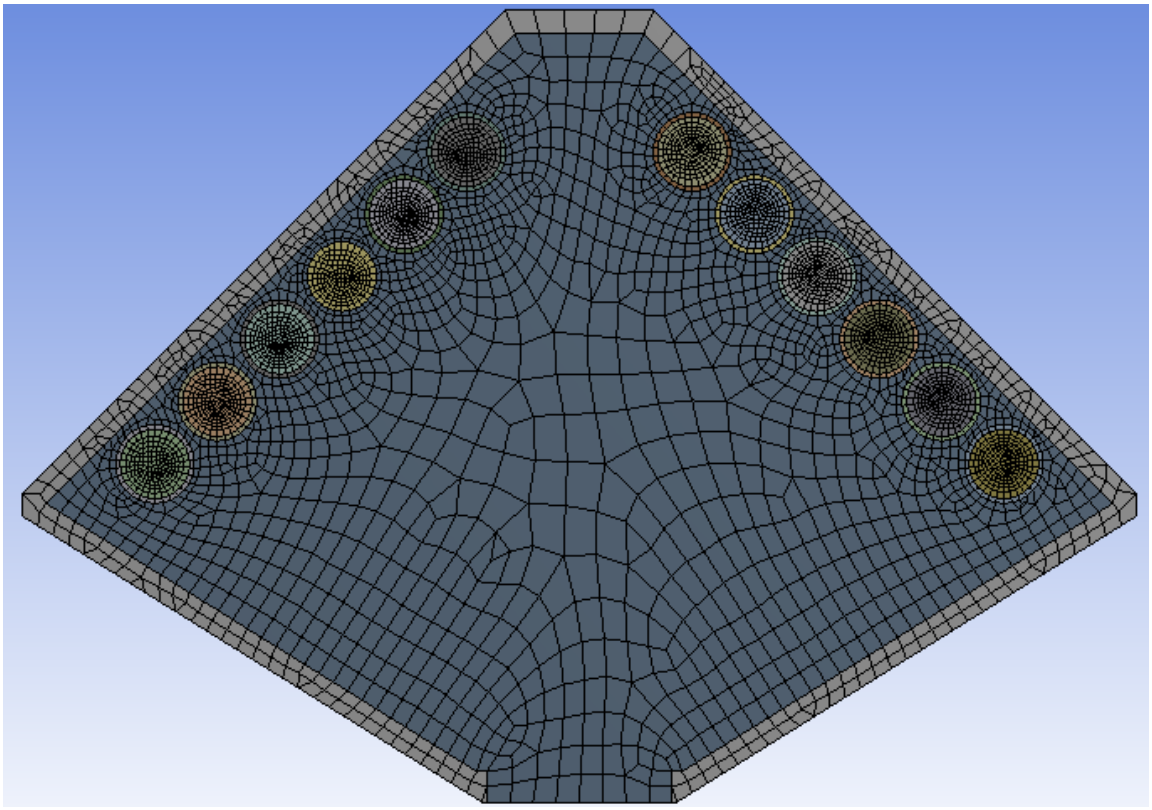

Figure 6.4: HTC Receiver Mesh (CR=20, θ=90^{o})

amount of radiation acting on the insulation coupled with a reflectivity of 0.97 results in a negligible amount of thermal absorption.

A convection and radiation boundary condition were also set on the outer surface of the insulation and bottom surface of the aperture in order to take into account air moving around the receiver as well as re-radiation to the sky.

An atmospheric pressure boundary condition was placed at the outlet of the receiver and a velocity boundary condition was placed at the inlet of the receiver. The mass flow rate flowing through the receiver was kept constant at 0.05kg/s. A volumetric heat source was generated using the results from the optical analysis and placed as a user-defined volumetric heat source placed on the absorber tubes.

6.5 RESULTS

The results of the simulations performed are presented in this subsection. The optical results are presented, followed by the heat-transfer results which are then analysed to determine the total thermal performance of the receiver.

6.5.1 STC RESULTS

Optical Results

The results of the optical and thermal analyses conducted on an STC receiver under different design configurations are presented in this sub-section. Figure 6.5 shows a SolTrace model of an STC receiver. All results and operating conditions of the investigation conducted on the STC receiver are listed in Appendix C.

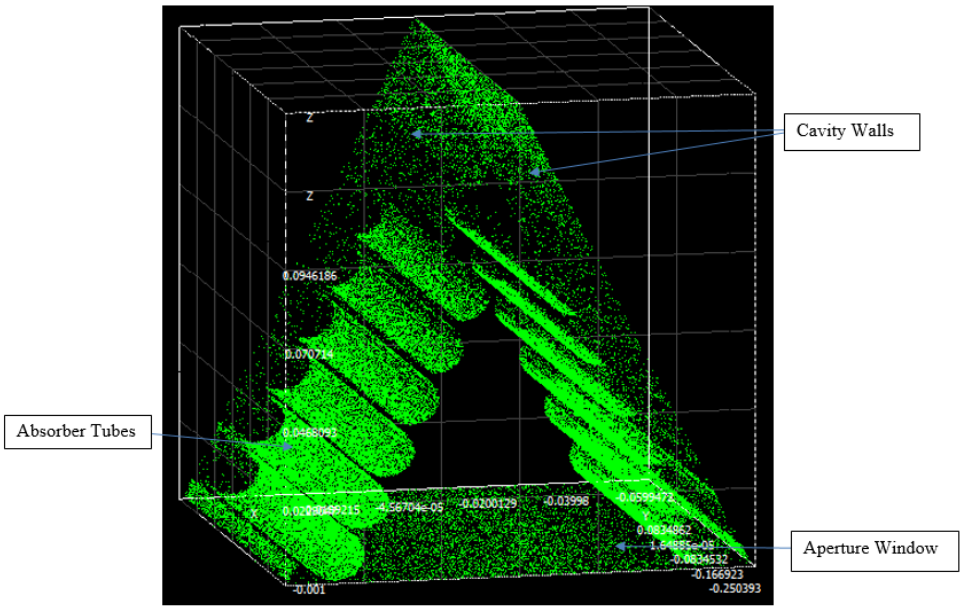

Figure 6.5: 3-D view of the SolTrace Model of an STC Receiver (CR=40, θ=45^0)

Figures 6.6 – 6.9 show the optical response of the STC receiver for cases A-D. The simulations show that many rays were reflected out of the receiver cavity. This is largely due to the wide aperture which accommodates for this re-radiation to occur leading to a loss in optical efficiency.

Figure 6.10 presents the optical efficiency of the STC receiver for configuration cases A-D. The results from the simulations of the different design configurations show that a change in concentration ratio does result in a change in optical efficiency. It was also found that a change in cone angle had an influence on the receivers' optical efficiency

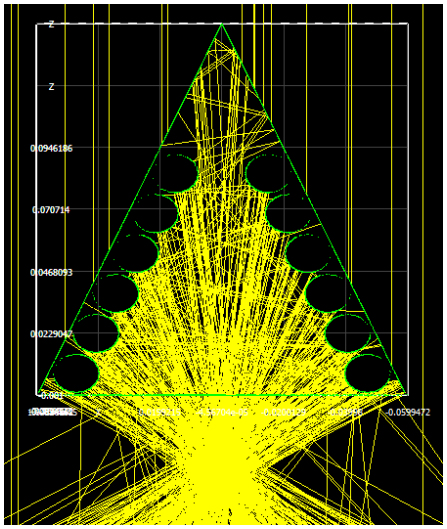

Figure 6.6: STC Receiver (Case A)

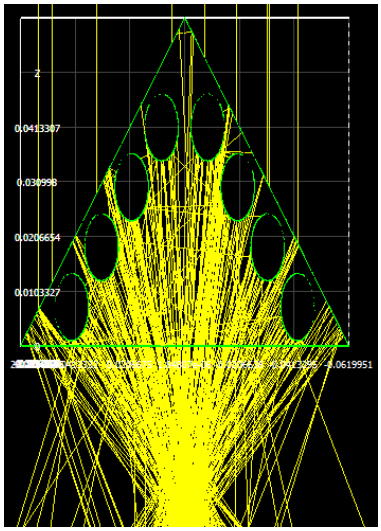

Figure 6.7: STC Receiver (Case B)

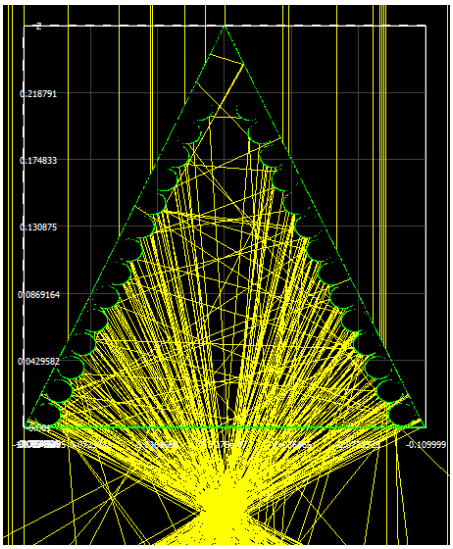

Figure 6.8: STC Receiver (Case C)

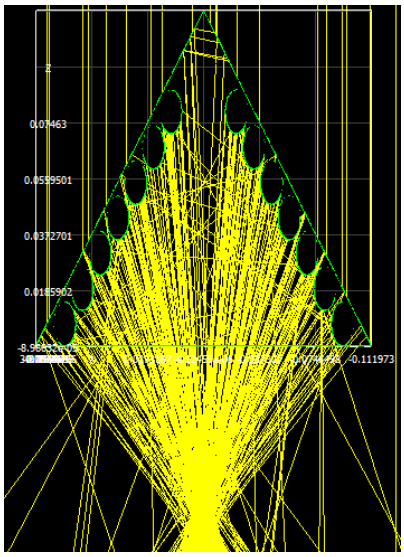

Figure 6.9: STC Receiver (Case D)

For an STC receiver with a concentration ratio of 40, a cone angle of 45^0 and 90^0, the optical efficiency was found to be 71.69% and 70.11% respectively. For an STC receiver with a concentration ratio of 20, a cone angle of 45^0 and 90^0, the optical efficiency was found to be 77.07% and 67.06% respectively. The highest optical efficiency occurs under configuration case C which showed a 5% higher optical efficiency than Case D which displayed the lowest optical efficiency.

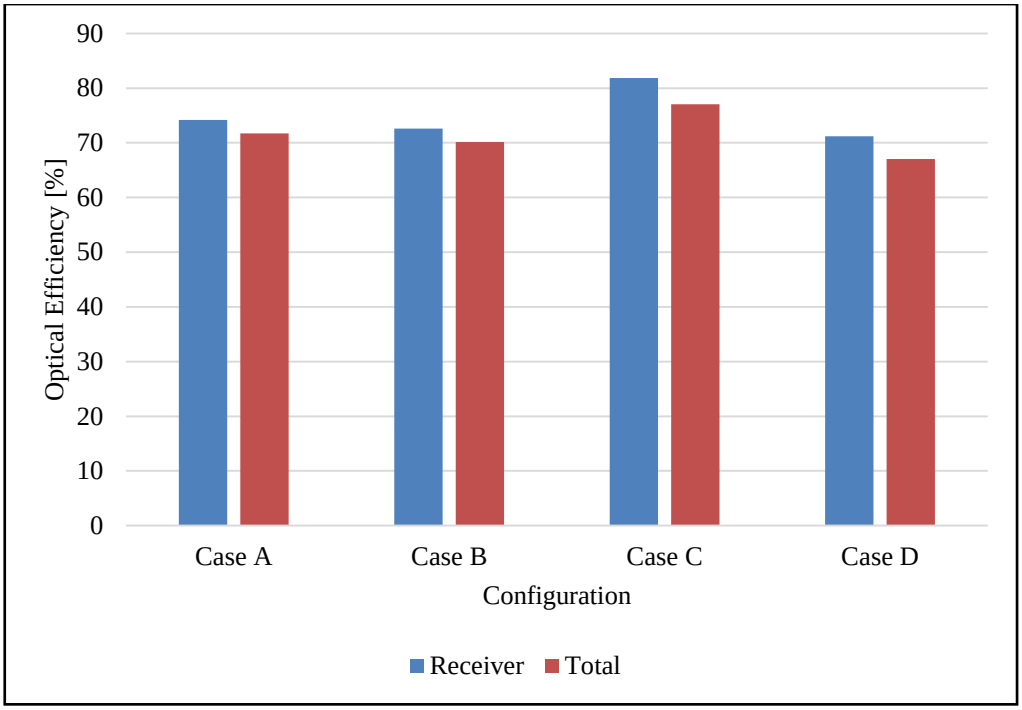

Figure 6.10: Optical Efficiency of STC Receiver

CFD Results

Figure 6.11 graphs the heat-transfer efficiency of the STC receiver for each configuration case.

The results show that the STC receiver with a concentration ratio of 20 and cone angle of 45^0 (Case C) has the highest thermal efficiency of 66%. The STC receiver with a concentration ratio of 20 and cone angle of 90^0 (Case D) has the lowest thermal efficiency of 61%.

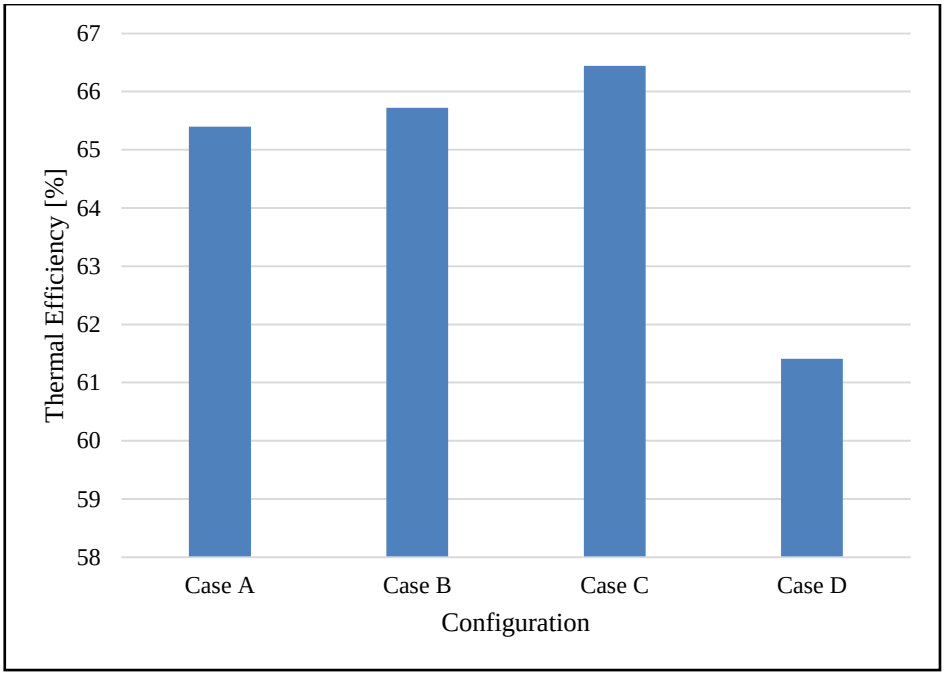

Figure 6.11: Thermal Efficiency of the STC Receiver

6.5.2 HTC RESULTS

The results of the optical and CFD simulations of the HTC receiver under configuration cases A-D are presented in this subsection.

Optical Results

Figure 6.12 shows a SolTrace model of an HTC receiver. Figures 6.13 – 6.16 display the optical response of the HTC receiver for configurations Cases A-D. It can immediately be noticed that there are less rays being reflected out of the receiver cavity. This is due to the small receiver aperture width which reduces the amount of re-radiation; hence reducing the amount of optical losses due to re-radiation leading to a higher optical efficiency.

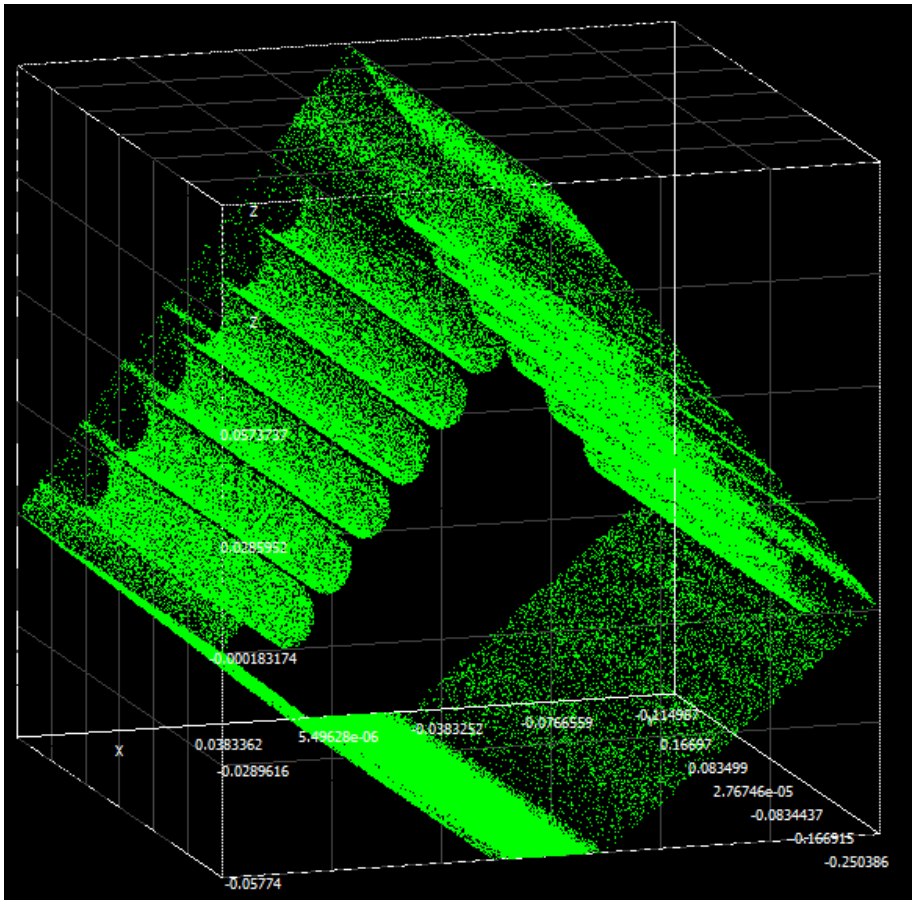

Figure 6.12: SolTrace Model of the HTC Receiver

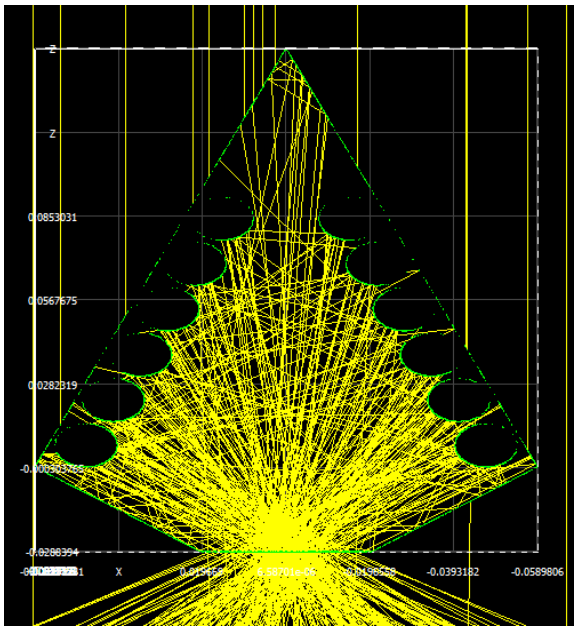

Figure 6.13: HTC Receiver (Case A)

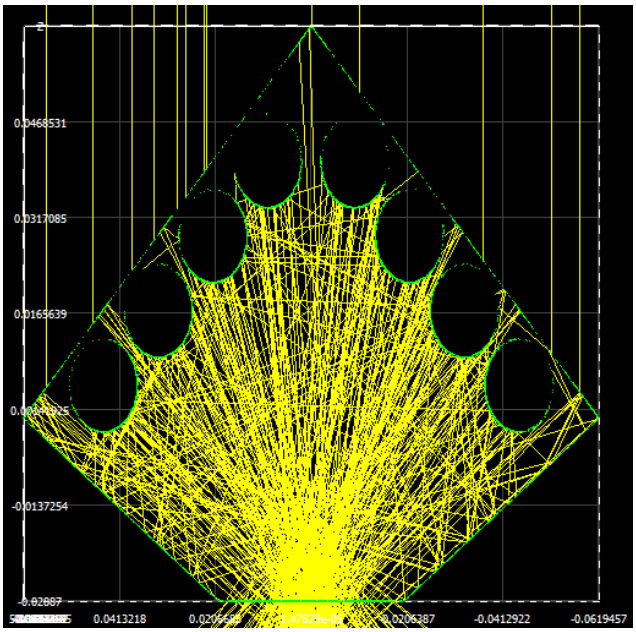

Figure 6.14: HTC Receiver (Case B)

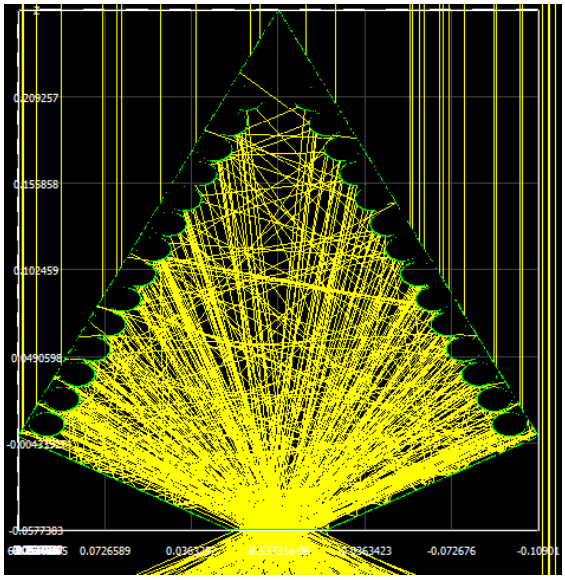

Figure 6.15: HTC Receiver (Case C)

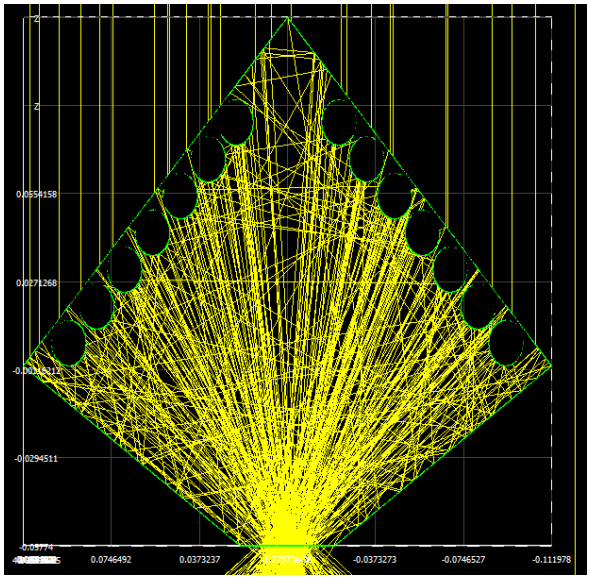

Figure 6.16: HTC Receiver (Case D)

Figure 6.17 graphs the optical efficiency of the HTC receiver for configuration cases A-D. The results show that there is a difference of 1% between the total optical efficiency of Case A and B and a difference of 8% between Case C and D. Case D displays the lowest total optical efficiency of 74%, while Case C exhibits the highest total optical efficiency of 82%

The results from the simulations of the different design configurations show that for a smaller receiver, a change in cone angle has very little effect on the receiver's optical efficiency as well as its overall optical efficiency. For a larger receiver, a change in cone angle has a greater effect on the receiver's surface area and cavity volume.

It is observed that the optical efficiency for the largest receiver is significantly higher than that of the other receivers simulated indicating that a larger inner cavity increases optical efficiency when the aperture width is kept constant.

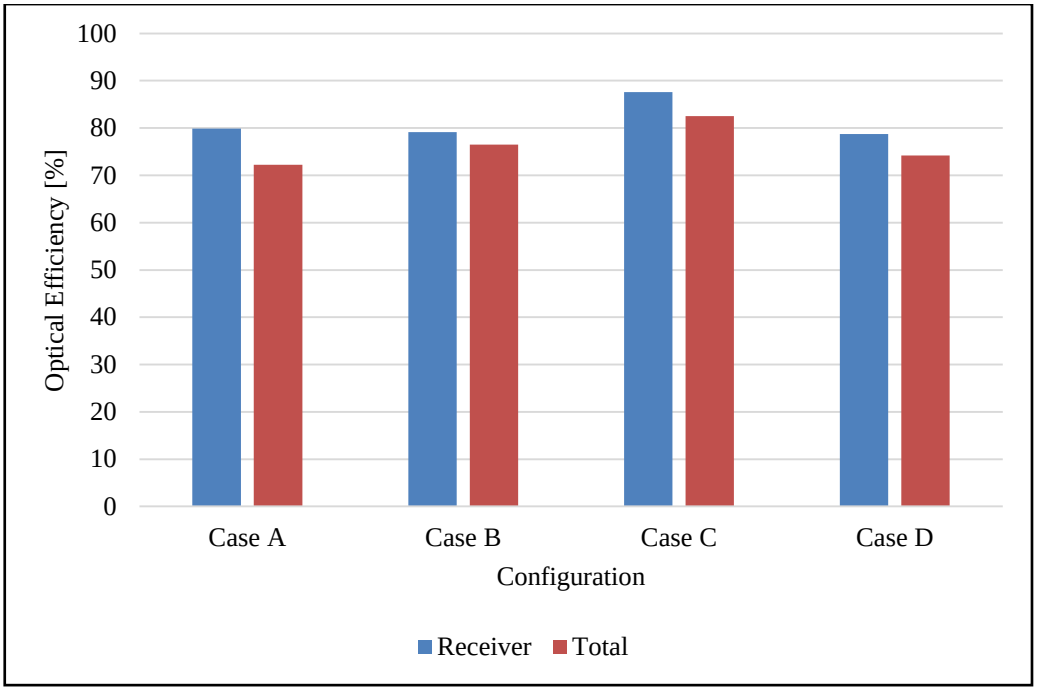

Figure 6.17: Optical Efficiency of HTC Receiver

CFD Results

Figure 6.18 graphs the heat transfer efficiency of the HTC receiver for configuration cases A-D.

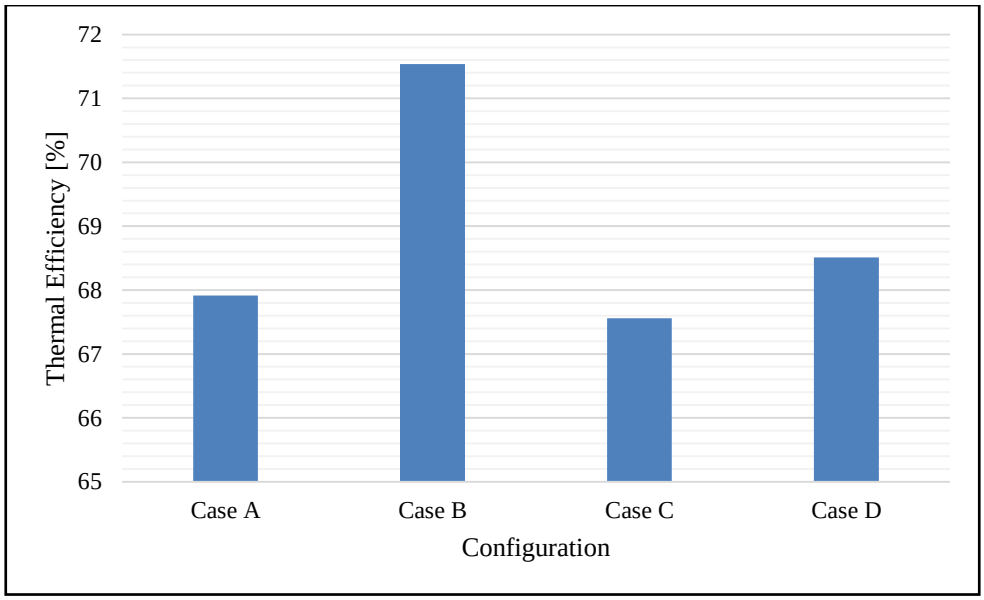

Figure 6.18: Heat-Transfer Efficiency of HTC Receiver

The results show that there is a difference of 4% between the maximum and minimum heat-transfer efficiency of the four configuration cases of the HTC receiver. The highest thermal efficiency is exhibited by Case B with an efficiency of 71.50%. The lowest thermal efficiency is

67.50% exhibited by Case C. The smallest receiver (Case B) has the smallest heat-transfer surface area and the largest receiver (Case C) has the largest heat-transfer surface area and these cases correspond to the highest and lowest heat-transfer efficiencies respectively. Therefore, the size of the HTC receiver does have a significant effect on heat-transfer efficiency as the size of the receiver affects the amount of heat loss that occurs due to natural and forced convection as well as losses due to radiation from the receiver.

6.6 DISCUSSION

The results showed that concentration ratio does have an effect on the thermal performance of the HTC receiver as there are significant differences between the thermal results of Cases A and B and Cases C and D for the HTC receiver. However, these differences could be attributed to the increase in heat loss due to convection and radiation as a result of the change in size of the receiver at different concentration ratios. However, a significant change in size of the receiver was found to affect the optical efficiency of the HTC receiver noticeably. It was found that an HTC receiver with a large cavity volume also produces a significant larger optical efficiency which can be seen when comparing Cases A, B and D to Case C where Cases A, B and D have optical efficiencies of approximately 80% and Case C has an optical efficiency of 88%. A larger volume seems to allow for less irradiation to escape the cavity of the HTC receiver.

The results of Cases A and B show that the HTC receiver is not significantly affected by varying its cone angle (cavity shape) when working with small receivers in which the cavity volume and outer heat transfer surface area does not vary significantly when varying the cone angle. However, the thermal results of Cases C and D applied to the HTC show that the cavity shape does have a significant effect on the thermal performance of the HTC receiver as the aperture width for these cases are large. Therefore, a significant change in cone angle results in a significantly large change in cavity volume and outer heat transfer surface area leading to larger heat losses due to convection and radiation.

The optical results of the STC receiver showed that a significant amount of irradiation is reflected out of the receiver due to its relatively large aperture width. The HTC receiver was found to have a significantly higher optical efficiency with an average increase of 6% upon the STC receiver. Due to the addition of the bottom inverted cone, a smaller aperture width was achievable leading to a significant reduction in re-radiation losses leading to a higher optical efficiency.

The HTC receiver is found to be more efficient than a typical cavity receiver, exhibiting a maximum thermal efficiency of 72% while the standard receiver showed a maximum thermal efficiency of 66%. This result proves that the addition of the lower inverted cone does improve efficiency and is effective is reducing reflective and heat losses.

6.7 SUMMARY

The numerical model described in this work was applied to the design of an STC and HTC receiver. An optical and thermal model was generated for each type of receiver and simulated under four design configuration cases.

The effect of concentration ratio and cavity shape on optical and thermal performance was investigated on both the STC and HTC receiver types. It was found that concentration ratio and cone angle (cavity shape) does affect the performance of an HTC receiver when working with significantly large receivers of this type but does not affect the performance of the receiver when working with smaller sizes.

It was found that the addition of the bottom inverted cone significantly reduced the amount of re-radiation without negatively affecting the receivers' thermal performance which resulted in producing a high-performance receiver design.

The HTC receiver was found to produce high optical efficiencies as well as high thermal efficiencies. Configuration Case B applied to the HTC showed the highest performance with a thermal efficiency of 72%.

CHAPTER SEVEN

7 ABSORBER TUBE OPTIMISATION

7.1 INTRODUCTION

Optimisation is the act of making the best or most effective use of a resource by finding the highest achievable performance of a system by varying some characteristic relative to a set of constraints.

This chapter presents the final stage of the three-step iterative optimisation process of the HTC receiver in the form of a numerical analysis of the HTC receiver under given constraints in order to maximise its total efficiency by varying its absorber tube parameters.

The chapter begins by formulating the optimisation problem which includes defining the objective function, variables, constraints and lastly the optimisation procedure used. The results of the optimisation are then presented, followed by a comprehensive discussion of the results. Thereafter, the HTC receiver's performance is given some context and relatability by comparing its performance to the performance of a receiver from previous work. To bring the chapter to a close, a summary of the findings is presented which includes the design configuration of an optimised HTC receiver.

7.2 OPTIMISATION PROBLEM FORMULATION

Due to the complexity of the modelling method and multiple modelling software packages used in this work to model a CSP system, typical analysis tools and algorithms are not applicable. Hence, an iterative manual analysis process was used to optimise the HTC receiver under its given constraints.

7.2.1 OBJECTIVE FUNCTIONS

An objective function is the function that is desired to be maximised or minimised. In this study, the objective function is to find the optima design configurations of an HTC receiver such that the outlet temperature of the heat transfer fluid is maximised under given operating conditions. In other words, the objective function is to maximise the total efficiency of the HTC receiver under specified operating conditions.

7.2.2 VARIABLES

Chapter 5 investigated the influence of concentration ratio and cone angle on the HTC receivers' optical efficiency. Chapter 6 investigated the influence of concentration ratio and cone angle of the HTC receivers' thermal efficiency and presented its overall efficiency while keeping the absorber tube diameter constant. In this study, the absorber tube diameter was set to be the variable and varied to reach the desired optimum result within a minimum and maximum diameter range.

7.2.3 CONSTRAINTS

The constraints are the limitations and constants placed on the design. In this study, the following are kept constant:

- DNI
- Mass flow rate
- Concentration Ratio (aperture and cavity width)
- Reflector geometric properties
- All optical properties
- All thermal properties

- Cone angle of the HTC receiver
- Absorber tube thickness
- Length of the receiver

7.2.4 METHOD

This sub-section describes the method followed to optimise the HTC receiver. Since typical optimisation methods are not applicable in this case, an iterative approach was employed. A minimum and maximum practical tube diameter was selected as well as a suitable increment between each subsequent tube diameter. Once a tube diameter is set, a SolTrace model of the HTC receiver with the specified tube diameter is constructed and executed. An interpolation file is generated to be used as a volumetric heat source in the CFD model.

The optical response of the system is then extracted and recorded. A CFD model is constructed according to the specified tube diameter. The boundary conditions are set according to the constraints and the volumetric heat source is interpolated onto the absorber tubes. The CFD module is then executed and allowed to run until convergence occurs. Thereafter, the thermal response of the receiver is extracted and recorded. Once the optical and thermal results were extracted, the overall performance of the receiver was determined and recorded. This process is then repeated for each specified tube diameter. The receiver performance results for each tube diameter are then compared and an optimised set of design configurations is determined. Figure 7.1 shows a flow chart of the iterative optimisation process.

Five different absorber tube diameters were decided on. These being 10mm, 15mm, 20mm, 25mm and 30mm diameter tubes – design points A, B, C, D and E respectively. In order to minimise the cost of computation, simulations were not carried out for each tube diameter for different cavity geometry configurations. The results of the varying cavity geometry simulations

were used to decide on a single cavity design configuration for which the varying absorber tube diameter simulations would be computed.

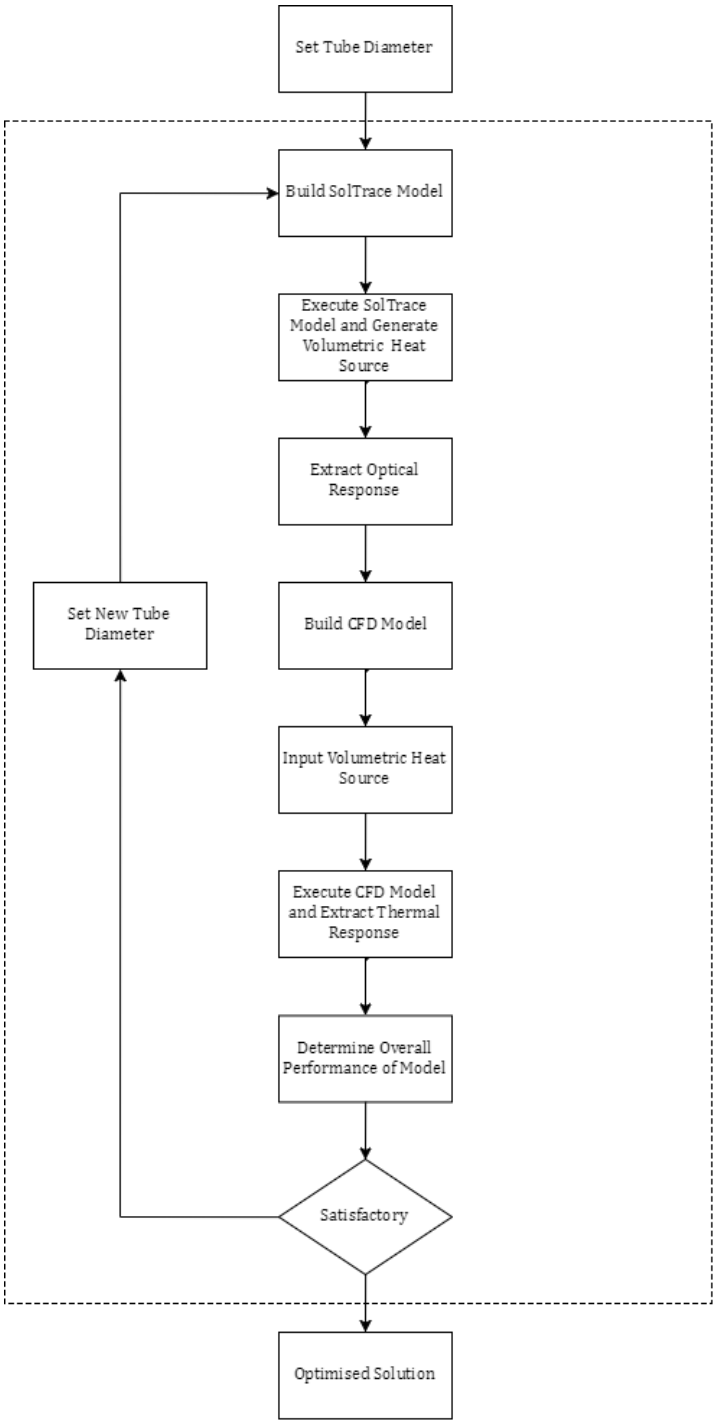

Figure 7.1: Optimisation Flow Chart

An optical model was generated and simulated for each of the five tube diameters, referred to design points from this point further, in which the optical response of the receiver was computed.

At the end of each computation an interpolation file (.ip file) was generated to be used in the thermal model of its respective design point configuration. The procedure of utilising ray-tracing and CFD together to model a CSP system is extensively described by M.A. Moghimi (Moghimi, et al., 2015). A CFD model was generated for each design point and the thermal response of the receiver was computed in which the interpolation file was used as a realistic volumetric heat source. The optical and thermal properties of the model are listed in Table 6.1 and Table 6.2 respectively. The operating conditions of the simulations are listed in Appendix C.

The thickness of the insulation and absorber tubes was kept constant at 5mm and 1mm respectively. The thickness of the aperture glass was fixed at 2mm along with the distance between the tube outer edge at 2mm.

7.2.5 MODEL SELECTION

The results of the investigation into the HTC receiver conducted in Chapter 6 were used to select the model to be optimised. The criterion used to select this model was a trade-off between the best performing receiver and the practicality in terms of size of the receiver.

The results of the investigations conducted in Chapter 5 and Chapter 6 showed that the optimum cavity configuration occurred at a CR of 10 and cone angle of 56º. This configuration was deemed too large to be practical and would consist of too many tubes which results in a low heat flux per tube. Therefore, considering the results of the aforementioned investigations, a CR of 20 (RCR = 5, r = 20cm) with a cone angle of 90º was selected as this configuration offers a high optical efficiency, a practical size and a high average heat flux per tube.

The geometric properties of the selected HTC receiver's cavity as well as position were kept constant and only the absorber tube diameter was varied in this study.

7.3 ANALYSIS RESULTS

Figure 7.2 shows the performance of the specified HTC receiver at each design point. The thermal efficiency across all five design points is above 65% and has a maximum difference between the highest and lowest thermal efficiency of approximately 9%. There is a lower difference noticed between the highest and lowest optical efficiency of approximately 7%. The results show that there could be a link between optical efficiency and thermal efficiency as it is observed that a lower optical efficiency corresponds to a lower thermal efficiency.

The highest optical efficiency occurs at an absorber tube diameter of 10mm which showed an optical efficiency of 79% and a thermal efficiency of 75%.

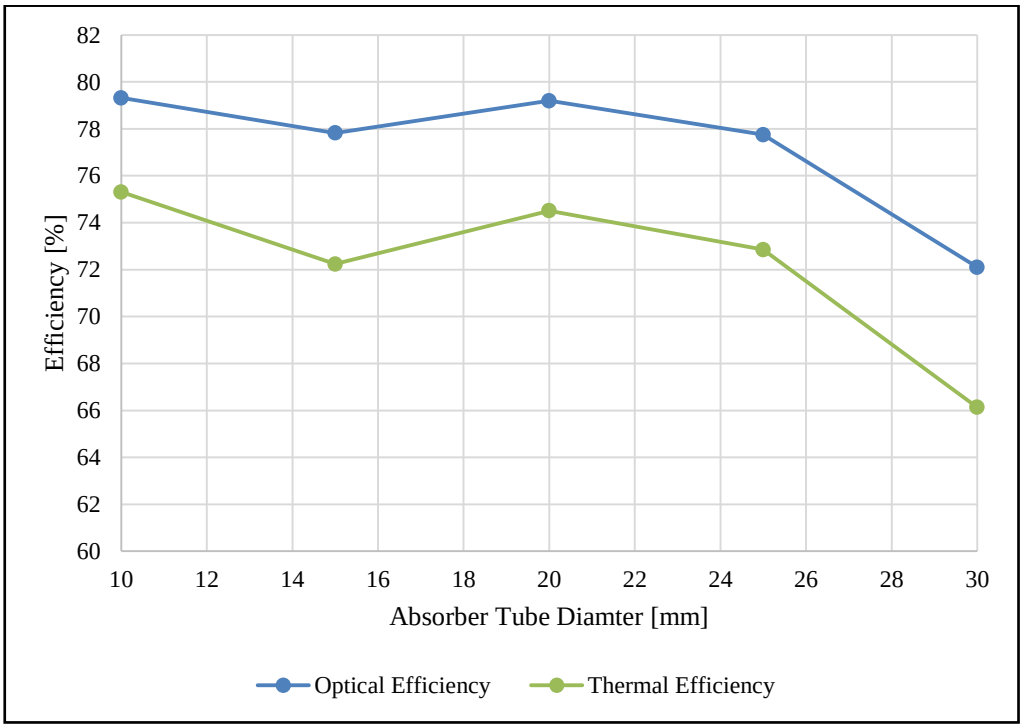

Figure 7.2: Performance of HTC Receiver for Varying Tube Diameters

The results show that the optimum absorber tube diameter for an HTC receiver with a cavity width of 20cm and cone angle of 90º for a parabolic reflector with a width of 4m is 10mm with a thermal efficiency of 75.30%. It must be noted that this result is not as obvious because at the thermal efficiency of the HTC receiver at a tube diameter of 20 mm is higher than that with a tube diameter of 15 mm showing that a smaller diameter tube does not indicate a higher efficiency and

that tube configuration plays a significant role in minimising losses. If one were to consider external factors such as the power required to pump the HTF through the receiver, the larger 20 mm diameter absorber tube would be the optimal choice as the difference in thermal efficiency between the 10mm and 20mm tube is less than 1% for the selected HTC receiver configuration.

7.4 DISCUSSION

Figure 7.3 and Figure 7.5 show that their respective tubes are irradiated the most and that their respective tubes overlap into the shadow region. Figures 7.4, 7.6 and 7.7 show that their respective tubes do not overlap into the shadow region but stop a small distance before the boundary of the shadow region. Comparing this observation of the receivers to their respective optical efficiencies, a correlation can be noticed between their optical efficiency and the distance between the last set of tubes and the shadow region.

These sudden dips or ‘shadow regions’ are caused by the lack of radiation being reflected and concentrated to and at this location due to the shadow that the receiver casts on the parabolic trough, shown in Figure 7.8. One could say that the shadow it casts is being cast back at it. This observation implies that the smaller the concentration ratio, the larger the shadow region.

The receivers with the highest optical efficiency are design points A and B and these are also the receivers whose tubes enter the shadow region. The receiver with the lowest optical efficiency is design point E which has the last set of tubes furthest from the shadow region. This means the tube diameter should be carefully considered such that the tubes cover the irradiated area in order to maximise optical efficiency.

Figures 7.9 and 7.10 show the heat flux distribution acting on an HTC receiver with absorber tubes with a diameter of design points A and E respectively. These figures show that both receivers experience similar heat flux distributions as the receivers at all the design points.

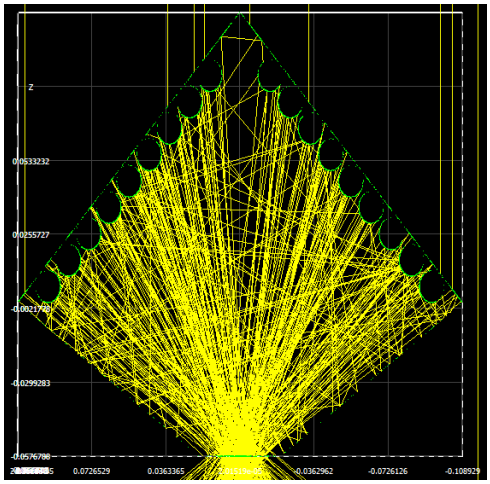

Figure 7.3: HTC, Design Point A

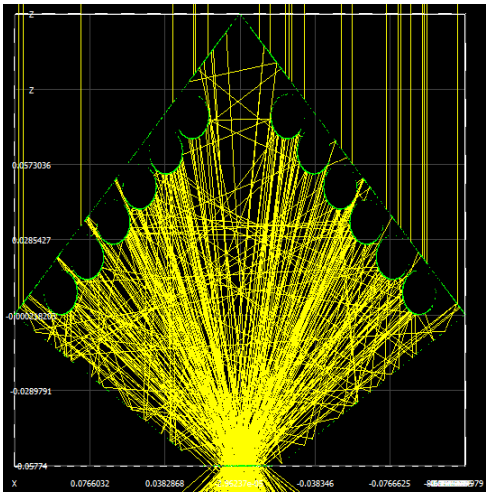

Figure 7.4: HTC, Design Point B

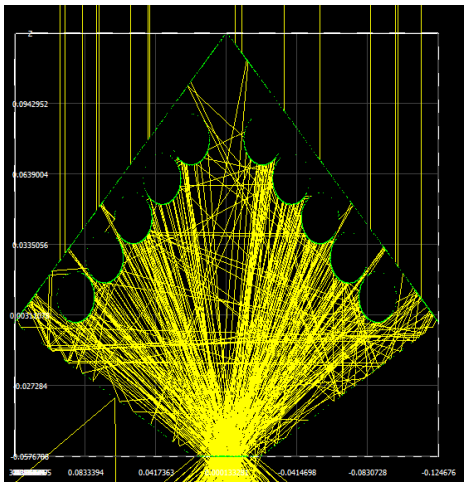

Figure 7.5: HTC, Design Point C

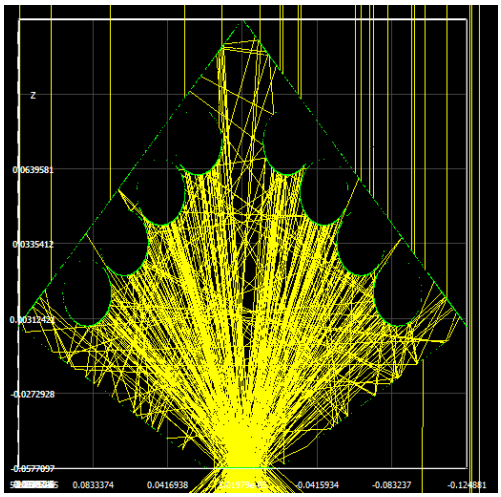

Figure 7.6: HTC, Design Point D

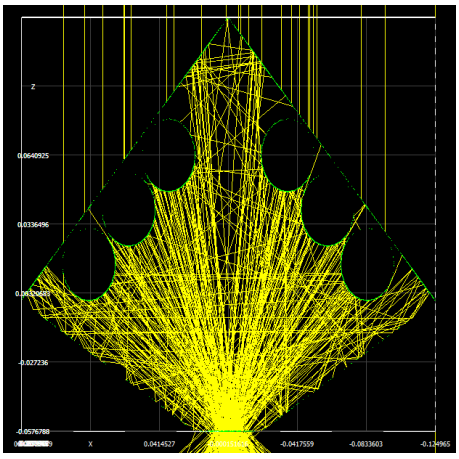

Figure 7.7: HTC, Design Point E

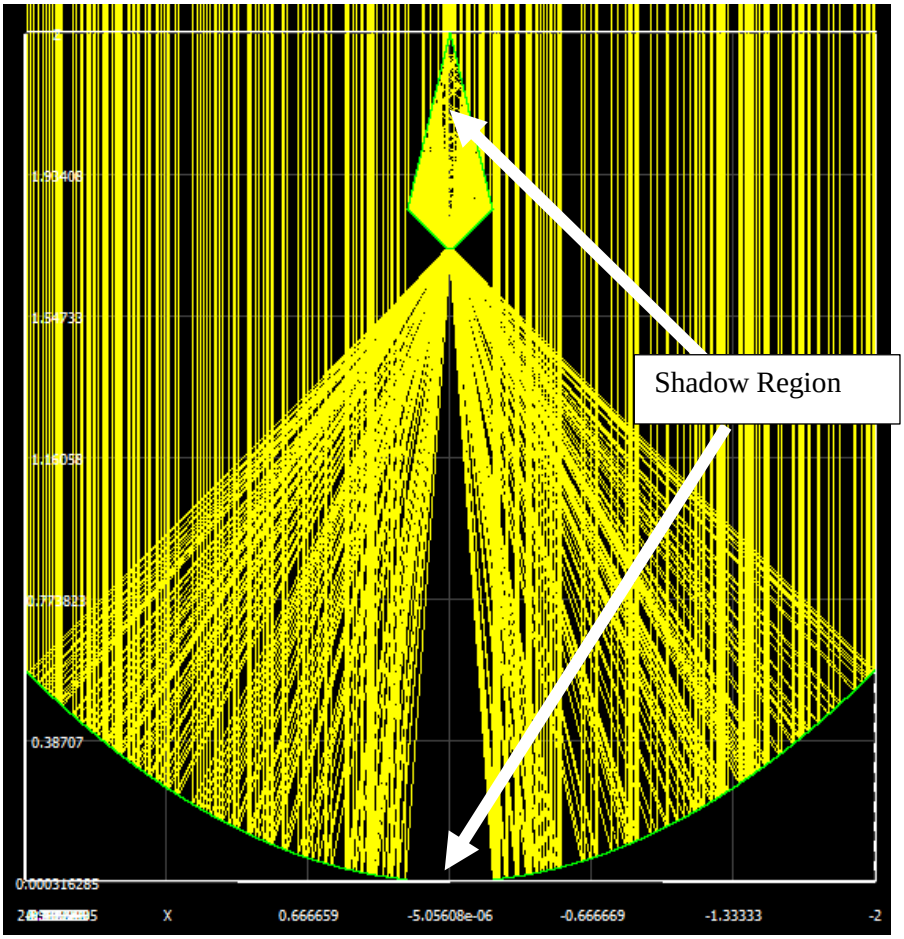

Figure 7.8: HTC Receiver Showing Shadow Region (CR=10, θ=45^0)

Figures 7.11 and 7.12 show the outlet temperature profiles of design points A and E. It is noticed that a smaller diameter tube allows for a more circumferential and uniform outlet temperature whereas a larger tube has a large centred volume of cold fluid with the outer parts of the fluid being at a much higher temperature than the centre resulting in a less uniform outlet temperature profile.

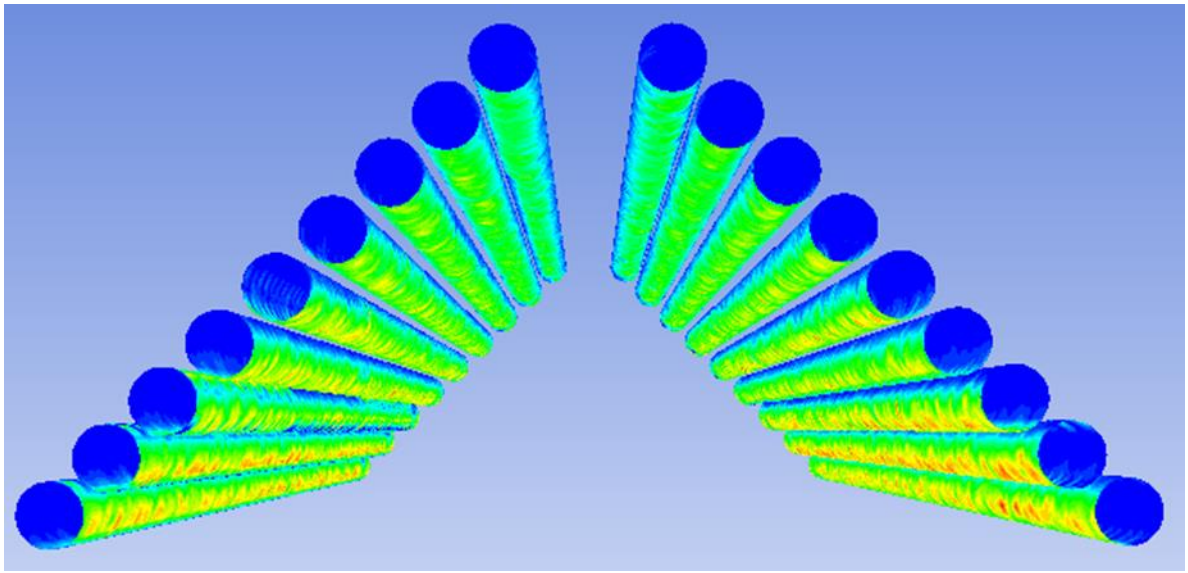

Figure 7.9: Heat Flux Profile (Design Point A)

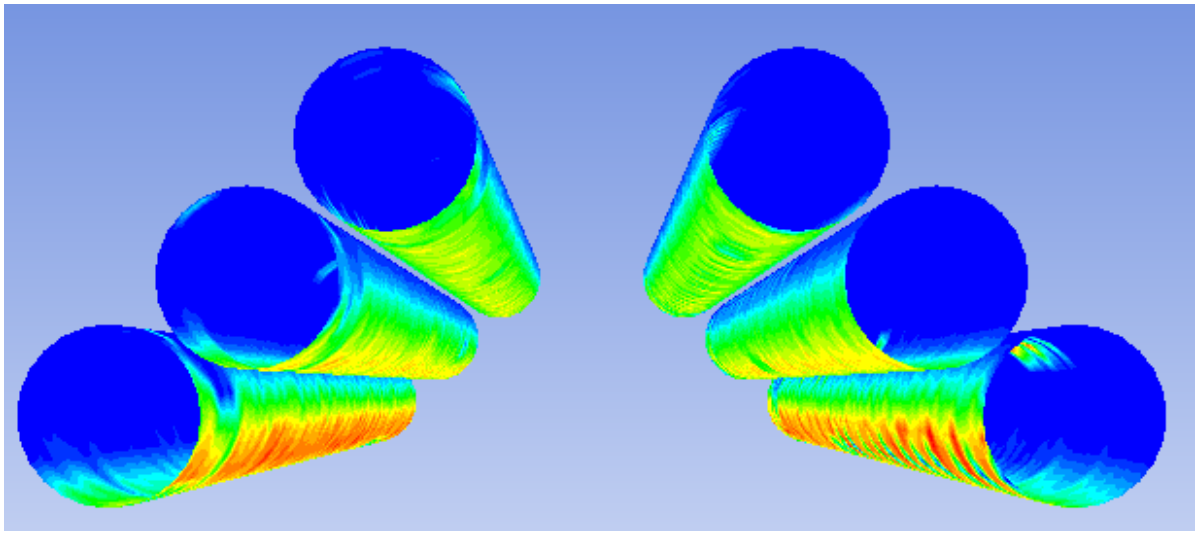

Figure 7.10: Heat Flux Profile (Design Point E)

The thermal efficiencies of the HTC receiver at all design points are close, with a difference of approximately 4% between the lowest and highest thermal efficiency. This difference could be due to the increasing non-uniformity in outlet temperature profiles as the tube diameter increases. The temperature

Figure 7.13 shows the temperature profile of the air within the cavity of the HTC receiver. The profile shows that the air is heated at the receiver aperture due to the aperture absorbing some of the concentrated irradiation which is then transferred to the cavity air. The temperature profile shows that the air surrounding the absorber tubes is the hottest, followed by the air in the centre

of the cavity, followed by the air near the bottom cone walls which is shown to be coldest. This temperature profile shows the flow of heat within the cavity air which is; the cavity air is absorbing heat from the absorber tubes which is then transferred to the surrounding via the bottom cone walls. This adds to the heat losses experienced by the HTC receiver.

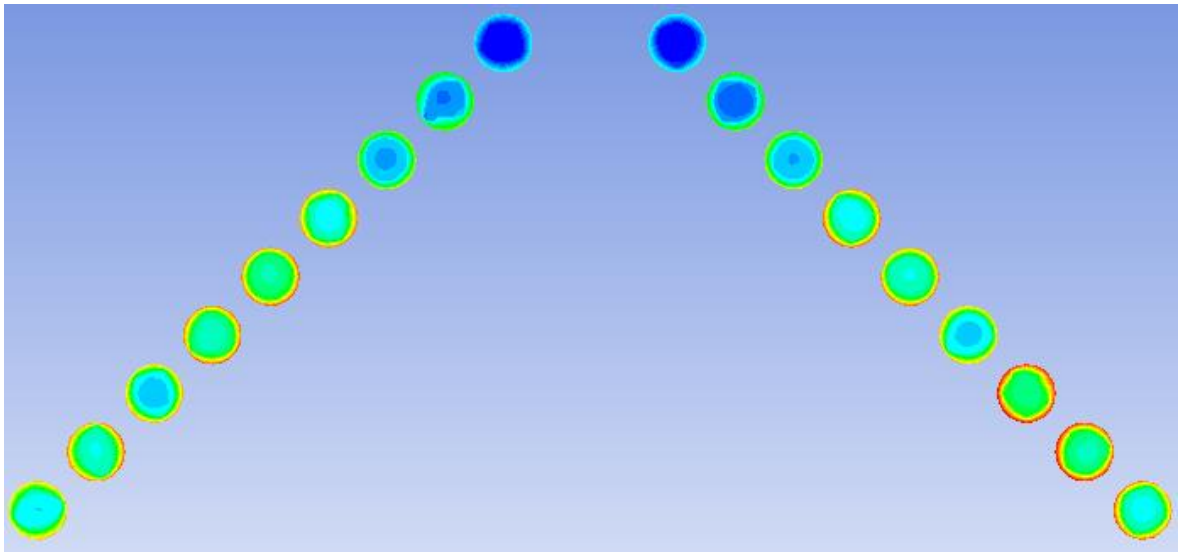

Figure 7.11: Outlet Temperature Profile (Design Point A)

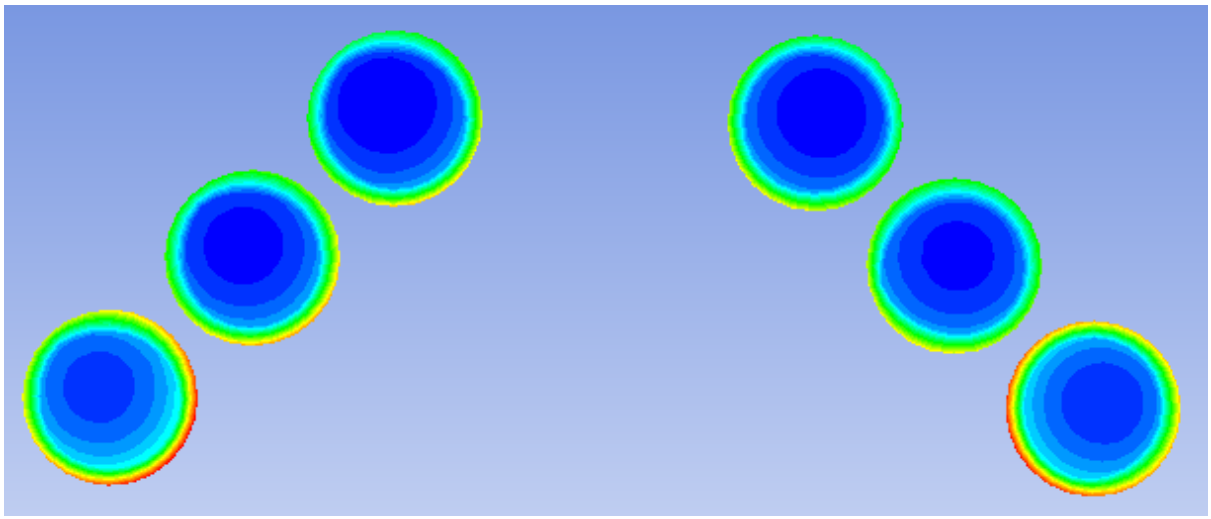

Figure 7.12: Heat Flux Profile (Design Point E)

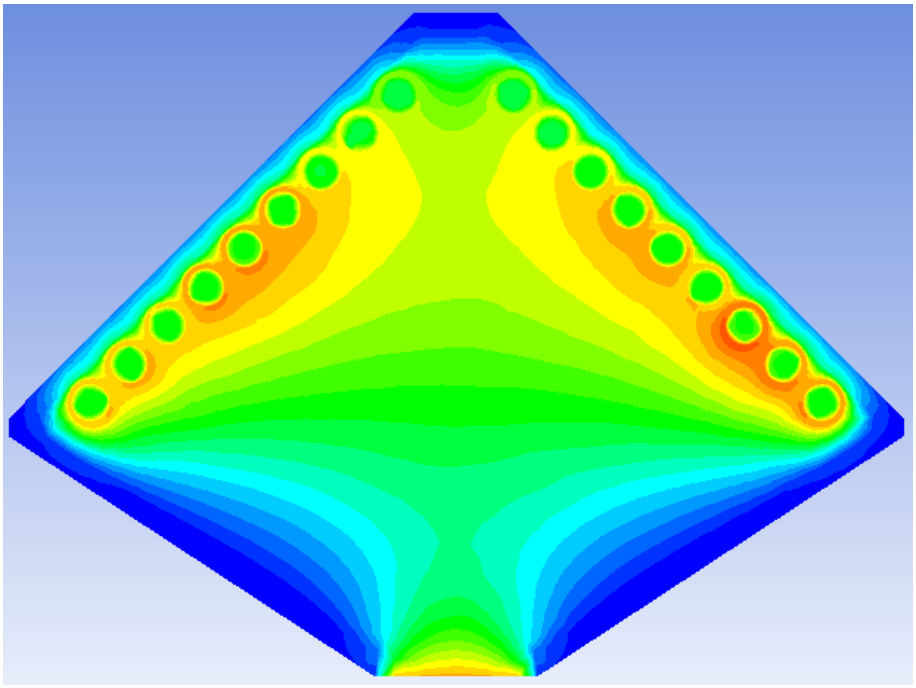

Figure 7.13: Temperature Profile of Cavity Air – HTC Receiver

Other factors that could be reducing thermal efficiency is increased re-radiation as each tube experiences a larger heat flux intensity as the number of tubes decreases as the tube diameter increases. Careful consideration of absorber tube diameter needs to be taken in order to maximise thermal efficiency.

7.5 HTC IN CONTEXT

In order to adequately comprehend the performance of a device, the performance of the device must be related to the performance of a well-known device. For example, one cannot fully understand how powerful or fast a 750hp Ford Mustang is unless they know how fast and powerful a common 75hp Hyundai i10 is and the best way to grasp the difference is by a drag race. It is good practise to compare new technology with current technology as a means of measuring if any progress has occurred.

To make the benefits of the HTC receiver more relatable, its performance was compared to a parabolic trough receiver that is widely used in massive solar power plants.

7.6 PREVIOUS WORK

In order to effectively compare this work to previous work, the previous work had to have utilised a tubular receiver, a parabolic trough, water as a heat transfer fluid, and an appropriate numerical model which considered all modes of heat transfer. The work done by Kalogirou (Kalogirou, 2012) was selected for this purpose.

The work done by Kalogirou was a detailed thermal analysis of a parabolic trough vacuum tube receiver. The thermal analysis considered all modes of heat transfer; convection into the receiver pipe, in the annulus between the receiver and the glass cover, and from the glass cover to ambient air; conduction through the metal receiver pipe and glass cover walls; and radiation from the metal receiver pipe and glass cover surfaces to the glass cover and the sky respectively. The receiver was numerically modelled and solved in Engineering Equation Solver (EES) and was validated with known performances of existing receivers.

Figure 7.14 shows a schematic of the parabolic trough collector modelled by Kalogirou.

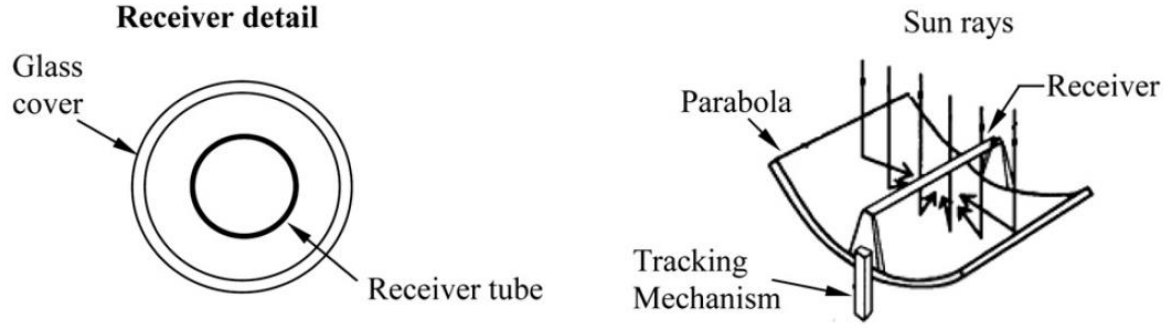

Figure 7.14: Schematic of Vacuum Tube Receiver (Kalogirou, 2012)

7.6.1 OPERATING CONDITIONS

The parabolic trough module used had a width of 1.208m, a length of 1.993m, a focal length of 0.647m and a reflectivity of 93.5%. A total of six modules were linked together. The receiver was

made from 304L stainless steel coated with a material with an absorptivity of 0.93. The absorber tube had an inner diameter of 25mm and an external diameter of 28mm.

The DNI used in the numerical model was kept constant at 900 W/m^2 with a constant ambient and inlet temperature of 25℃. The mass flow rate and wind speed were kept constant at 8.8g/s and 0.45m/s respectively.

The total irradiance acting on the reflector is the product of the DNI and the reflector area normal to the incoming irradiation. Therefore, the total irradiance acting on the reflector is 2166.78W/module.

To fairly compare the performance of the aforementioned receiver and the optimised HTC receiver, the HTC receiver was simulated under these operating conditions. The parabolic trough used for the vacuum tube receiver was 1.208m by 1.993m and the parabolic trough used in this work was 0.5m by 4m. Therefore, using the same DNI used in Kalogirou's work would result in a lower total incoming irradiance which would yield less similar operating conditions. To accommodate for this, the total incoming irradiance was used as an operating condition instead of the DNI. The DNI applied to this work's numerical model was determined by dividing the total irradiance per module of the previous work by the perpendicular reflector area of this work's parabolic trough which yielded a DNI of 1083.39W/module which provided the same supply of energy to the HTC receiver as the vacuum tube receiver.

7.6.2 RESULTS

The total efficiency of the vacuum tube was compared to the total efficiency of the optimised HTC receiver at different heat transfer fluid operating outlet temperatures. Figure 7.15 plots the results of the aforementioned comparison.

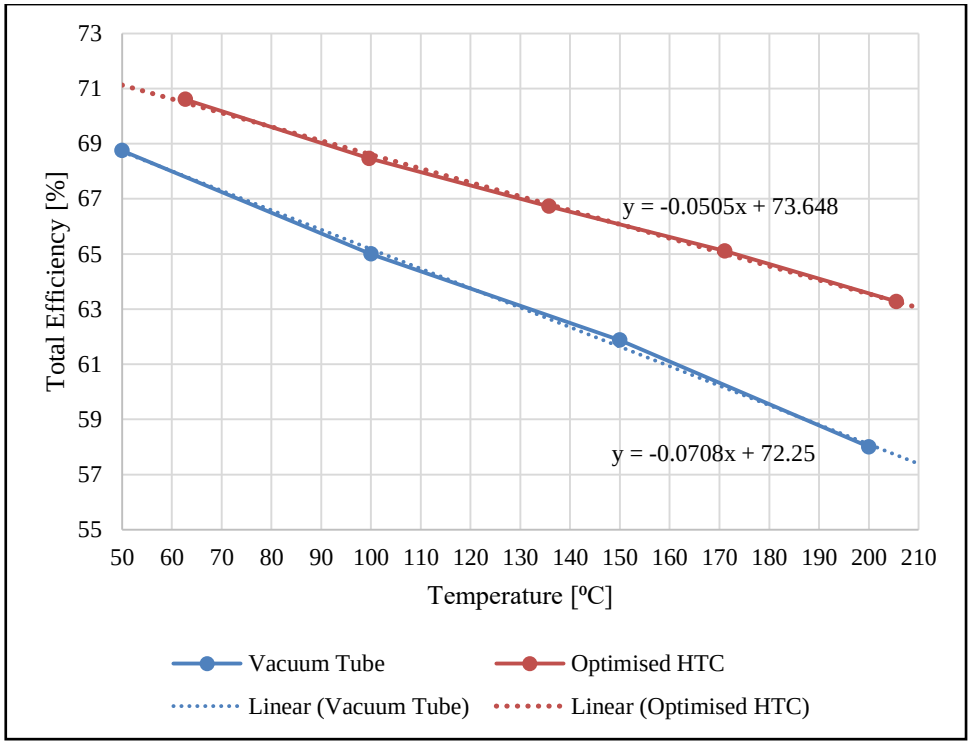

Figure 7.15: Performance Comparison – HTC vs Vacuum Tube Receiver

Figure 7.15 shows that the HTC is more efficient than the vacuum tube receiver in the operating temperature range of 50-210℃. The efficiency of the vacuum tube receiver at 50℃ was approximately 69%. The results of the vacuum tube receiver showed a linear pattern. Therefore, a linear trendline was applied to its results and extrapolated to 210℃ for which vacuum tube receiver showed an efficiency of approximately 57%. The results of the HTC receiver also displayed a linear pattern; hence a linear trendline was applied to its results. At an operating temperature of 210℃, the HTC receiver exhibited an efficiency of approximately 63%. The HTC receiver was found to operate at an approximate efficiency of 71% at an operating temperature of 50℃.

The Equations of the linear trend-lines show that the HTC is capable of operating at significantly higher efficiencies at higher operating temperatures as the rate at which its efficiency decreases with temperature is 30% lower than the rate at which the vacuum tube losses efficiency with an increase in temperature.

7.7 SUMMARY

The absorber tube diameter of an optimised HTC cavity was optimised using an iterative analysis method. The results of the analysis showed that there is a relationship between optical efficiency and thermal efficiency of the HTC receiver. It was found that the shadowing and the shadow region significantly affects performance and must be considered when selecting the diameter of the absorber tube in an HTC receiver.

A comparison was conducted between the optimised HTC receiver and a widely utilised vacuum tube receiver. It was found that the HTC receiver performs better than the vacuum tube receiver at all considered operating temperatures. It was found that the HTC receiver is capable of operating at higher efficiencies than the common vacuum tube receiver at higher operating temperatures and exhibits a lower decrease in performance per temperature rise than the vacuum tube receiver.

The optimum configuration of an HTC receiver for a parabolic trough with a width of 4m and focal length of 1.732m was found to be at a concentration ratio of 20, a cone angle of 90^0 and an absorber tube diameter of 10mm which produced a maximum efficiency of 75.30%.

CHAPTER EIGHT

8 SUMMARY, CONCLUSION AND RECOMMENDATIONS

8.1 SUMMARY

The need for efficient solar power as a means of providing a source of usable energy has increased because of the rise in pollution, cost of conventional fossil fuels and depleting non-renewable energy resources. Various studies are being conducted to investigate methods of reducing heat loss via convection and re-radiation as well as proposing novel design concepts that are more cost effective and efficient. Dominating factors that affect the efficiency of CSP systems are being investigated and new methods of increasing efficiency are being proposed.

In this dissertation, relevant information was provided in the literature about some of these studies and the basic concept and workings of CSP systems were presented in chapter 2. A numerical approach to modelling complex CSP systems efficiently was presented in chapter 3 which separated the numerical model into two models and combined their results to form one complete model. A method was presented to model the optical response of a CSP receiver and a separate method which used the data from the optical model was presented to model the thermal response of a CSP system.

A validation study was performed and presented in chapter 4 in which the proposed numerical model was validated against experimental results. An experiment which involved the testing of a parabolic trough system with a single absorber tube receiver under various operating conditions was selected because this experiment involved multiple operating conditions, a tubular receiver and a parabolic reflector which provided a system that tested both the optical and thermal capability of the numerical model.

A novel receiver design as well as a comparative design was presented in Chapter 5. The novel design included geometric shapes and properties that had the potential to produce high optical and thermal efficiencies by reducing losses due to re-radiation and convection through its shape. An alternative design was also presented to act as a benchmark design which the results of the novel design would be compared to in order to show that the design concept shape achieves its task of producing high efficiencies. Chapter 5 presented an optical investigation into these two designs. Performance results, heat flux distributions and areas of efficiency losses were presented and compared for each design under varying geometric conditions in order to identify which geometric properties affect optical efficiency.

A thermal study into the novel design and comparative design was performed and presented in Chapter 6. The thermal study was focused on studying the performance of each receiver design under different design configurations and observing which aspects affect thermal efficiency and how effective the novel design was at reducing losses. Heat flux distributions, cavity air and outlet temperature profiles were presented in order to identify how the novel design is able to achieve high efficiencies as compared to other typical tubular receivers.

An optimisation study was conducted on the novel design and presented in Chapter 7 in which the novel design's shape was fixed and its absorber tube diameter was varied to maximise thermal efficiency. An iterative manual optimisation approach was utilised. A new numerical model was generated at each design point and the optical and thermal performance results were extracted and compared to find the absorber tube diameter which maximised the receiver's thermal efficiency.

A comparison was conducted between the optimised HTC receiver and a widely utilised vacuum tube receiver as a means of benchmarking the HTC receiver. The HTC receiver was observed to experience a decrease of 6% compared to the commercial vacuum tube receiver which experienced a drop of 13% from operating at temperatures of 50ºC-210ºC. The HTC receiver exhibited a lower decrease in performance per temperature rise than the vacuum tube receiver.

This dissertation was a three-phase development and optimisation process of a novel tubular cavity thermal receiver in which its cavity geometry was optimised optically in Chapter 5 and thermally in Chapter 6 and its absorber tube diameter optimised in Chapter 7. This provided a fully optimised novel receiver for a specified parabolic trough reflector.

8.2 CONCLUSION

Based on several simulations performed, including a validation study, a successful computational method and model as well as an optimised novel receiver design was developed and presented.

The proposed numerical method was validated against experimental results produced by the numerical model, which on average, were 1.69% higher than the experimental results; showing a strong alignment between the model and real conditions. Therefore, the proposed numerical method is a suitable method for accurately modelling complex CSP systems effectively and efficiently.

The optical investigation performed on the HTC receiver cavity geometry showed that the geometry of the HTC receiver successfully performed in significantly reducing radiation and reflection losses. After a thorough investigation into the optical and thermal performance of the STC and HTC receiver, it was observed that the HTC receiver is between 9% and 12% more efficient than an STC receiver; confirming that the HTC design successfully increases optical and thermal efficiency.

The optimum results obtained in this study have confirmed the existence of an ideal design configuration and the steps to be followed to achieve it on an HTC receiver that would maximise both the optical and thermal efficiency of the receiver. The optimised HTC receiver, for practical purposes, had an overall thermal efficiency of 71%.

The HTC was shown to be a more efficient and effective high performance solar thermal CSP receiver than the commercial vacuum tube receiver capable of operating more efficiently at

temperatures in excess of 210^0C. The HTC receiver exhibits a low decrease in performance in high temperature operating conditions.

In conclusion, the Heteroconical Tubular Cavity receiver; a successfully performing high efficiency novel tubular cavity thermal receiver was proposed, designed, investigated and optimised.

8.3 RECOMMENDATIONS

Despite the success of this study, recommendations can be made to aid in any further research and development of complex solar thermal receivers.

The method of computationally modelling the complex solar receiver was validated. However, the accuracy of this method can be increased when modelling an evacuated cavity receiver as the method does not account for the fluid within the cavity affecting the optical efficiency.

Further investigation into evacuated complex cavity receivers could be done in order to design complex receivers with higher efficiencies.

Complex cavity receivers produce high efficiencies, but at what cost? One could investigate the economical aspect of implementing complex cavity receivers and conduct a trade-off between energy efficiency and economic efficiency.

In order to increase the overall efficiency of a cavity receiver, further research should be conducted into the optical aspect of a cavity receiver as the thermal efficiency is already significantly larger than the optical efficiency.

REFERENCES

Alucobond Architecture , 2012. *Solar and Light Reflectivity Values for Alucobond Colours and Finishes,* Melbourne: Halifax Vogel Group.

ANSYS, 2012. *Fluent 14.5 User's Guide.*

Avila-Marin, A., 2011. Volumetric receivers in Solar Thermal Power Plants with Central Receiver System Technology: A Review. *Solar Direct,* Issue 85, pp. 891-910.

Bakker, A., 2006. *Applied Computational Fluid Dynamics,* s.l.: s.n.

Behar, O., Khellad, A. & Mohammedi, K., 2013. A review of studies on central receiver solar thermal power plants. *Renewable and Sustainable Energy Reviews.*

Bugaje, I. M., 2004. Renewable Energy for Sustainable Development in Africa: a review. *Renewable and Sustainable Energy Reviews,* Volume 10, pp. 603-612.

Burkholder F, K. C., 2009. *Heat Loss Testing in Schott's 2008 PTR70 Parabolic Trough Receiver,* s.l.: NREL.

Cengel, Y. & Ghajar, A., 2011. *Heat and Mass Transfer: Fundamentals and Applications.* Fourth ed. New York City: McGraw-Hill.

Craig, K., Gauche, P. & Kretzschmar, H., 2014. *CFD Analysis of Solar Tower Hybrid Pressurized Air Receiver (HPAR) using a Dual-Banded Radiation Model,* Pretoria: University of Pretoria.

Craig, O. O., 2015. *A Stand-alone Parabolic Dish Solar Cooker,* Stellenbosch: University of Stellenbosch.

CSP-Today, 2012-2013. *Concentrated Solar Power Markets Report,* London: FC Business Intelligence Ltd..

DOE, 2018. *South African Department of Energy.* [Online]
Available at: http://www.energy.gov.za/files/coal_frame.html
[Accessed 9 May 2018].

Dunham, M. T. & Iverson, B., 2014. High Efficiency Thermodynamic Power Cycles for Concentrated Solar Power Systems. *All Faculty Publications.*

Feldhoff, F., 2012a. *Direct Steam Generation Technology Overview.* Almera, SFERA Summer School.

Feldhoff, F., 2012b. *Linear Fresnel Collectors A Technology Overview.* Almeria, SFERA Summer School.

Garbrecht, O., Al-Sibai, F., Kneer, R. & Wieghrdt, K., 2013. CFD-simulation of a new receiver design for a molten salt solar power tower. *Solar Energy,* Volume 90, pp. 94-106.

García-Valladares, O. & Velázquez, N., 2009. Numerical simulation of parabolic trough solar collector: Improvement using counter flow concentric circular heat exchangers. *International Journal of Heat and Mass Transfer,* Volume 52, pp. 597-609.

Gehring, B. J., 2013. *Modeling and Analysis of Latent Heat High Temperature Thermal Energy Storage for Concentrating Solar Power Plants,* San Diego: San Diego State University.

Giostri, A., Silva, P., Macchi, E. & Manzolini, G., 2011. *Comparison of Two Linear Collectors in Solar Thermal Plants: Parabolic Trough vs Fresnel.* Washington, ASME.

Govaerts, Y., 1998. Raytran: A Monte Carlo Ray-Tracing Model to Compute Light Scattering in Three-Dimensional Heterogeneous Media. *IEEE Transactions on Geoscience and Remote Sensing,* 36(2), pp. 493-505.

Green Rhino Energy, 2016. *Concentrated Solar Thermal System.* [Online]
Available at: http://www.greenrhinoenergy.com/solar/technologies/cst_systems.php
[Accessed 14 June 2017].

Gunther, M., Joemann, M. & Csambor, S., n.d. *Parabolic Trough Technology.* 1 ed. s.l.:enerMENA.

Ho, C. K. & Iverson, B. D., 2014. Review of high-temperature central receiver designs for concentrating solar power. *Renewable and Sustainable Energy Reviews,* Volume 29, pp. 835-846.

Homann, C., 2015. *Effects of Solar Hybridization on the Performance of a Gas Turbine,* Stellenbosch: Stellenbosch University.

Izweik, H. T., Ahmed, A. M. & Albusefi, A. A., 2016. Design, Construction and Experimental Testing of a Parabolic Trough Collector for Process Heat APplications. *International Journal of Innovative Research in Science, Engineering and Technology,* 5(9), pp. 15890-15900.

Kajiya, J. T., 1986. The Rendering Equation. *Siggraph,* 20(4), pp. 143-150.

Kalogirou, S. A., 2012. A detailed thermal model of a parabolic trough collector receiver. *Energy,* Issue 48, pp. 298-306.

Karni, J. et al., 1997. The DIAPR: a high-pressure, high-temperature solar receiver. *Journal of Solar Energy Engineering, Transactions of the ASME,* 1(119), pp. 74-78.

Kayofa, L., 2015. *Feasibility study and business plan for manufacturing a 3 kW-electrical solar Stirling engine and dish for stand-alone power supply units,* Stellenbosch University: M.S. Thesis.

Laforgia, D., 2013. *Transparent Parabolic Trough Collector Based on Gas-phase Nanofluids.* [Online]
Available at: http://www.solar.unisalento.it/TPTC.htm
[Accessed 20 May 2018].

Launder, B. D. S., 1974. The numerical computation of turbulent flows. *Computer Methods in Applied Mechanics and Engineering,* 3(2), pp. 269-289.

Litt, D., 2016. *Greenhouse Gases versus Glass Greenhouse.* [Online]
Available at: http://berkeleysciencereview.com/greenhouse-gases-versus-glass-greenhouses/
[Accessed 29 May 2018].

Maleka, E., Mashimbye, L. & Goyns, P., 2010. *South African Energy Synopsis 2010.* Pretoria, South African Department of Energy.

Meyer, A., 2011. *The South African Refit: Solar Resource Assesment Options for CSP Developers.* Stellenbosch , The South African Refit.

Meyer, A. J. & van Niekerk, J. L., 2011. *Roadmap for the Deployment of Concentrating Solar Power Systems,* Pretoria: s.n.

Mills, D., 2004. Advances in Solar Thermal Electricity Technology. *Solar Energy,* Volume 76, pp. 9-31.

Milwaukee Area Skywarn Association, 2011. *Wind Speed Estimates.* [Online]
Available at: www.mke-skywarn.org/hail_wind.htm
[Accessed 15 June 2018].

Moghimi, M., Craig, K. & Meyer, J., 2015. A novel approach to combine the optical and thermal modelling of linear fresnel collectors using the finite volume method. *Solar Energy,* Volume 116, pp. 407-427.

Moghimi, M., Craig, K. & Meyer, J., 2015. *A Novel Computational Approach to Combine the Optical and Thermal Modelling of Linear Fresnel Collectors using the Finite Volume Method.* Kruger National Park, South Africa, s.n.

Ngo, L., Bello-Ochende, T. & Meyer, J., 2016. *Numerical Modelling and Optimisation of Natural Convection Heat Loss Suppression in a Solar Cavity Receiver with Plate Fins,* Cape Town: University of Pretoria and University of Cape Town.

Patel, M. R., 2006. *Wind and Solar Power Systems - Designs, Analysis and Operation.* New York: Taylor & Francis.

Piyawat Chalermkanjana, K. T., 2008. *wikidot.* [Online]
Available at: http://me1065.wikidot.com/solar-stirling-engine
[Accessed 17 June 2016].

Prometheus Turbine, 2013. *The Prometheus Turbine Project.* [Online]
Available at: http://www.prometheusturbine.info/solar_gas_turbine.html
[Accessed 14 June 2017].

Rajesh Bhaskaran, L. C., 2017. *Introduction to CFD Basics,* s.l.: s.n.

Reddy, K. & Sendhil, N., 2008. Combined laminar natural convection and surface radiation heat transfer. *International Journal of Thermal Sciences,* Issue 47, pp. 1647-1657.

Shih, T., 1995. A new k-ε eddy viscosity model for high Reynolds number turbulent flows. *Computers and Fluids,* 24(3), pp. 227-238.

Solar Energy Technologies Office, 2013. *Dish/Engine System Concentrating Solar Power Basics.* [Online]
Available at: https://www.energy.gov/eere/solar/articles/dishengine-system-concentrating-solar-power-basics
[Accessed 17 June 2017].

Solar Energy Technologies Office, 2013. *Line Concentrating Systems.* [Online]
Available at: https://www.energy.gov/eere/solar/articles/linear-concentrator-system-basics-

concentrating-solar-power
[Accessed 17 June 2016].

Solar Energy Technologies Office, 2013. *Power Tower System Concentrating Solar Power Basics.* [Online]
Available at: https://www.energy.gov/eere/solar/articles/power-tower-system-concentrating-solar-power-basics
[Accessed 17 June 2017].

Versteeg, H. W. M., 2007. *An introduction to computational fluid dynamics: The finite volume method.* s.l.:Pearson Education Limited.

Watt, A. D., 1978. *On the Nature and Distribution of Solar Radiation,* s.l.: U.S. Department of Energy.

Wendelin, T. & Wagner, M., 2018. *SolTrace Open-Source Software Project,* Colorado: National Renewable Energy Laboratory.

Wild, S., 2015. *Is Greenpeace right to say S. Africa is the world's third best solar location?.* [Online]
Available at: https://africacheck.org/reports/is-south-africa-really-the-worlds-third-best-solar-location/
[Accessed 29 May 2018].

William, B., Geyer, S. & Geyer, M., 2001. *Power from the Sun.* s.l.:s.n.

Wu, S., Xiao, L., Cao, Y. & Li, Y., 2010. Convection heat loss from cavity receiver in parabolic dish solar. *Solar Energy,* Issue 84, pp. 1342-1355.

Yakhot, V., 1992. Development of turbulence models for shear flows by a double expansion technique. *Physics of Fluids,* 4(7), pp. 1510-1520.

A. APPENDIX A – VALIDATION STUDY

Table A.1: Physical Properties of Experiment (Izweik, et al., 2016)

Property	Value
Parabolic Trough Collector	
Surface Material	Aluminium Foil
Reflectivity	0.85
Aperture Width	1m
Aperture Length	4.8m
Focal Length	0.5m
Concentration Ratio	15.76
Absorber Tube	
Tube Material	Mild Steel coated with Black Paint
Absorptivity	0.83
Inner Diameter	0.017m
Outer Diameter	0.021m

Table A.2: Experimental Data (Izweik, et al., 2016)

	Date	DNI [W/m^2]	$\dot{m}$ [kg/s]	T_{amb} [K]	T_{in} [K]	η_{th} [%]
Exp. 1	04-01-2016	243	0.004	291	291.3	52.7
Exp. 2	07-01-2016	263	0.004	284	284.6	40
Exp. 3	14-01-2016	280	0.004	288	288.7	45.2
Exp. 4	20-01-2016	460	0.004	278	278.5	45.6
Exp. 5	26-01-2016	420	0.004	284	284	42.7

Table A.3: Numerical Results of Experiment

	Result	*Simulation*				
		Exp. 1	**Exp. 2**	**Exp. 3**	**Exp. 4**	**Exp. 5**
SolTrace	DNI [W/m^2]	243	263	280	300	480
	$\dot{Q}_{trough}$[W]	1166.4	1262.4	1344	1440	2304
	$\dot{Q}_{abs}$[W]	699.87	757.47	806.43	864.03	1382.45
	η_{opt}	0.60	0.60	0.60	0.60	0.60
Fluent	$\dot{Q}_{abs}$[W]	691.004	747.88	796.22	853.09	1364.95
	$\dot{m}$[kg/s]	0.004	0.004	0.004	0.004	0.004
	T_{sky}[K]	274.02	264.19	269.79	255.86	264.19
	T_{amb}[K]	291	284	288	278	284
	T_{in}[K]	291.3	284.6	288.7	278.5	284
	T_{out}[K]	327.08	316.89	324.99	318.61	347.14
	ΔT_{htf}[K]	35.78	32.29	36.29	40.11	63.14
	$\dot{Q}_{htf}$[W]	598.53	540.15	607.06	670.96	1056.21
Thermal Efficiency	$\boldsymbol{\eta_{th}}$	**0.5196**	**0.4333**	**0.4574**	**0.4719**	**0.4643**

Table A.4: Experimental Results vs Numerical Results – Validation Study

Thermal Efficiency [%]	**Exp. 1**	**Exp. 2**	**Exp. 3**	**Exp. 4**	**Exp. 5**	**Average**
Experimental	52.7	40	45.2	45.6	42.7	45.24
Numerical	51.96	43.33	45.74	47.19	46.43	46.93
Discrepancy	0.74	3.33	0.54	1.59	3.73	1.69

B. APPENDIX B – DESIGN CONFIGURATIONS

Table B.1: Cavity Geometry Configurations

	CR	RCR	r [cm]
Case 1	40	2.5	10
Case 2	20	5	20
Case 3	13.33	7.5	30
Case 4	10	10	40

Table B.2: Receiver Design Configurations

	CR	RCR	r [cm]	θ [^{0}]
Case A	40	2.5	10	45
Case B	20	5	20	90
Case C	40	2.5	10	45
Case D	20	5	20	90

Table B.3: Optimisation Design Points

Design Point	D_t [mm]
A	10
B	15
C	20
D	25
E	30

C. APPENDIX C - NUMERICAL MODEL RESULTS

Table C.1: Optical Results – STC Receiver

Property	**STC Receiver**			
	Case A	**Case B**	**Case C**	**Case D**
DNI [W/m^2]	1000	1000	1000	1000
$\dot{Q}_{trough}$[W]	2000	2000	2000	2000
Ppr [W/ray]	0.002	0.002	0.002	0.002
Tube Intersections	716907	701143	770700	670612
Aperture Intersections	966699	966060	941758	941848
$\dot{Q}_r$[W]	1933.398	1932.12	1883.516	1883.696
$\dot{Q}_{abs}$[W]	1433.814	1402.286	1541.4	1341.224
$\eta_{opt,r}$	0.741603	0.725776	0.818363	0.712017
η_{opt}	**0.716907**	**0.701143**	**0.7707**	**0.670612**

Table C.2: Thermal Results – STC Receiver

Property	**STC Receiver**			
	Case A	**Case B**	**Case C**	**Case D**
C_p [$\mathbf{J/kg \cdot K}$]	4182	4182	4182	4182
$\dot{Q}_{abs}$[W]	1407.98	1405.62	1584.95	1348.81
Number of Tubes	12	8	28	14
$\dot{m}$[kg/s]	0.05	0.05	0.05	0.05
v_{in} [m/s]	0.03351	0.05026	0.01436	0.02872
T_{sky}[K]	276.84	276.84	276.84	276.84
T_{amb}[K]	293	293	293	293
T_{in}[K]	300	300	300	300
T_{out}[K]	306.141	306.3	306.533	305.906
η_{th}	0.6539	0.6572	0.6644	0.6141

Table C.3: Optical Results – HTC Receiver

Property	HTC Receiver			
	Case A	**Case B**	**Case C**	**Case D**
DNI [W/m^2]	1000	1000	1000	1000
$\dot{Q}_{trough}$[W]	2000	2000	2000	2000
Ppr [W/ray]	0.002	0.002	0.002	0.002
Tube Intersections	772393	765212	825452	742232
Aperture Intersections	967101	967187	942178	942646
$\dot{Q}_r$[W]	1934.202	1934.374	1884.356	1885.292
$\dot{Q}_{abs}$[W]	1544.786	1530.424	1650.904	1484.464
$\eta_{opt,r}$	0.798668	0.791173	0.87611	0.787392
η_{opt}	**0.772393**	**0.765212**	**0.825452**	**0.742232**

Table C.4: Thermal Results – HTC Receiver

Property	HTC Receiver			
	Case A	**Case B**	**Case C**	**Case D**
C_p [$\mathbf{J/kg \cdot K}$]	4182	4182	4182	4182
$\dot{Q}_{abs}$[W]	1362.186	1549.464	1712.411	1523.076
Number of Tubes	12	8	28	14
$\dot{m}$[kg/s]	0.047116	0.050468	0.050472	0.050472
v_{in} [m/s]	0.03351	0.05026	0.01436	0.02872
T_{sky}[K]	276.84	276.84	276.84	276.84
T_{amb}[K]	293	293	293	293
T_{in}[K]	300	300	300	300
T_{out}[K]	306.4991	306.8635	306.64	306.661
η_{th}	0.6791	0.7154	0.6756	0.6851

Table C.5: Optical Results - Optimisation

Property	Tube Outer Diameter				
	10mm	**15mm**	**20mm**	**25mm**	**30mm**
DNI [W/m^2]	1000	1000	1000	1000	1000
$\dot{Q}_{trough}$[W]	2000	2000	2000	2000	2000
Ppr [W/ray]	0.002	0.002	0.002	0.002	0.002
Tube Intersections	747761	733648	746635	732963	679652
Aperture Intersections	942721	942688	942742	942702	942646
$\dot{Q}_r$[W]	1885.442	1885.376	1885.484	1885.404	1885.292
$\dot{Q}_{abs}$[W]	1495.522	1467.296	1493.27	1465.926	1359.304
$\eta_{opt,r}$	0.793194381	0.778251129	0.791982324	0.777512936	0.721004
η_{opt}	0.747761	0.733648	0.746635	0.732963	0.679652

Table C.6: Thermal Results - Optimisation

Property	Tube Outer Diameter				
	10mm	**15mm**	**20mm**	**25mm**	**30mm**
C_p [$\mathbf{J/kg \cdot K}$]	4182	4182	4182	4182	4182
$\dot{Q}_{abs}$[W]	1401.41	1335.51	1432.13	1398.65	1313.48
Number of Tubes	18	12	10	8	6
$\dot{m}$[kg/s]	0.05	0.05	0.05	0.05	0.05
v_{in} [m/s]	0.03544	0.02363	0.01595	0.01276	0.01181
T_{sky}[K]	273	273	273	273	273
T_{amb}[K]	293	293	293	293	293
T_{in}[K]	300	300	300	300	300
T_{out}[K]	306.47	305.97	306.48	306.31	305.82
$\dot{Q}_{htf}$[W]	1330.47	1239.69	1347.35	1310.48	1204.83

Table C.7: Thermal Efficiency - Optimisation

	Tube Outer Diameter				
	10mm	**15mm**	**20mm**	**25mm**	**30mm**
$\eta_{th,r}$	0.753	0.7224	0.7451	0.7284	0.6613
η_{th}	0.7099	0.681	0.7024	0.6867	0.6234

D. ETHICS FORM

Application for Approval of Ethics in Research (EiR) Projects
Faculty of Engineering and the Built Environment, University of Cape Town

APPLICATION FORM

Please Note:
Any person planning to undertake research in the Faculty of Engineering and the Built Environment (EBE) at the University of Cape Town is required to complete this form **before** collecting or analysing data.The objective of submitting this application *prior* to embarking on research is to ensure that the highest ethical standards in research, conducted under the auspices of the EBE Faculty, are met. Please ensure that you have read, and understood the **EBE Ethics in Research Handbook**(available from the UCT EBE, Research Ethics website) prior to completing this application form: http://www.ebe.uct.ac.za/usr/ebe/research/ethics.pdf

APPLICANT'S DETAILS		
Name of principal researcher, student or external applicant		Neelesh Maharaj
Department		Mechanical Engineering
Preferred email address of applicant:		Mhrnee002@myuct.ac.za
If a Student	Your Degree: e.g., MSc, PhD, etc.,	MSc
	Name of Supervisor (if supervised):	Prof. Tunde Bello-Ochende
If this is a researchcontract, indicate the source of funding/sponsorship		Click here to enter text.
Project Title		Thermodynamic analysis of a heteroconical tubular receiver for maximum power generation

I hereby undertake to carry out my research in such a way that:

- there is no apparent legal objection to the nature or the method of research; and
- the research will not compromise staff or students or the other responsibilities of the University;
- the stated objective will be achieved, and the findings will have a high degree of validity;
- limitations and alternative interpretations will be considered;
- the findings could be subject to peer review and publicly available; and
- I will comply with the conventions of copyright and avoid any practice that would constitute plagiarism.

SIGNED BY	Full name	Signature	Date
Principal Researcher/ Student/External applicant	Neelesh Maharaj		**19 Sep 2016**

APPLICATION APPROVED BY	Full name	Signature	Date
Supervisor (where applicable)	Tunde Bello-Ochende Click here to enter text.		Click here to enter a date. 26/09/2016
HOD (or delegated nominee) Final authority for all applicants who have answered NO to all questions in Section1; and for all Undergraduateresearch (Including Honours).	Tunde Bello-Ochende Click here to enter text.		26/09/2016 Click here to enter a date.
Chair : Faculty EIR Committee For applicants other than undergraduate students who have answered YES to any of the above questions.	Click here to enter text.		Click here to enter a date.

Page 1 of 1